Debonding in Bi-layer Material Systems under Moisture Effect: A Multiscale Approach
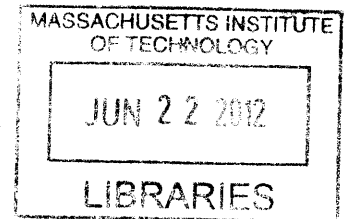
by

Tak Bun Denvid Lau

B.Eng. Civil Engineering
The University of Hong Kong, 2004

M.Phil. Structural Engineering
The University of Hong Kong, 2006

S.M., Civil and Environmental Engineering
Massachusetts Institute of Technology, 2009

SUBMITTED TO THE DEPARTMENT OF CIVIL & ENVIRONMENTAL ENGINEERING IN
PARTIAL FULFILLMENT OF THE REQUIREMENTS FOR THE DEGREE OF

DOCTOR OF PHILOSOPHY IN THE FIELD OF STRUCTURES AND MATERIALS
AT THE
MASSACHUSETTS INSTITUTE OF TECHNOLOGY

JUNE 2012

Signature of Author: _____
Department of Civil and Environmental Engineering
May 15, 2012

Certified by: _____
Oral Büyüköztürk
Professor of Civil and Environmental Engineering
Thesis Supervisor

Accepted by: _____
Heidi M. Nepf
Chair, Departmental Committee for Graduate Students

Debonding in Bi-layer Material Systems under Moisture Effect: A Multiscale Approach

by

Tak Bun Denvid Lau

Submitted to the Department of Civil and Environmental Engineering
on May 15, 2012 in Partial Fulfillment of the
Requirements for the Degree of Doctor of Philosophy in the Field of
Structures and Materials

ABSTRACT

Bi-layer material systems are found in various engineering applications ranging from nano-scale components, such as thin films in circuit boards, to macro-scale structures such as adhesive bonding in aerospace and civil infrastructure applications. They are also found in many natural and biological materials such as nacre or bone. One of the most human-related applications of bi-layer material systems is the artificial tooth involving the bonding between the natural tooth and the metal cap glued with a polymer based material. The structural integrity of a bi-layer system depends on properties of both the interface and the constitutive materials. In particular, interfacial delamination has been observed as a major integrity issue. In this research, a comprehensive investigation on the interfacial debonding mechanism has been conducted both computationally and experimentally using an epoxy-silica system. In the computational approach, a multiscale model which can predict the intrinsic strength between organic and inorganic materials, based on a molecular dynamics simulation approach, is presented. The intrinsic strength between epoxy and silica derived from the molecular level can be used to predict the structural behavior of epoxy-silica interface at the macroscopic length-scale by invoking a finite element approach using a cohesive zone model developed in this research. In order to understand the moisture effect in a more comprehensive way, the free energy profile of the epoxy-silica bonded system describing the debonding process has been reconstructed for both dry and wet conditions and it is found that the adhesion between epoxy and silica, which is dominated by the van der Waals force and Coulombic interaction, can be weakened significantly (more than 68% reduction) in the presence of water. Experimental work involving two different approaches, namely "nanoindentation" and "superlayer" approaches, in characterizing the interfacial fracture toughness are presented and the advantages and disadvantages of these two approaches are discussed. The morphology of material in the vicinity of the interface has also been captured using the scanning electronic microscope (SEM). Experimental results show that the interface fracture energy decreases significantly after 4 weeks of moisture conditioning. Both the experimental and computational results show that water plays a main role in the interfacial deterioration. The mechanism of interfacial deterioration is explained using molecular dynamics simulation and a multiscale model of the epoxy-silica bonded system which is capable of predicting the macro-scale structural behavior based on the reconstructed free energy profile of the bonded system at the nano-scale. The multiscale modeling used in this research provides a powerful new approach to link nano-level to macro-level for complex material behavior.

Thesis Supervisor: Oral Büyüköztürk

Title: Professor of Civil and Environmental Engineering

This thesis is dedicated to my love Ant

Acknowledgement

4

Here, I want to say an honorable thank you to my parents, Jimmy and Candy Lau, for bringing me up. They have given me the most time, effort, guidance, care and support throughout the first twenty years of my life, and I acknowledge the many great biblical values they have implanted in me. Also, I will always have my appreciation and love to my younger sister, Ivy Lau, who has been very supportive throughout these years.

I would like to express my deepest gratitude to the love of my life, Joey Ngai, for her prayer, encouragement and continuous support. Without her sacrifice and tenacity, I would never have had such an enjoyable experience at MIT. I am so grateful for having someone like her who is willing to run this race with me. I dedicated this book to her as a diminutive way of saying "thank you".

Last but my most heartfelt thanks to my Lord! Thank you for giving me the chance to come across all these people in my life. Thank you for showering upon me the tremendous amounts of blessings all along, more than I could ever count or notice. But most importantly, thank you for granting me difficulties and struggles throughout the time at MIT, you made me realize how small a person I am but how great the God you are. Thank you Lord and I believe you have made me a finer person, more prepared and equipped now for the many challenges ahead.

Denvid Lau
Cambridge, Massachusetts
2012

Contents

List of Figures

BE RECONSTRUCTED BY THE PROFILE OF EXTERNAL ENERGY APPLIED DURING THE PROCESS. 36

10

12

List of Tables

1.1 Background

1.1.1 Debonding of bi-layered material system

An earlier development of molecular dynamics simulation was reported in 1957 (Alder and Wainwright 1957) for a study on the dynamics of a hard sphere system consisting of several hundreds of particles. Since then, advancement of molecular dynamics simulation has been observed with the evolution of computational power in the last few decades. Molecular dynamics simulation represents a powerful tool for potential applications in various research fields including physics, chemistry, biology, bio-engineering and medicine (Allen and Tildesley 1989; Rapaport 1997). Recently, efforts have been made for applying the method to structural mechanics and engineering. Traditionally, the classical continuum mechanics theories have been the basis for most computational methods used in various engineering fields including civil and mechanical engineering; examples are finite elements, finite difference, finite volume and boundary element methods. The capability of the continuum approach is limited when structural solution at a small length scale is of concern, or if predictions about material behavior should be made from a fundamental bottom-up perspective.

Molecular dynamics simulation is based on modeling at atomistic level when the discrete nature of the matter at that level is explicitly considered. In an atomistic model the atomic distance provides a natural measure for the spatial discretization. The smallest unit in the atomistic model is an atom; the motion of each in the material is modeled over the course of a simulation time span. Collective behavior of the atoms allows one to understand how the material undergoes structural deformation. Atomistic models provide a fundamental chemistry-based description of material properties and processes, and molecular dynamics simulation is capable of solving the dynamic evolution of equilibrium and non-equilibrium processes. Thus, a particular and detailed insight into the physics of fundamental processes can be obtained. The atomistic approach has been shown to be powerful in obtaining solutions for small scale structural mechanics problems such as, localized fracture processes in materials (see, for example (Buehler and Ackbarow 2007) and references therein).

Study of organic-inorganic interfaces for various applications has been of interest to numerous researchers. Development of molecular dynamics simulation based on the atomic and molecular motions has offered opportunities for the application of the method to interface problems. The study of organic-inorganic interfaces using molecular dynamics was mainly carried out in the fields of biological and chemical engineering since the early 1990's (Galema et al. 1994; Sprous et al. 1999) but typically not focused on mechanical properties. With the expansion of the computational

methods and capabilities, application can now be extended to structural mechanics and engineering problems. An example of organic-inorganic interface in structural engineering is the layered bonded material systems. Deterioration and debonding of interfaces in a multi-layer material system is of concern since such failures at local regions might lead to a system or structural failure. One example is the possible premature failure of reinforced concrete (RC) structural elements strengthened by fiber reinforced polymer (FRP) after prolonged exposure to moisture affecting the FRP/concrete interface. In practice, FRP-strengthening system for a RC beam is typically designed such that failure occurs in the form of either steel reinforcement yielding followed by concrete crushing, or FRP rupture, providing early warning when the load capacity is exceeded (ACI440.2R-08 2008). However, when the interface becomes weak, failure can occur in the form of delamination in a tri-layer material system formed by the FRP, epoxy adhesive (organic), and the concrete material (inorganic) at various critical locations along the beam soffit, leading to a significantly lower load capacity of the FRP-retrofitted system. Fig. 1.1 shows possible debonding configurations in a FRP-retrofitted reinforced concrete beam.
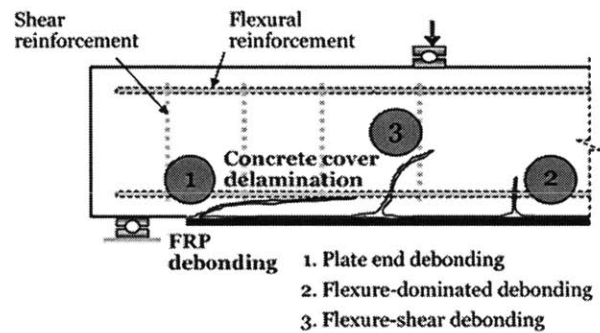
Fig 1.1 Typical failure modes of FRP-retrofitted reinforced concrete beam (Büyüköztürk et al. 2004)

When a strengthened RC beam is loaded to failure, cracks can initiate and propagate in different interfaces and material locations depending on loading configuration, and mechanical properties of the constituent materials and the interfaces. In general, crack can either propagate in bulk materials (material decohesion) or along the interfaces (interface separation). Reported empirical and analytical formulae available to predict interfacial fracture behavior include crack kinking by energy release rate (Hutchinson and Suo 1992; Nishioka et al. 2003), crack kinking by maximum hoop stress (Yuuki and Xu 1992), and crack kinking by zero complex stress intensity factor, K_{II} (Akisanya and Fleck 1992).

However, these criteria may not fully explain the interface fracture behavior involving complex material interaction when the interface is under moisture attack. Knowledge on the debonding behavior of FRP-concrete bonded systems under the effect of moisture is crucial in predicting the service-life and improving the safety of civil structures strengthened using this technique. Interface fracture tests were conducted on tri-layer specimens consisting of carbon FRP, epoxy adhesive, and

15

concrete (Au and Büyüköztürk 2006a; Au and Büyüköztürk 2006b; Lau and Büyüköztürk 2010). The specimens were loaded under displacement control in peel and shear loading configurations separately. Effect of moisture on bond strength was studied by conditioning specimens in various moisture levels at room and elevated temperatures. It was found that the presence of moisture may significantly decrease fracture toughness of the tri-layer material system. Furthermore, for both peel and shear loadings, while the dry specimens failed by concrete delamination, in all cases the wet specimens failed by epoxy/concrete interface separation. Using material properties (Young's modulus and Poisson's ratio) from material characterization test program, the crack kinking criterion could well predict crack propagation observed in the dry specimens. However, these criteria failed to explain the decrease in strength and shift in failure mode observed in wet specimens, in which interaction at the material level between water, epoxy, and concrete may have occurred in the bulk material and at the interface. The two possible explanations may be that, first, there may be a toughened epoxy-penetrated concrete layer in the vicinity of the interface under moist environment (Fig. 1.2a). As a result, the initial crack at the interface between concrete and epoxy may not propagate into concrete due to this toughened top concrete layer staying at the interface instead. Second, the adhesive force at the interface may be weakened due to interaction between epoxy and water (Fig. 1.2b). The initial crack, therefore, may stay at the interface which requires less energy for crack propagation. There is a need to study the debonding mechanism of the interface under the presence of water molecules using a more fundamental approach. Atomistic modeling approach employing molecular dynamics simulation may be used as a basis for a fundamental study.
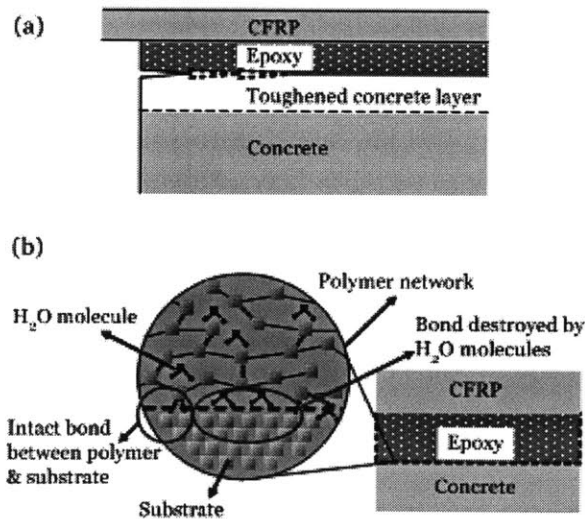
Fig 1.2 (a) Plasticization of epoxy-penetrated concrete layer, (b) weakening of bond between epoxy and concrete

1.1.2 Molecular dynamics simulations

Molecular dynamics simulation is a numerical modeling technique for studying

the molecular behavior of different substances (Allen and Tildesley 1989; Rapaport 1997; Fermeglia et al. 2003; Shevade et al. 2003; Fermeglia et al. 2004; Gardebien et al. 2004; Minisini and Tsobnang 2005). The modeling process involves several key steps, namely, (1) construction of the atomistic geometry; (2) definition of atomic interaction; (3) governing equations for the system; (4) initialization and energy minimization; (5) conditions of simulation; (6) integration scheme and (7) calculation of concerned properties. These steps are incorporated in the flowchart of the numerical approach shown in Fig. 1.3.

The first step in molecular dynamics simulation is an accurate construction of the atomistic geometry which refers to a clear definition of the atomic location, the element type (i.e. the atomic mass and associated chemical properties) and the partial charge of each atom, the bond connectivity among all atoms and the boundary conditions. This information is required for evaluating the inter-atomic interactions that describe the chemical properties. With this approach, determination of the system energy is critical throughout the simulation process, and force fields (potentials) play an important role in the accuracy of the computer modeling studies by proper description of the interaction among atoms (Lewis and Catlow 1985). There are a number of force fields available in the literature for different types of interactions among atoms (Allen and Tildesley 1989; Rapaport 1997; Buehler 2008). The choice of force field is left to the discretion of the user, based purely on the knowledge of nature of forces acting between atoms for the specific material. The potential should be chosen in such a way that it mimics the nature of atomic interactions in a realistic or appropriate way, given a particular application of the model. There are different kinds of chemical bonds that exist in different substances for holding the material together; namely, ionic bonds, covalent bonds, metallic bonds, hydrogen bonds and van der Waals bonds. Each type of bond has varied strengths.
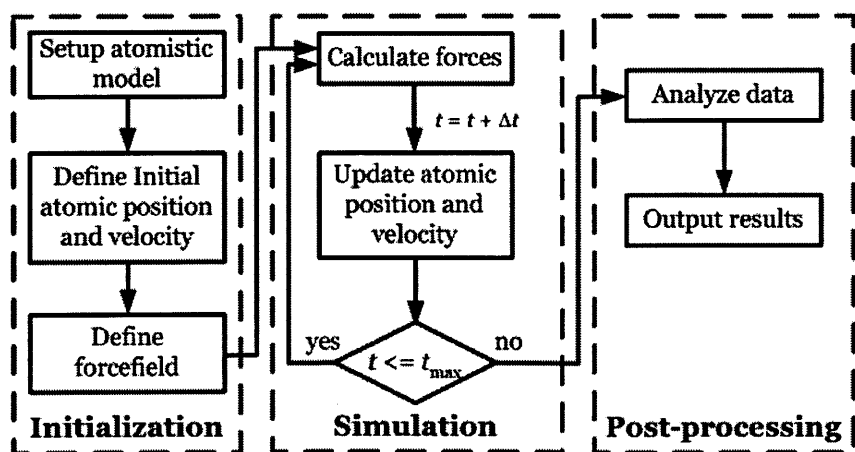
Fig 1.3 Numerical approach of molecular dynamics simulation

Molecular dynamics methods rely on Newton's second law of classical mechanics, which is given by

$$F_i = m_i a_i \qquad\qquad\qquad\qquad\qquad\qquad\qquad\qquad\qquad (1.1)$$

where F_i is the force acting on an atom, m_i is the mass of the atom, and a_i is the acceleration of the atom. The total potential energy of the system is determined by summing up the potential energy associated with all bonded and non-bonded interactions. The total potential energy (U) is expressed as $U = U_{bond} + U_{nonbond}$, where U_{bond} refers to the potential energy of the bonded atoms and $U_{nonbond}$ refers to the potential energy of the non-bonded atoms. The force (F_i) acting between a pair of atoms is determined by evaluating the negative gradient of the potential energy with respect to the separation distance (r_{ij}). This is given by $F_i = -\partial U / \partial r_{ij}$. The net force acting on an atom 'i' is calculated by summing up the interactions between atom 'i' and the surrounding atoms 'j'. Once the net force is known, the acceleration of the individual atom can be determined using Eq. (1.1) as the atomic mass has been defined previously during the construction of the atomistic model. Finally, velocities and positions can be obtained by numerical integration of the equations of motion, given that their initial values are known.

Before conducting the computational experiment, initialization and energy minimization should be carried out. Similar to the process of solving a partial differential equation in continuum mechanics, for example, initial conditions are necessary for a defined solution. Initial positions of all the atoms are defined by the coordinates of the corresponding atoms in the simulation cell. Here, simulation cell refers to a space in which simulation takes place. The total potential energy of the system (U) can be calculated as U is a function of the current atomic positions. The entire system is then subjected to a minimization of potential energy by varying the atomic position. The new atomic positions after energy minimization is used in the subsequent computational experiment as these positions refer to the most stable structure in the concerned domain. It should be mentioned that the energy minimization is carried out under absolute zero temperature which means the kinetic energy is zero as well.

After the stages of initialization and energy minimization, the constraints of the simulation are defined. The purpose of applying these constraints is to control the simulation process such that the computational experiment can be accurately performed; this is similar to the concept of applying boundary conditions in a finite element analysis. Here, the concept of "ensemble" is introduced, which is a probability measure on the set of all possible microscopic configurations that are consistent with the macroscopic state of the system. The microscopic state of a system is defined by the atomic positions and momenta which constitute the coordinates in a multidimensional imaginary space called "phase space". For a system of N particles, this space has $6N$ dimensions as each particle is associated with three position variables and three momentum variables. A single point in phase space represents the state of a system. A molecular dynamics simulation generates a collection of points in phase space as a function of time. An ensemble can be defined as a collection of points in phase space satisfying the conditions of a particular thermodynamic state. In advance of the

computation, it is necessary to fix the type of ensemble that the system is desired to perform during the computation experiment, just like when finite element analysis is being performed the boundary conditions need to be defined at the beginning of the analysis. There are three commonly used ensembles in molecular dynamics: (1) micro-canonical (*NVE*), where the number of atoms (*N*), the volume (*V*) and the energy (*E*) of the system are kept constant; (2) canonical (*NVT*) where, the number of atoms (*N*), the volume (*V*) and the temperature (*T*) of the system are constant; (3) Gibb's ensemble (*NPT*), where, the number of atoms (*N*), the pressure (*P*) and the temperature (*T*) of the system are maintained constant. Depending on the type of ensemble used, a thermostat or barostat need to be chosen for the molecular dynamics simulations. Generally, thermostats are intended to control the temperature of the system. Some of the popular barostats used to control the pressure of the system (*NPT*) are Berendsen and Nose-Hoover barostat (Allen and Tildesley 1989; Rapaport 1997). It should be mentioned that macroscopic quantities are always related to their associated microscopic quantities. For instance, temperature (*T*) is a macroscopic quantity and its associated microscopic quantity is the atomic velocity (*v*). Their relationship can be established by considering the kinetic energy stored in the system macroscopically and microscopically, and given by the following equation:

$$\frac{3}{2}k_BT = \frac{1}{N}\sum_i \frac{1}{2}m_iv_i^2 \tag{1.2}$$

where k_B is the Boltzmann constant and m_i is the mass of the ith atom. The left hand side of Eq. (1.2) describes the kinetic energy of the system from a macroscopic point of view using the quantity T, while the right hand side of Eq. (1.2) describes the kinetic energy of the system from a microscopic point of view using the quantity v.

As mentioned earlier, the fundamental equation governing the molecular motion is the Newton's second law. In the simulation process, integration of this governing equation must be carried out. There are several numerical algorithms for integrating Eq. (1.1) using finite difference methods. A relatively simple algorithm called Verlet algorithm is discussed in this thesis. Besides Verlet algotithm, the velocity-Verlet algorithm and the leapfrog-Verlet or the r-RESPA integration schemes are also widely used for implementation. The Verlet algorithm is one of the commonly used methods in molecular dynamics simulation and is described as,

$$r_i(t_0 + \Delta t) = 2r_i(t_0) - r_i(t_0 - \Delta t) + a_i(t_0)\Delta t^2 \tag{1.3}$$

where $r_i(t_0)$ is the position vector at time t_0, $r_i(t_0-\Delta t)$ is the position vector at time $t_0-\Delta t$, and $a_i(t_0)$ is the acceleration vector at time t_0. This representation assumes that the atomic positions, velocities and accelerations can be approximated by a Taylor series expansion and uses the positions and accelerations at time t_0, and the positions from previous time step at time $t_0-\Delta t$ to calculate the new positions at the next time step at time $t_0+\Delta t$. Hence, once the initial conditions in terms of atomic position in the system, as well as a well-defined force field which is used for evaluating the acceleration vector,

are obtained the subsequent motion can be calculated by this algorithm.

In order to reduce the computation time, a cut off radius (r_{cut}) is usually specified in the simulation to limit the number of interactions associated with individual atoms. A list of neighboring atoms is generated for each atom in the system so that only the interactions with those listed in the neighbor list are accounted for the force calculation. This avoids the time consuming step of calculating all possible interactions between an atom and the rest in the system for each time step.

Based on Eq. (1.3), the atomic displacements for all atoms can be calculated from a pre-set time step which is usually 1 fs (1×10^{-15} s), and the atomic velocities can be calculated accordingly. After computing the atomic displacements, velocities and accelerations for all atoms under a desirable ensemble, the material properties can be determined and interpreted through post-processing of the calculated quantities. Usually an existing post-processing program, such as the visualization tool in Visual Molecular Dynamics (VMD) ((Humphrey et al. 1996)), is used. Interpreting the molecular dynamics results usually means performing time averages of physical properties. Post-processing using appropriate theoretical models are required in order to evaluate some of the material properties from the molecular dynamics simulation result, such as the adhesive energy of a bonded system. Fig. 1.3 shows the various steps involved in a typical molecular dynamics algorithm.

1.1.3 Multiscale modeling

There are several examples where mechanical properties from molecular simulations match reasonably well with those measured experimentally at larger scales (see, for example case studies discussed by (Buehler 2008)). However, deformation mechanisms at the interface can be complicated and can change across different length scales. Besides the change of deformation mechanisms, the disparity in time- and length-scales also leads to the discrepancies between molecular dynamics simulation and the experimental results. Hence, there is a need to connect the atomistic level to macroscale such that a prediction on mechanical properties using a bottom-up approach becomes feasible.

Multiscale modeling in physics usually refers to the calculation of material properties or system behaviors on one level using information or models from different levels. On each level particular approaches are used for describing the concerned system. In general, the following levels can be distinguished, namely:

- level of quantum mechanical models which includes the information about electrons,
- level of molecular dynamics models which includes the information about individual atoms,
- level of nano or mesoscale which includes the information about groups of atoms and molecules,
- level of continuum models in which material is treated as an entire continuum.

Each level addresses a phenomenon over a specific length scale and time scale. Multiscale modeling is particularly important in integrated computational materials science and engineering since this modeling approach is capable in predicting the material properties or system behavior based on knowledge of the atomistic structure and properties of elementary processes, which are fundamentally governed by physics and chemistry.

1.2 Research Objective

The objective of this research is to develop an in-depth mechanistic understanding on the moisture affected debonding mechanism between epoxy and silica under various length scales, with the extensibility of understanding the general adhesion problem between organic and inorganic materials so as to form the basis for designing a mechanically strong interface in applications such as those found in medical field including artificial bone and tissue, as well as civil infrastructure application.

1.3 Research Approach

From the review of prior studies on strengthening and retrofitting of reinforced concrete systems using FRP composites, it can be seen that while FRP-bonded concrete system has been extensively studied, the structural performance of FRP-bonded concrete system when subjected to moisture ingress at the interface remains largely uncertain and unanswered. In particular, little is known regarding the durability of concrete/epoxy interface which has been shown as a critical region under the effect of moisture. Prior research has demonstrated that moisture effect significantly leads to the degradation in concrete composite system. In order to understand the origin of this deterioration, a fundamental understanding of the physics and chemistry at the vicinity of the interface is required. In view of the limitation of the conventional fracture mechanics concept which is unable to predict the behavior when chemical effects are involved, molecular dynamics simulation is used in this research which is capable in describing the interaction between the material system and the surrounding (water molecules in this case).

Both computational and experimental approaches are used for a comprehensive investigation on the debonding at epoxy-silica interface under the effect of moisture. Molecular dynamics simulation is used for studying the interaction among various materials (epoxy, silica and water). The result from the molecular dynamics simulation can be interpreted in a larger length scale through an appropriate multiscale modeling, which can then be compared with the experimental result. In this research, two different experimental approaches in characterizing the interfacial fracture toughness will be presented. The pros and cons of these two approaches will be described in detail in Chapters 4 and 5.

This research is motivated from the interfacial durability concerns of the strengthened and retrofitted concrete structures. It is anticipated that this work can

21

yield much needed scientific knowledge and quantitative information; and through the studies on the epoxy-silica interface, it can provide the essential knowledge as a basis for understanding the adhesion between general organic and inorganic materials that can be beneficial to many engineering related application including the fabrication of Micro-Electro-Mechanical System (MEMS) and medical devices which have a direct impact on human wellbeing.

1.4 Thesis Organization

The thesis consists of seven subsequent chapters.

Chapter 1   presents a review on the debonding of bi-layer material system, with a focus on FRP-bonded concrete system and concrete/epoxy interface. A general background on molecular dynamics simulations and multiscale modeling approach is described which form the basis of my Ph.D. research.

Chapter 2   describes the application of molecular dynamics simulation in structural engineering problems. The durability study of epoxy-silica system is used as an example for demonstration.

Chapter 3   presents the derivation of the intrinsic strength at epoxy-silica interface through the reconstruction of the free energy landscape and the worm-like-chain based fracture model.

Chapter 4   presents the experimental approach in characterizing the fracture toughness at epoxy-silica interface using nanoindentation.

Chapter 5   presents the experimental approach in characterizing the fracture toughness at epoxy-silica interface using superlayer approach.

Chapter 6   presents the multiscale analysis which links the result from molecular dynamics simulation to continuum through the implementation of cohesive zone model in the finite element analysis.

Chapter 7   summarizes the thesis and draws conclusions from the work. Areas for future investigation are also presented.

Molecular Dynamics Simulations
for Structural Engineering Problem

2.1 Molecular Dynamics Simulation of Epoxy-Silica Interface

One of the challenges in molecular dynamics simulation is to construct an atomistic model which can accurately describe the system. A known chemical formula for the concerned material is necessary in order to create a realistic atomistic model. Concrete is a heterogeneous material which is primarily composed of hydrated cement and aggregate. However, among all the constituent materials in concrete, silica, which has a well-defined chemical formula, constitutes a large proportion as aggregate, usually more than 40 percent by weight of the solid ingredients. By investigating the silica-epoxy interface in an atomistic scale, it is expected that the structural behavior of concrete-epoxy interface can also be interpreted. Note that the chemical formula for hydrated cement has also been provided in a recent study on cement chemistry (Pellenq et al. 2009).
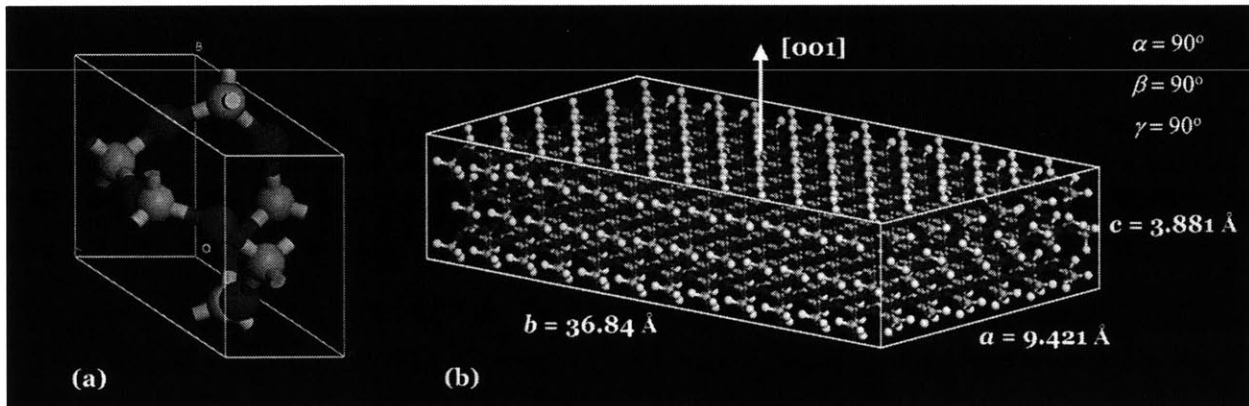
Fig 2.1 (a) Unit cell of SiO_2, (b) Atomistic model of SiO_2 substrate
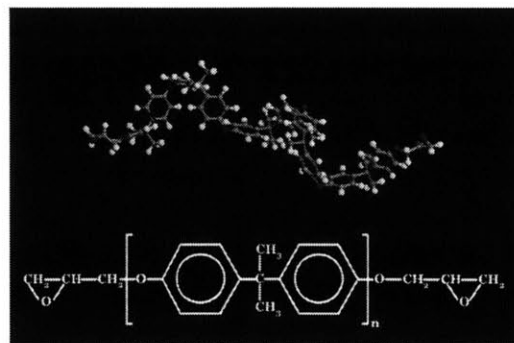
Fig 2.2 Molecular structure and chemical formula of DGEBA with n=5

In our study, the atomistic model consists of crystalline silica (SiO_2) and a single chain of epoxy. Fig. 2.1 shows the atomistic model of the crystalline silica used in molecular dynamics simulation. A silica block was constructed from a unit cell of crystalline silica shown in Fig. 2.1(a). By repeating the unit cell in x-, y-, and z-directions, a bulk silica crystal can be obtained as shown in Fig. 2.1(b). The bulk silica crystal is then cleaved in such a way that the normal vector of the cleaved surface (to be in contact with epoxy) is at [001] direction. All the atoms in the crystalline silica are covalently bonded by a harmonic bond potential. Non-periodic boundary conditions are applied on the SiO_2 substrate which means that hydrogen atoms are used for bond termination at the free surface of the SiO_2 substrate as shown in Fig. 2.1b. The entire SiO_2 substrate has dimensions a = 9.421Å, b = 36.84 Å, c = 3.881 Å, with $\alpha = 90°$, $\beta = 90°$, $\gamma = 90°$ and consists of 2540 atoms. The epoxy employed in this thesis is diglycidyl ether of bisphenol A (DGEBA) and its molecular structure is shown in Fig. 2.2. For simplification, there is no hardener included in the atomistic model. Only one chain of DGEBA, with five repeating units (n=5 as shown in Fig. 2.2), is used in this model. In the case describing a wet environment, a water box is created which embraced the SiO_2-DGEBA system entirely. Fig. 2.3 shows the models for both dry (Fig. 2.3a) and wet (Fig. 2.3b) cases. Partial charges of all atoms in the simulation cell are calculated by the charge equilibrium (QEq) method (Rappe and Goddard 1991).
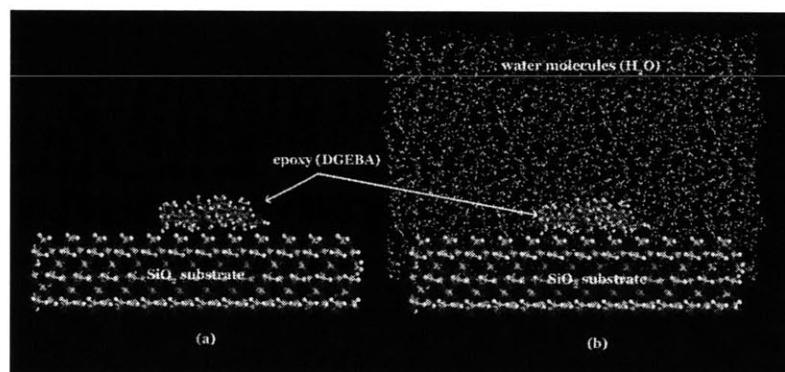
Fig 2.3 (a) Simulation model for dry case, (b) Simulation model for wet case

Interaction between dissimilar molecular entities such as polymer and silica is formulated through the definition of force field. This is similar to the concept of constitutive model used in FEM to formulate the material behavior. For different atoms, the corresponding parameters adopted in the chosen force field are obtained either by experimental methods such as nuclear magnetic resonance (NMR) spectroscopy or from rigorous ab initio quantum mechanics calculations. Some of the commonly used force fields are Amber (Weiner et al. 1984; Weiner et al. 1986), DREIDING (Sotomayor and Schulten 2007), CHARMM (Brooks et al. 1983; Momany and Rone 1992), consistent force field (CFF91) (Hagler and Ewig 1994; Hwang et al. 1994; Maple et al. 1994) and consistent valence force field (CVFF) (Dauber-Osguthorpe et al. 1988; Maple et al. 1988). These force fields were optimized and well tested for simulating different proteins and polymers. Epoxy is a typical polymer in which the above mentioned force fields are

24

applicable. Meanwhile, efforts have been made to parameterize the CVFF for inorganic materials including silica as well as the interface between silica and epoxy. Therefore, CVFF is applied for studying the interaction between silica and epoxy under both dry and wet condition.

The total potential function in CVFF is represented by the superposition of valance and non-bonded interactions. The valance terms are the bonded interactions consisting of bond stretch, bond angle bending, dihedral angle torsion terms, while non-bonded interactions consist of Van der Waals and electrostatic terms. Fig. 2.4 shows the potential terms adopted in the CVFF.

Bond Stretch   **Bond Angle Bending**

Dihedral Angle Torsion
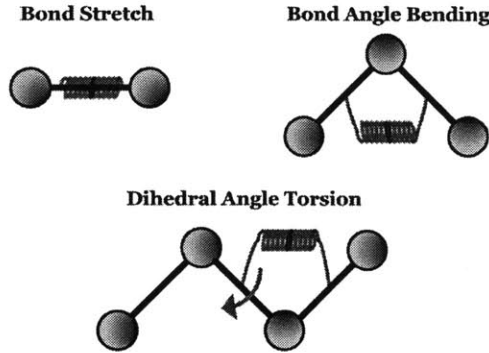
Fig 2.4 Major potential terms in the CVFF used here, applied to describe the silica substrate, epoxy chain and water

In this simulation, the CVFF potential energy function given by (Maple et al. 1988) is used. This is a reduced form of CVFF potential function using harmonic form for bond stretching term, which is useful for simulating structures consisting of organic and inorganic phases (Ritschla et al. 2002). In this reduced form, the CVFF potential function is described as,

$$E = \sum_{b} K_{b}(b - b_{o})^{2} + \sum_{\theta} K_{\theta}(\theta - \theta_{o})^{2} + \sum_{l} K_{\phi}(1 + s \cos n\phi)$$
$$+ \sum_{i,j} \varepsilon_{ij} \left[\left(\frac{r_{ij}^{*}}{r_{ij}} \right)^{12} - \left(\frac{r_{ij}^{*}}{r_{ij}} \right)^{6} \right] + \sum_{i,j} \frac{q_{i}q_{j}}{\varepsilon r_{ij}}$$

(2.1)

where K_{b}, K_{θ}, K_{ϕ} are force constants, b_{o}, θ_{o} and s are equilibrium bond length, equilibrium bond angle and dihedral angle, respectively; b and θ are bond length and bond angle, r_{ij} is the distance between the ith and j^{th} particles with charges q_{i} and q_{j}, respectively. The terms ε_{ij} and r_{ij}^{*} determine the minimum and zero values of the van der Waals terms, respectively. The CVFF has been parameterized against a wide range of experimental observables for amino acids, water, and a variety of other functional groups, as well as some inorganic materials including silica (details and parameters described in (Maple et al. 1988)). The parameters of the force field used in this thesis are included in the Appendix A. In this thesis, the CVFF water potential is adopted, a three-site model with internal geometry corresponding to the gas-phase experimental structure (Lau et al. 1994). Flexibility of water molecules is modeled through the use of

harmonic bond stretching and angle bending potentials. With the exception of the hydrogen atom size, the non-bonded parameters are comparable to those of simple point charge (SPC) model. An important aspect of choosing an interaction function for the epoxy-silica system including explicit water molecules is the consistency between different parts of the interatomic function, for example the epoxy-silica, epoxy-solvent, silica-solvent and solvent-solvent terms. When combining a water model with a force field used in the epoxy-silica system, the definition of the solvent-related interaction requires special attention. In most cases, this interaction is defined using the so-called combination rules (Gunsteren et al. 1994). If epoxy-silica system and solvent force fields are of different types, the application of combination rules may lead to an imbalance between epoxy-silica, epoxy-solvent, silica-solvent, and solvent-solvent interactions.

Initiation and energy minimization of the simulation cell containing silica and epoxy (and water in the wet condition) were then performed. After constructing the atomistic models for both dry and wet cases with the clear definition of the model geometry and the interaction among atoms, the following computation experiments were carried out under NVT ensemble at 300 K in an existing molecular dynamics code called LAMMPS (Plimpton 1995). A sample script of atom definition in LAMMPS can be found in Appendix B.

Computational peel and shear tests on the silica-epoxy system were performed through steered molecular dynamics (SMD) by systematically varying the pulling velocity over four orders of magnitude, ranging from 2 to 1000 m/s. The basic idea of SMD is to apply an external force to one or a group of atoms, while keeping another group of atoms fixed and study the behavior of the molecule. Essentially, the SMD approach applies a moving spring force under constant velocity (i.e. the force is not constant). The SMD approach mimics an atomic force microscope (AFM) experiment. In our simulation, only the silica substrate is fixed. All atoms in water and silica are allowed to move freely. The end carbon atom in the epoxy was connected to a virtual spring in the entire process of SMD. The pulling direction to this carbon atom is normal away from the silica-epoxy interface under peeling condition and parallel with the interface under shear loading. Fig. 2.5 describes the peel and shear computational experiments schematically.
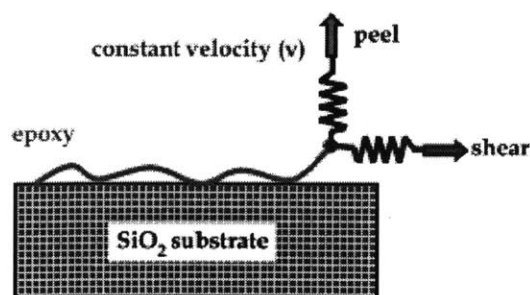
Fig 2.5 Schematic diagram of the computational experiments for both peel and shear loading

As discussed previously, a suitable model is required in quantifying certain mechanical property. Here, the applicability of the model as done previously for investigating the adhesion between protein structures is extended (Ackbarow et al. 2007). It is based on the conventional Bell model (Bell 1978) which was developed and applied to the study on cell adhesion at larger scales. Similar to earlier work (Ackbarow et al. 2007) here Bell's approach is applied so that simulation at various pulling speeds can be used to gain information on the free energy landscape of the bi-material system, postulating a phenomenological theory in explaining the competing process due to the mechanical induced stabilities. Through the Bell analysis, the energy barrier E_b and the distance between the equilibrated state and the transition state x_b (see Fig. 2.6) can be found. In the modified Bell model (Ackbarow et al. 2007), a relationship between the pulling speed and the bond associated properties can be written as:

$$v = v_0 \exp\left(\frac{f \cdot x_b}{k_B T}\right) \tag{2.2}$$

where f is the external applied force, k_B is the Boltzmann constant, T is the temperature, with v_0 as the natural bond breaking speed, which is defined as

$$v_0 = \omega_0 \cdot x_b \cdot \exp\left(-\frac{E_b}{k_B T}\right) \tag{2.3}$$

Substituting Eq. (2.3) into Eq. (2.2) and rearranging the equation with f as the subject,

$$f = \left(\frac{k_B T}{x_b}\right) \ln v - \frac{k_B T \ln v_0}{x_b} = A \cdot \ln v + B \tag{2.4}$$

where $A = k_B T / x_b$ and $B = k_B T \cdot \ln v_0 / x_b$. Eq. (2.4) predicts that the applied force depends logarithmically on the pulling speed in a non-equilibrated system. It should be mentioned that the maximum force recorded through the whole simulation process under the constant velocity was taken as the value of f for the Bell analysis. By plotting f against ln(v), the E_b and x_b for this system can be quantified through the slope of y-intercept of the curve. The resulting value of E_b represents the adhesive energy between silica and epoxy in an atomistic scale.
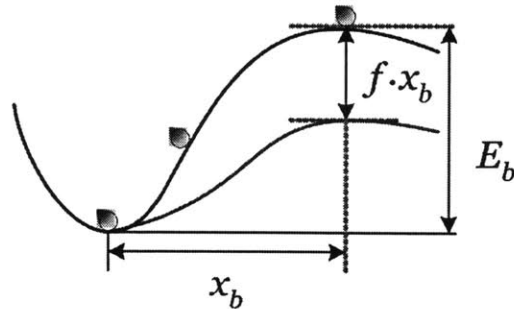
Fig 2.6 Schematic diagram of the energy profile

The maximum force f is plotted as a function of the pulling speed in Fig. 2.7a and Fig. 2.7b for the peel case under dry and wet conditions, respectively. Fig. 2.7c and Fig. 2.7d show the maximum force f for the shear case as a function of the pulling speed under dry and wet conditions, respectively. It should be mentioned that v^* is for the normalization purpose which equals 1 m/s. By fitting the extended Bell theory to the molecular dynamics results of the peel case, $E_b = 9.10$ kcal/mol and $x_b = 0.69$ Å for the dry condition are obtained. In the wet case, $E_b = 7.74$ kcal/mol and $x_b = 0.16$ Å. Similar values are found for the shear case. For the dry case, the obtained values are $E_b = 7.06$ kcal/mol and $x_b = 0.48$ Å. In the wet case, $E_b = 5.99$ kcal/mol and $x_b = 0.11$ Å. These results are summarized in Fig. 2.8. The decrease in the adhesive energy E_b from 9.10 to 7.74 kcal/mol in the peel case and from 7.06 to 5.99 kcal/mol in the shear case, indicates that the adhesive strength between silica and epoxy is weakened in the presence of water with 14.9% reduction in the peel case and 15.2% reduction in the shear case. A close examination of the molecular dynamics simulation process under wet condition shows that some water molecules can seep into the gap between silica and epoxy as shown in Fig. 2.9. Hence, the interaction between silica and epoxy is interfered by the presence of these water molecules, causing a change in the epoxy-silica interface from a bonded stage to a detached stage, which results in a reduction of energy barrier. The trend of deterioration is consistent with the results from meso-scale fracture based studies of the concrete-epoxy specimens (Lau and Büyüköztürk 2010) and FRP-bonded concrete specimens (Au and Büyüköztürk 2006b). In these papers, it is reported that there is a substantial decrease in the interfacial fracture toughness of concrete-epoxy system under prolonged moisture, which is accompanied with a shift of failure mode from material decohesion to interface separation. Both the experimental and simulation works show the reduction in the energy required for debonding in the presence of water. The molecular dynamics result validates our hypothesis that the adhesive strength of the interface is weakened due to interaction between epoxy and water and provides an atomistic-based view on the mechanical properties of the interface.

(a) — $y = 54.46x + 560.12$, $R^2 = 0.9171$

(b) — $y = 239.08x + 2,213.68$, $R^2 = 0.8288$

(c) — $y = 88.55x + 525.51$, $R^2 = 0.7964$

(d) — $y = 341.80x + 2,181.11$, $R^2 = 0.8922$
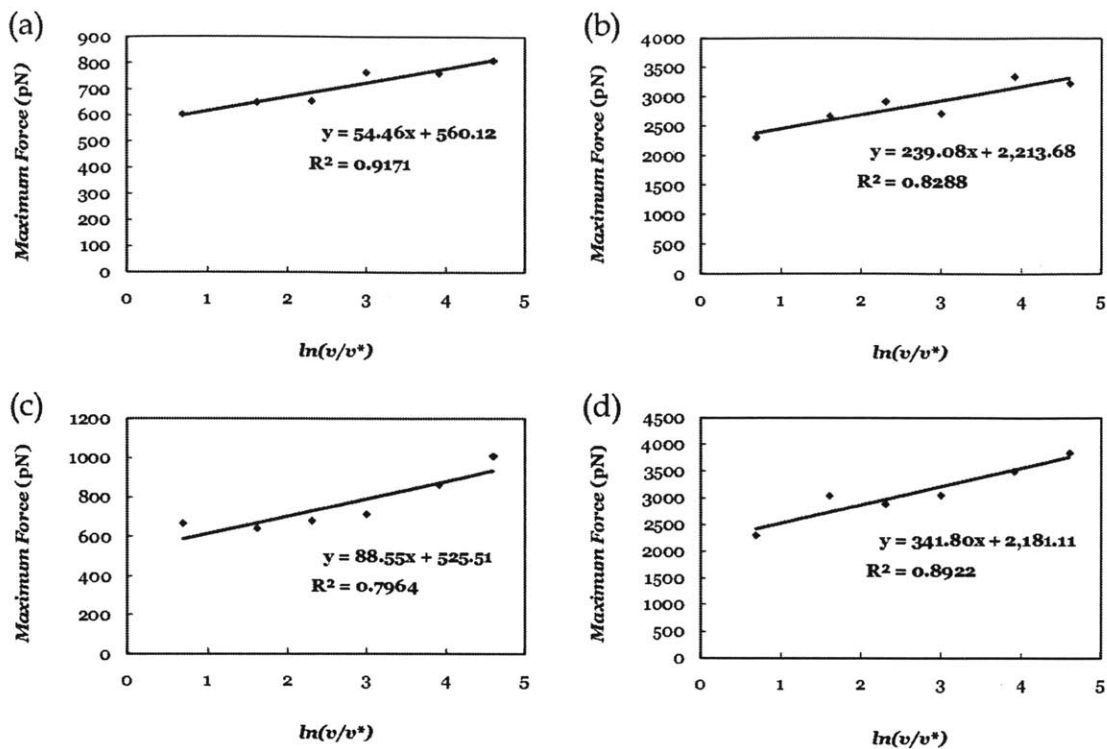
Fig 2.7 Maximum force as a function of varying pulling speed under (a) peel and dry conditions, (b) peel and wet conditions, (c) shear and dry conditions, and (d) shear and wet conditions.
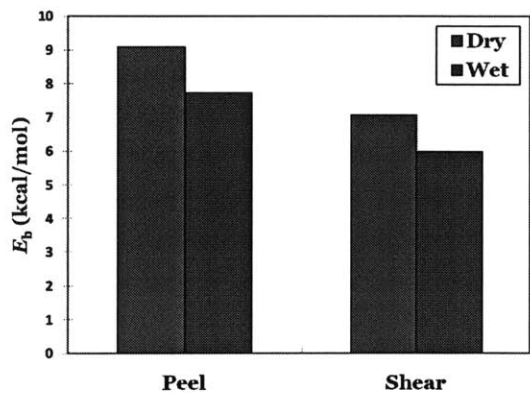
Fig 2.8 Summary of the difference between peel and shear loading cases under both dry and wet conditions. This result implies that adhesion between silica and epoxy is weakened by about 15% in the presence of water.

29
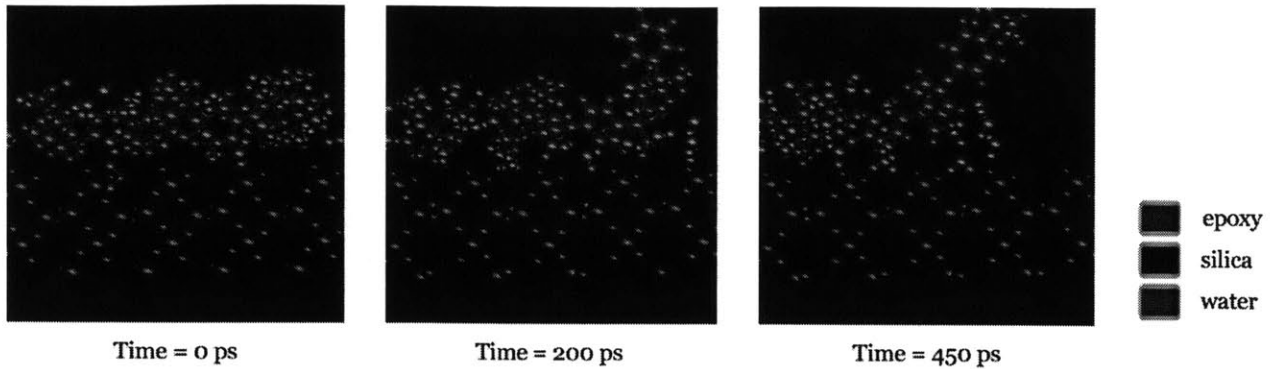
Fig 2.9 Snapshots of the MD simulation in wet condition

2.2 Summary Comments

Research on molecular dynamics simulation contributes to our understanding of the interaction between structural materials and environment at an atomistic scale providing a bottom-up approach to structural engineering. Especially, molecular dynamics is useful for studying the fracture related problems which can be intrinsically described in this length scale. The work reported in this chapter has demonstrated that solution from molecular dynamics simulation can give us an insight on the failure mechanism of layered material system under moisture effect. The bonded structural system consisting of silica and epoxy was investigated and it was found that the weakening of the adhesive strength between silica and epoxy can be quantified by the decrease of the energy barrier E_b. However, the results from standard molecular dynamics simulation only describe the considered system correctly on limited length and time scales. A bridging technique which links the nano-scale and macro-scale together is required. Research work in this area is still at infant stage, and in particular applying the method to important problems in the field that often span many structural scales. It is anticipated that the long term impact of my Ph.D. work will be in extending our ability to perform structural engineering at the macro-scale, as related to the local phenomena that is modeled at the nano-scale. In the following chapter, adhesive strength of the interface will be quantified through the reconstruction of the free energy profile of the bonded system. It is believed that a better understanding on the debonding mechanism can be obtained through the free energy profile.

Intrinsic Strength of Epoxy-Silica Interface

3.1 Introduction

Organic-inorganic interface exists in many material systems that can be found broadly in natural and synthetic materials, such as mineral-protein interfaces seen in bone and epoxy-silica interfaces found in concrete buildings and bridges. The study of such interfaces has been the subject of investigations in various research fields, including biomechanical engineering, electrical engineering, materials science and structural engineering because of its biological, scientific and technological significance. Based on prior research on interfacial properties of bonded systems (Au and Büyüköztürk 2006b; Sharratt et al. 2007; Lau and Büyüköztürk 2010; Tuakta and Büyüköztürk 2011b), it is known that the structural and mechanical integrity of the interface is highly affected by the physical and/or chemical interactions between the interface and the surrounding region at the nanoscale. With the development of molecular dynamics as a powerful method to describe the mechanics of interfaces from fundamental chemical principles upwards, information about the mechanical behavior of the interfacial region through the observation of atomic and molecular motions can be acquired (Buehler 2008; Büyüköztürk et al. 2011). In particular, the integrity of the bonded material system can be studied from a fundamental perspective by monitoring the interactions and the deformation mechanism between two materials along the interfacial region at a molecular level. More recently, there are several examples where mechanical properties from molecular simulations match reasonably well with those measured experimentally at larger scales. However, deformation mechanisms at the interface can be complicated and can change across different length scales. Besides the change of deformation mechanisms, the disparity in time- and length-scales also leads to the discrepancies between molecular dynamics simulation and the experimental results. Hence, there is a need to connect the atomistic level to macroscale such that a prediction on mechanical properties using a bottom-up approach becomes feasible.

The underlying principle of this work is to understand the adhesion problem between an organic and an inorganic material, using epoxy-silica system as a simple example. Epoxy, bonded with silica in many engineering applications, is chosen as the representative of an organic material because of its extensive application as an adhesive. Also, its chain structure with cross-links can be found readily in many other polymers. Silica is commonly found material in nature in the form of sand or quartz, as well as in the cell walls of diatoms and is the most abundant mineral in the Earth's crust (Korzhinsky et al. 1995) and is thus a good model for a mineral. The epoxy-silica interface serves as a representative system for an interface dominated by relatively weak and non-covalent chemical interactions. In many cases, the interatomic and intermolecular bonds at organic-inorganic interfaces are of non-covalent nature. The

focus of this study is to study the effect of the nonbonded interactions (van der Waals forces and Coulombic interactions) between polymer chains and a mineral surface, incorporating the effect of the spacing between polymer chains towards the structural behavior of the interface at the macroscale. Also, the proposed model should be able to describe the interfacial debonding mechanics, which is dominated by the sliding of the polymer chains on the substrate. With these considerations, this model is constructed at the nanoscale (~2-3 nm) such that the adhesion between a small piece of crystalline silica and a single polymer chain can be carefully investigated. The effect of the spacing between polymer chains is studied at a larger length scale in which each polymer chain is connected through cross-linking, using a simplified symmetrical grid system with a spacing "s" as shown in Fig. 3.1. Even though this simplified model may not be able to describe all details in the vicinity of the interface (e.g. the variation of the partial charges, kinematic barriers and changes during debonding, or alternative deformation mechanisms at larger scales), this model provides a basic description of interfacial properties of this system.
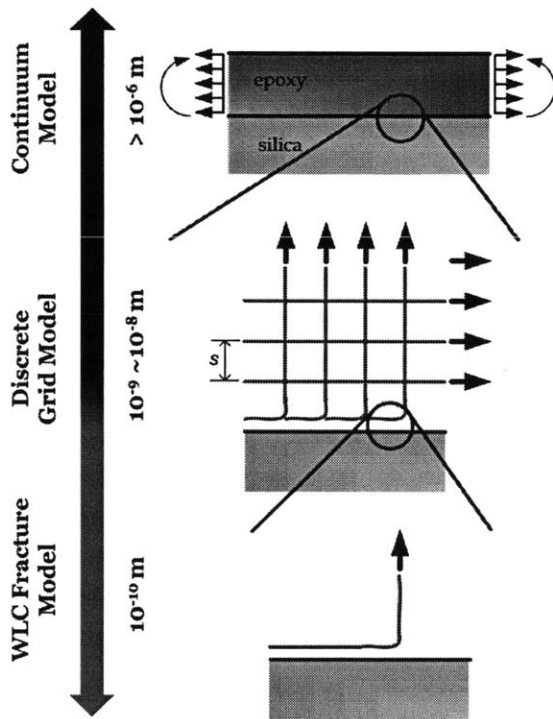
Fig 3.1 The continuum epoxy-silica interface can be represented by a discrete grid model when the length scale goes down to nano-scale. The adhesion between each epoxy chain and the silica substrate can be represented by the WLC fracture model. The proposed multiscale analysis is to deliver the mechanical properties derived in the WLC fracture model to the continuum macroscale through the implementation of a finite element analysis.

In what follows, the approach of developing this model starting from the atomistic scale will be demonstrated. The result from the molecular dynamics simulation will be interpreted as intrinsic strength of an individual epoxy chain by applying the rubber-like elasticity, which can then be converted to continuum interfacial properties through the use of cohesive elements in finite element modeling. The prediction at the macroscale will then be conducted through finite element model and a comparison between our prediction and existing experimental results will be made.

32

3.2 Materials and Methods

The multiscale approach used here involves a systematic determination of interfacial parameters, starting from the surface energy, a material property that characterizes the energy required to create new surface. The surface energy is characterized by deriving a free energy profile of the bonded system that describes the free energy change from an attached stage referring to the lowest free energy state to a detached stage when the separation between two materials is larger than 10 Å, which is the cutoff distance of the pair potential (the free energy is the energy that is convertible to work) used in the molecular dynamics simulation. The difference in the free energy between the attached and detached stages, normalized by an associated area of molecular attachment (computed as the surface area of epoxy chain projected onto the silica substrate), yields an estimate of the upper bound of the surface energy between epoxy and silica. The identification of the free energy surface is achieved using the metadynamics method (Laio and Parrinello 2002; Laio and Gervasio 2008).

After obtaining the surface energy between epoxy and silica from molecular dynamics simulation, a worm-like-chain (WLC) based fracture model (Keten and Buehler 2008) is adopted to estimate the intrinsic strength at the interface. The WLC fracture model is based on the rubber elasticity concept and is used to describe the debonding mechanism at the molecular level as a molecular peeling process. The intrinsic strength at the epoxy-silica interface derived from the WLC fracture model is then used to determine the macroscale material interfacial behavior through the implementation of a cohesive zone model (CZM), which describes the debonding mechanics through the traction-separation relation. By using cohesive elements in finite element modeling, the behavior is represented at the continuum level to describe the macroscopic debonding mechanism at the interface. This prediction is eventually compared with existing experimental data for demonstrating the applicability of the model in predicting the structural behavior in a macroscale based on the molecular dynamics simulation results.

The atomistic model consists of a slab of crystalline silica (SiO_2) and a single chain of epoxy which is similar to that in Chapter 2. Fig. 3.2 shows the atomistic model of the epoxy-silica system used here. The entire SiO_2 substrate has dimensions $a = 42.2$ Å, $b = 42.2$ Å, $c = 25.1$ Å, with $\alpha = 90°$, $\beta = 90°$, $\gamma = 90°$ and consists of 4,749 atoms. The epoxy employed in this study is diglycidyl ether of bisphenol A (DGEBA) with only one repeating unit. Typically, non-reactive force fields are fitted to thermodynamic properties and not to kinetic barriers. However, based on the prior work on epoxy-silica system shown in Chapter 2 in which CVFF was used to govern the interaction between epoxy and silica, the applicability of using CVFF with the Bell model to quantify a reasonable energy barrier for the adhesion problem has been demonstrated (Büyüköztürk et al. 2011). It is emphasized that the breaking of bonds of interest here are weak bonds, not covalent, which can be described with CVFF. By using the non-reactive force field CVFF, it is understood that the partial charges in the system do not change in the entire molecular dynamics simulation process. Although the partial

33

charges along the interface may not be accurately described in the entire debonding process by using CVFF, the case demonstrated in this chapter is based on the prior work shown in Chapter 2. Partial charges of all atoms in the simulation cell are calculated by the charge equilibrium (QEq) method (Rappe and Goddard 1991). It has been demonstrated that the charge distributions from QEq lead to good agreement with experimental data and *ab initio* calculations (Rappe and Goddard 1991). The QEq approach uses only readily available experimental data (ionization potential, electron affinity and atomic radius) and thus can be applied to any combination of atoms. Based on the prior work on epoxy-silica system using the CVFF and the similar description of nonbonded interaction among various non-reactive force fields, it is decided to choose CVFF for studying the adhesion between silica and epoxy and extended the application of CVFF to include epoxy-silica interaction as this is not included in the original version. Besides for modeling the interaction between epoxy and silica, CVFF is also used to describe SiO$_2$. The properties that are correctly captured by CVFF are the elastic constants, including the Young's modulus. It should be mentioned that the reduced form of CVFF potential function using harmonic form for bond stretching term is used which has been shown in Eq. (2.1) (Ritschla et al. 2002).
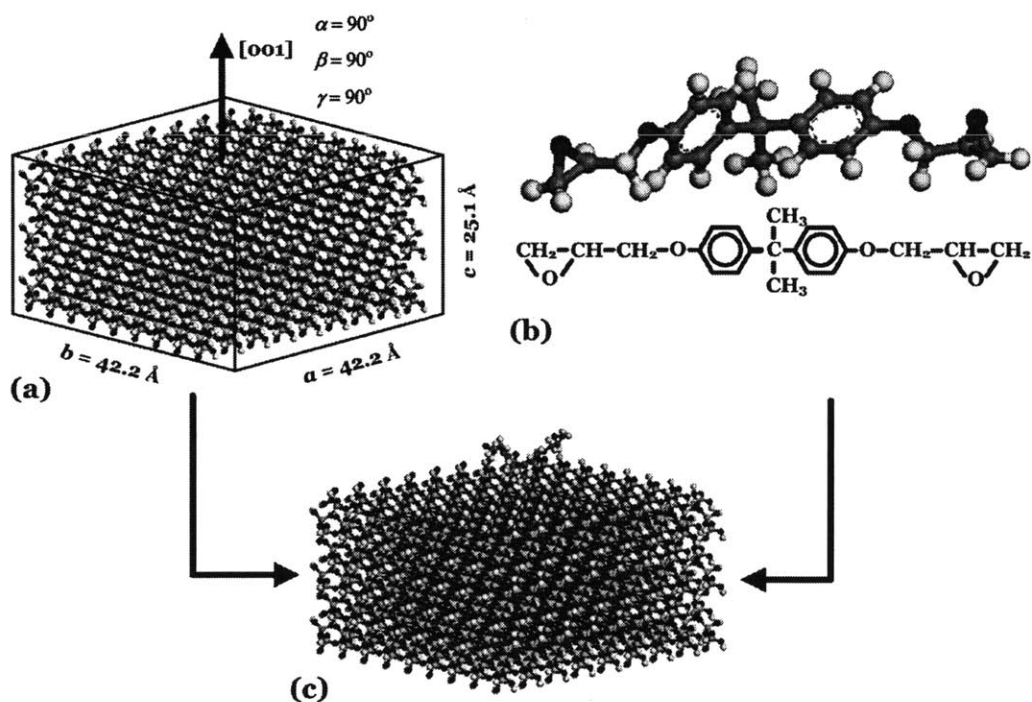
Fig 3.2 (a) Atomistic model of the silica substrate in which the surface is cleaved in [0 0 1] crystallographic plane, (b) the epoxy chain with only one repeating unit, (c) the epoxy chain is moved manually onto the silica substrate before carrying out the simulation.

3.2.1 Metadynamics analysis for adhesion energy of a single epoxy chain

The free energy surface (FES) of the epoxy-silica system from an attached stage to a detached stage is reconstructed by the metadynamics approach (Laio and Parrinello

2002; Laio and Gervasio 2008). This is a powerful algorithm that can be used for both reconstructing the free energy and for accelerating rare events in the system. The principle of this algorithm can be qualitatively understood by filling the actual FES by a series of Gaussians. By keeping track on the filled Gaussians, the FES can be calculated. Metadynamics requires the identification of a set of collective variables (CVs) which are assumed to be able to describe the process of interest. The dynamics in the space of the chosen CVs is enhanced by a history-dependent potential constructed as a sum of Gaussians centered along the trajectory followed by the CVs. In metadynamics, the sum of Gaussians is exploited to reconstruct iteratively an estimator of the free energy. The Gaussian potential (V_G) acting on the system at time t is given by

$$V_G\left(S(x),t\right)=\omega\sum_{\substack{t'=\tau_G,2\tau_G,\cdots\\t'<t}}\exp\left(-\frac{\left(S(x)-s(t')\right)^2}{2\delta s^2}\right),$$ (3.1)

where $s(t) = S(x(t))$ is the value taken by the CV at time t. Three parameters are introduced in the definition of the V_G, namely the Gaussian height (ω), the Gaussian width (δs) and the frequency (τ_G) at which the Gaussians are added. These parameters influence the accuracy and efficiency of the free energy reconstruction. Qualitatively, they define the amount of external energy being added to the actual FES. If the Gaussians are large, the FES will be explored in a fast pace, but the reconstructed profile will be affected by larger errors. Instead, if the Gaussians are small or are placed infrequently, the reconstruction will be accurate, but the trade-off is to take a longer time for achieving a uniform sampling. Fig. 3.3 demonstrates the metadynamics approach graphically. After careful adjustments of these parameters, it is found that a Gaussian of height (ω) = 0.005 and width (δs) = 0.35 added every 100 steps is good in reconstructing a reliable FES of our system.

Besides the parameters in Gaussian potential, the reliability of metadynamics is strongly influenced by the choice of the CVs. Ideally, the CVs should be chosen such that they can clearly distinguish, as a special interest to us, the initial stage from the final stage. Meanwhile, they should describe all slow events that are relevant to the process of interest and the number of CVs should not be too large in order to avoid a long time for filling the FES. In our case, the distance between the center of mass (CM) of the epoxy chain and the silica surface is chosen to be the CV for this study as shown in Fig. 3.4(a). All metadynamics calculations are performed by using the PLUMED plug-in package (Bonomi et al. 2009). The results are then interpreted by plotting with different simulation time until convergence is obtained (ensured when reconstructed free energy profiles overlap with each other). Sample input scripts for LAMMPS and PLUMED can be found in Appendix C and Appendix D respectively.
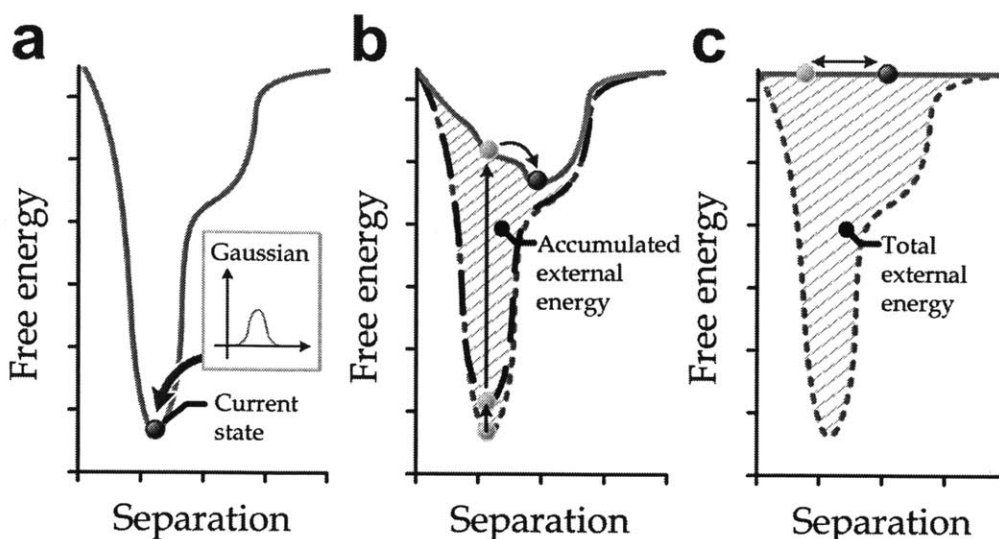
Fig 3.3 (a) Gaussians are continuously added to the molecular system, (b) Because of the additional external energy source, the free energy profile of the system varies during the simulation process, (c) At the end of the procedure, the system can translate from one state to another freely since the free energies at different states are roughly the same. The actual free energy profile can then be reconstructed by the profile of external energy applied during the process.

The surface energy is obtained by dividing the free energy barrier (E_b) between the attached and detached stages by the entire contour length of the epoxy chain (L_o), *i.e.*

$$\gamma_s = \frac{E_b}{L_o}.$$

(3.2)
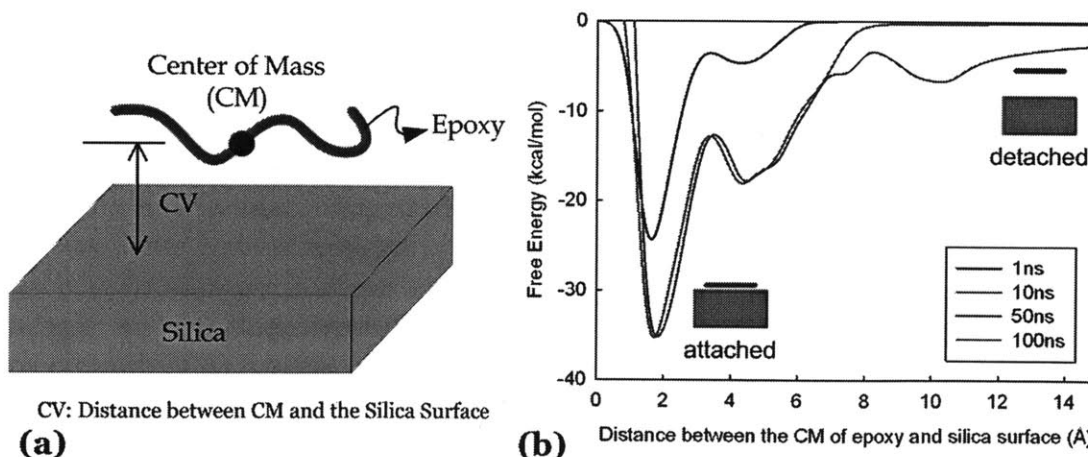
Fig 3.4 (a) Schematic diagram showing the definition of CV in epoxy-silica system, (b) It shows the convergence of the free energy surface in the epoxy-silica-system under different processing times. The surface energy of the system can be calculated by taken the energy difference between the attached and detached stages.

3.2.2 Worm-like-chain (WLC) based fracture model

The method described in Section 3.2 gives an estimate of the adhesion energy of the epoxy chain at the surface. In this calculation the debonding mechanism of the bonded system is assumed to be homogenous. This mechanism, however, will likely not represent the detachment mechanism when a single epoxy chain is separated from the silica surface by mechanical load acting at the far end of the epoxy chain (see schematic in Fig. 3.1 for the boundary conditions at different scales). To address this issue, the consideration is extended by invoking a WLC based fracture model that allows us to predict the force needed to detach an epoxy chain from the substrate. The intrinsic strength can in principle be found by applying a force at the end of the epoxy chain. However, the result predicted through this method is likely higher than the actual strength, and the discrepancy depends on the asymptotic nature between rupture force and the pulling speed for the material system at hand. The dependence on the pulling speed in molecular dynamics studies has been widely investigated in the literature (Ackbarow et al. 2007; Sotomayor and Schulten 2007; Büyüköztürk et al. 2011). In order to interpret the result from atomistic simulation with the experimental data, it is necessary to overcome the difference in time scale between atomistic simulations and experiment such that the intrinsic strength limit, which corresponds to the limit of zero pulling speed, can be evaluated. Based on the previous work shown in Chapter 2, the intrinsic strength limit of hydrogen-bond assemblies in protein has been investigated (Keten and Buehler 2008). Here, their work is extended such that the intrinsic strength at the organic-inorganic interface governed by non-directional and continuous interactions can be quantified. A simple model as shown in Fig. 3.5 is used to describe the rupture behavior of a single epoxy chain attached on a silica substrate.

A combination of WLC model (Marko and Siggia 1995) and a fracture approach (Keten and Buehler 2008) is an appropriate model that suits our purpose. Epoxy is a polymer and its elasticity is primarily due to entropic rather than energetic effects at low to intermediate force levels. This model is one of the most widely used expressions to predict the entropic elasticity of polymer chains, and has been adopted here as the elastic description of the epoxy backbone. Previous studies provide substantial evidence that this model is a good model for the behavior of individual, unconstrained polymer chains (Rief et al. 1997; Oberhauser et al. 1998; Rief et al. 1998; Fisher et al. 1999; Bustamante et al. 2000). By adopting the WLC model, the energy release rate (G) is obtained through an expression of how the free energy changes as a function of detachment of the polymer from the substrate; and at the stage just before the onset of rupture, the critical energy release rate (G_c) is equal to the surface energy between epoxy and silica (γ_s; determined as describe above), and hence

$$G_c(\alpha) = \frac{k_B T}{4\xi_p}[\alpha(1-\alpha)^{-2} - (1-\alpha)^{-1} + 2\alpha^2 + 1] = \gamma_s \tag{3.3}$$

The rupture force F_{break} is then given as a function of α_{cr} and the persistence length (ξ_p), where α_{cr} is the ratio between the end-to-end chain length (x) and the contour length (λ)

at the moment of fracture obtained from the condition:

$$G_c(\alpha_{cr}) = \gamma_s \tag{3.4}$$

The intrinsic strength (F_{break}) of the epoxy-silica interface can then be expressed as:

$$F_{break} = \frac{k_B T}{4\xi_p}[(1 - \alpha_{cr})^{-2} + 4\alpha_{cr} - 1] \tag{3.5}$$
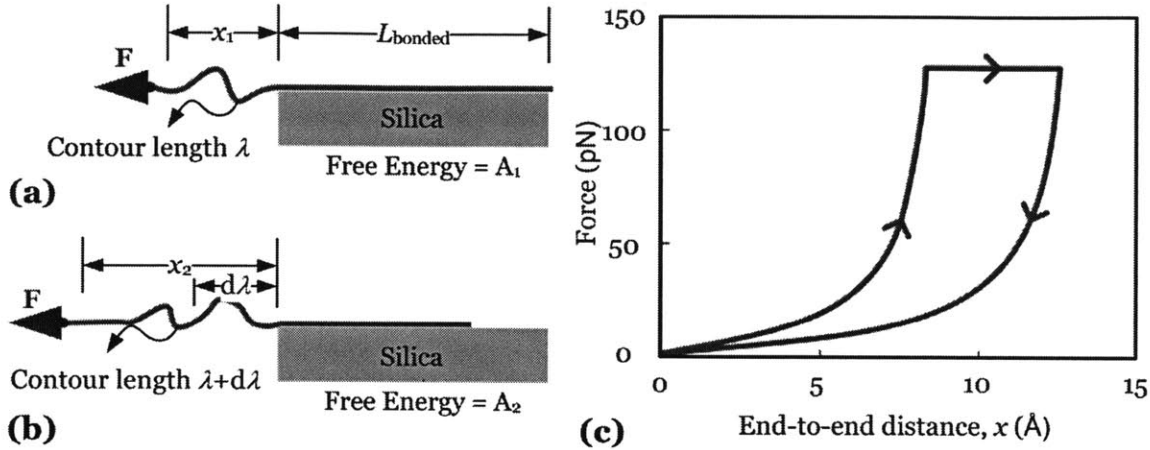
Fig 3.5 (a) Single chain epoxy with a length L_{bonded} bonded with the silica substrate by a continuous van der Waals and Columbic interactions is strained at the free end under a constant force F, (b) At the onset of rupture, the contour length increases due to the detachment of a piece of chain, (c) Qualitative description of the force-displacement behavior before and after debonding, with an illustration of the dissipation energy. It is noted that the model does not require the applied force to be in the shear direction as shown in panels (a) and (b). In fact, it is valid for other loading angles (shear, tear, or mixed) as we only consider the free energy change in the overhang of the epoxy chain.

3.2.3 Upscaling

The surface energy (γ_s) and the nanoscale asymptotic force limit (F_{break}) presented above can be used to quantify the relationship between the stress and the crack tip opening displacement at the interface, which acts as a bridge between the discrete atomistic model and the finite element model. The continuum epoxy-silica bi-layer system can be visualized as a series of cross-linked polymer chains connected to the silica surface through the adhesion at the chain tail. Here, the crosslink network of the polymer chains is simplified by imagining that it is a regular grid system with a grid size spacing equal s as shown in Fig. 3.1. For each chain adhered to the silica surface, we can treat it as an individual WLC fracture model such that the mechanical properties of the single chain system can be evaluated. In order to predict the structural behavior of the bonded system in a larger length scale, these evaluated mechanical properties based on the single chain system are incorporated in the finite element model of epoxy-silica interface using the cohesive elements. These elements are formulated based on the concept of cohesive zone model (CZM) which was originally proposed by Dugdale

38

(Dugdale 1960) and Barenblatt (Barenblatt 1962). CZM was first introduced as a technique to study fracture or void nucleation in quasi-brittle materials such as ceramic and concrete. CZM collectively describes all the mechanisms related to fracture, such as plastic deformation, void growth, and crack coalescence, in the process zone ahead of the crack tip; its structural behavior is governed by a given traction-separation relation. Conventionally, such a relation is calibrated with results from micromechanical modeling or experiments on fracture specimens of various configurations (Karbhari and Engineer 1996; Elices et al. 2002; Qiao and Xu 2004; Au and Büyüköztürk 2006b; Frigione et al. 2006; Ouyang and Guoqiang 2009). An alternative approach is provided for estimating the important parameters in defining a traction-separation relation based on the WLC fracture model from a nanoscale point of view that enables us to predict the global structural behavior of epoxy-silica interface (at the macroscale) using an appropriate finite element model.

The parameters characterizing the traction-separation relationship include the initial stiffness, damage initiation threshold, and damage evolution properties. In general, the fracture toughness of a material system, which defines the damage evolution, can be measured experimentally in a reliable manner. However, the peak traction in the traction-separation relation and the initial stiffness of the cohesive element are usually hard to be determined and are adjusted by controlling the mesh density in the finite element model. The WLC fracture model with parameters fed from the metadynamics approach enables us to determine the maximum debonding stress (σ_{th}), the fracture energy (Γ_s), and the Young's Modulus (E) of the cohesive element. By considering the bonded area of each epoxy chain adhered onto the silica surface with the associated s value, σ_{th} can be predicted as F_{break}/s^2. Γ_s in this simplified grid system also depends on the parameter "s" and can be predicted by a theoretical one-dimensional fracture model as $\sigma_{th}^2 H/2G$, where H is the thickness of epoxy and G is the shear modulus of epoxy. Finally, E can be quantified by the equation $E = kL/A_o$, where k is the interfacial stiffness which can be estimated by considering the second derivative of the FES with respect to the chosen CV, L is distance between the epoxy chain and the silica surface and A_o is the contacted area. After defining these three parameters, together with the linear assumption between stress and crack tip opening displacement at the interface, the traction-separation relation becomes well-defined and can be used in the finite element model accordingly.

3.3 Results and Discussion

Fig. 3.4(b) shows the FES of our system at different simulation times. By observing the free energy profiles, the well depth is getting deeper with convergence when the time of simulation is longer. Based on the simulation result shown in Fig. 3.4(b), the E_b between the attached and the detached stages is 31.22 kcal/mol (21,688 × 10^{-23} J) which can be obtained using the above chosen Gaussian parameters using the simulation time of 100 ns. The parameter L_o is measured as 21.44 Å. Based on the metadynamics approach, γ_s is equal to 101 pJ/m (1.46 kcal mol^{-1} Å^{-1}) using Eq. (3.2),

which is a material property for the epoxy-silica system. It is noted that in Eq. (3.5) there are only two model parameters, namely the surface energy at epoxy-silica interface (γ_s) and the persistence length of the epoxy chain (ξ_p). Here, ξ_p = 0.5 nm, which is roughly half of the repeating unit length of the polymer chain, and T = 300 K (and a widely accepted good approximation). It is found α_{cr} = 0.873 and the corresponding asymptotic force limit is estimated to be F_{break} = 134 pN. This force limit is comparable to that of hydrogen bond clusters as identified in earlier studies (Keten and Buehler 2008). Under an assumed increase of the persistence length by a factor of four, the predicted rupture force only decreases by 14%. This implies that the dependence of rupture strength on the persistence length is weak, a phenomenon that has also been found in the study of other organic structures (Keten and Buehler 2008).
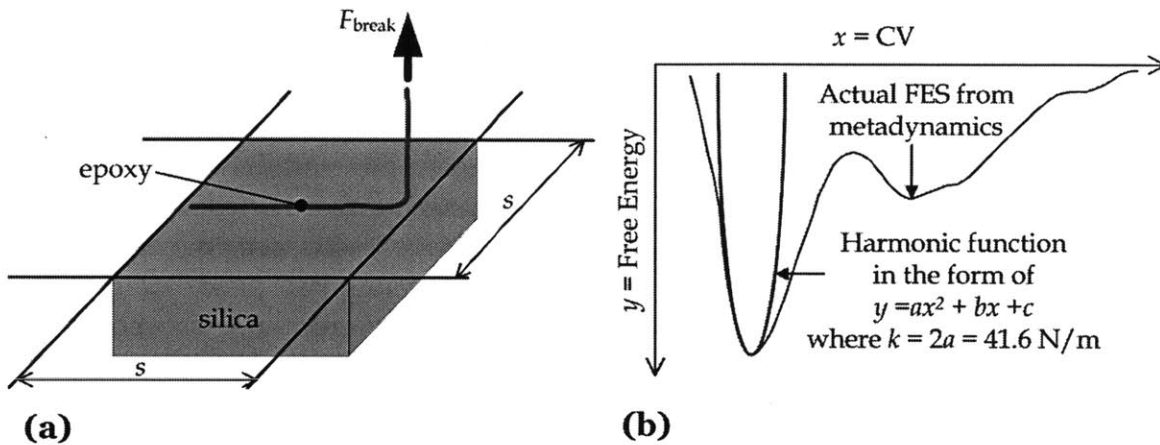
Fig 3.6 (a) The derivation of the maximum stress in the traction-separation relation for the epoxy-silica interface by considering the tributary area (s × s) for a single epoxy chain, (b) the prediction of k by curve fitting from the molecular dynamics data via a harmonic function.

In the discrete grid model as shown in Fig. 3.1, we use a parameter s that defines the spacing of the grid system. The value of s depends on the distance between the two epoxide groups in one polymer chain that form cross-links as shown in Fig. 3.6(a). Here, we pick three different values of s for analysis, namely, 2 nm, 4 nm and 8 nm, which are reasonable distances between two epoxide groups in an epoxy chain based on the reported crosslink density in several common types of epoxy (Yarovsky and Evans 2002). By considering the bonded area of each epoxy chain adhered onto the silica surface with the associated s value, the corresponding maximum stress in the traction-separation relation can then be predicted as 33.5 MPa, 8.38 MPa and 2.09 MPa, respectively, by $\sigma_{th} = F_{break}/s^2$. Before evaluating Γ_s, it is necessary to know the thickness of the adhesive. Here, we use H to be 1 mm which is a well adopted thickness in civil engineering practices and G equals 1.923 GPa corresponding to the Young's Modulus (E) = 5 GPa and the Poisson's ratio (ν) = 0.3. The E value is taken from the molecular dynamics result, which corresponds to the stiffness at the interface. In fact, it is noticed that the Young's modulus of epoxy (from existing data, see e.g. (May 1987)) is

very close to that of the interface predicted from the molecular dynamics result. The corresponding fracture energies are 292 J/m², 18.2 J/m², 1.14 J/m², respectively, with respect to the various chosen s values as shown above. The estimation of E requires the characterization of interfacial stiffness (k), which involves the second derivative of the FES with respect to the chosen CV. In order to avoid a large fluctuation of its second derivative due to a small variation in the FES, a harmonic function is used to fit the FES in the vicinity to the lowest free energy state which corresponds to the attached stage as shown in Fig. 3.6(b). Based on the fitted harmonic curve, the second derivative of the FES with respect to the chosen CV is predicted to be 41.6 N/m. As mentioned previously, the debonding mechanism described by the FES refers to a homogenous debonding which may not reflect the actual failure mechanism between epoxy polymer chain and silica. In view of this, we now study the sensitivity of our predicted strength to the variation of E. A parametric study on E is performed by considering that L changes from 1 Å to 5 Å with A_o = 91.76 Å² (estimated from our atomistic model presented above). The calculated E ranges from 4.54 GPa to 22.7 GPa and it is noted that the predicted strength of our multiscale model is insensitive to the change of E within the above range.
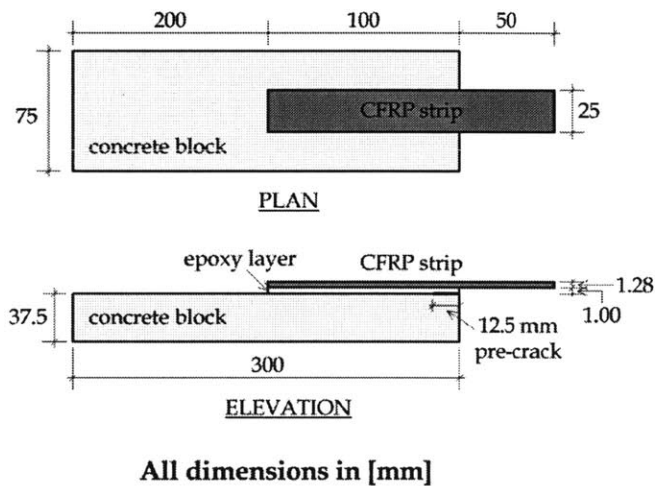
Fig 3.7 Configuration of the interface fracture specimen that are tested by applying a peel load at the end of the CFRP strip.

This multiscale approach of modeling the epoxy-silica interface is then compared with the existing experimental. The experimental work involved concrete-epoxy interface. Since the research on atomic model of concrete is still ongoing, a reasonable and reliable atomic model should be chosen based on our best understanding. Concrete consists of cement, aggregates and water and involves various crystallographic and amorphous materials inside. In this heterogeneous material system, silica is the major constituent material in concrete (about 40% by mass). The comparison between our simple epoxy-silica model and the complex epoxy-concrete system is believed to give us some key insights on complexity of a real interface problem. We set up a finite element model to describe an epoxy-concrete bonded specimen with the same dimensions and the same material properties of the constituent materials as reported in the literature (Au and Büyüköztürk 2006b). The finite element model is created based on the

41

schematic diagram shown in Fig. 3.7. The interface between epoxy and concrete is modeled by two dimensional cohesive elements and the corresponding traction-separation relation is characterized based on our predicted σ_{th}, Γ_s and E from the above epoxy-silica bonded system. The global critical fracture energy determined in that experiment is used for the determination of the damage evolution of the cohesive element and a linear softening in the traction-separation relation is adopted. The other constituent materials are modeled using plane strain elements and the assumption of perfect bonding between CFRP strip and epoxy is made since the CFRP-epoxy interface remained intact throughout that experiment. There are 10 cohesive elements per adjacent continuum element in the mesh according to the rule-of-thumb for choosing the size of cohesive elements (Diehl 2008).

(a)

(b)

(c)
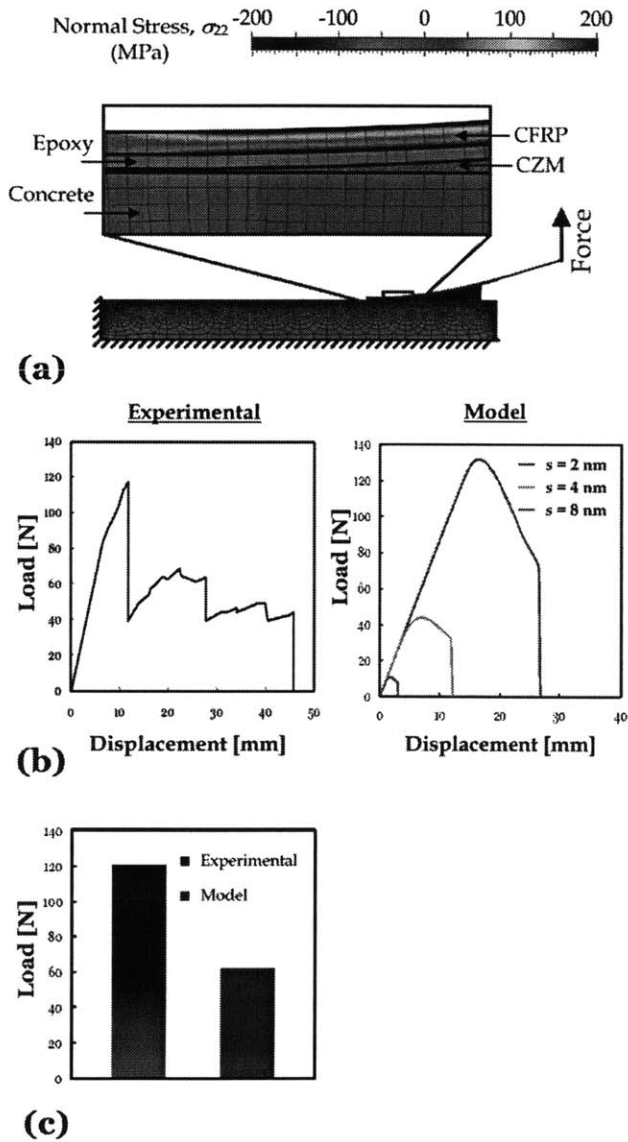
Fig 3.8 (a) The stress (σ_{yy}) distribution of the specimen at the peak of the load-displacement curve. Separation between epoxy and the substrate can be captured by the deformation of the cohesive element as shown in the close-up, (b) The load-displacement curves from the predictive model and experiment are shown. The peak of the load-displacement curve from the experiment is close to the prediction when s = 2 nm which is a reasonable distance between adjacent crosslinks for a fully cured epoxy. The good agreement between our prediction and the experimental result implies that our multiscale model of interface can provide a reasonable estimate of the global structural behavior of the epoxy-silica interface, (c) A quantitative comparison of between the maximum load measured from the experiment and the predicted average peak load based on the three chosen s values is shown using a bar plot.

Fig. 3.8(a) shows the stress distribution on the deformed bonded system and Fig.

3.8(b) shows the load-displacement curves from both the reported experimental data and our simulation result. Although there are variations of the predicted peak load from the three chosen s values, the agreement within the same order of magnitude implies that our model can be used as a preliminary prediction on mechanical properties of the epoxy-silica interface. The variation of predicted peak load implies that the macroscale strength at the interface is very sensitive to the density of the attached epoxy tail on the silica surface. It is an important observation which can explain the general large deviation when characterizing the interfacial mechanical properties as the local effect of several polymer chains (spacing between them) may significantly affect the macroscale structural behavior. It should also be mentioned that there is no noticeable change in the predicted load-displacement curves within our concerned range of E values. The discrepancy between the experiment and modeling could potentially come from various reasons, including:

(i)   the limitation of using a non-reactive force field CVFF which may not be able to accurately describe the energy barrier for interface separation,

(ii)   the difference in atomic structure between concrete and silica,

(iii)   the possible defects at the material interface during the fabrication process,

(iv)   the possible change of the material structures from nanoscale to macroscale,

(v)   the effects of the mechanical interlock and the surface roughness which are hard to be avoided in the macroscale experiment.

Even though it is a rough comparison in view of the above reasons, the good agreement between our prediction and the experimental result with a difference in the peak load by a multiple of two as shown in Fig. 3.8(c), implies that the nanoscale rupture strength derived from the metadynamics approach and the WLC fracture model is able to preliminarily predict to global structural behavior at a larger length scale. More importantly, such agreement indicates that the individual chain failure at the end of the epoxy chain attached on the silica surface is probably the origin leading to the global structural failure at the epoxy-silica interface. It also implies that the application of CVFF and the QEq method (*i.e.* insignificant change of partial charges during epoxy-silica interface separation) for describing the epoxy-silica interaction is feasible as a simplified approach. Table 3.1 summarizes the major predictions of the mechanical properties at the epoxy-silica interface based on this proposed approach. The results reported in this chapter have been published in peer-reviewed journal (Lau et al. 2012a).

Table 3.1 Predictions of the material properties at epoxy-silica interface

γ_s (pJ/m)	ξ_p (nm)	F_{break} (pN)	Γ_s (J/m^2)	σ_{th} (MPa)	E (GPa)
101	0.5	134	292	33.5	4.54

The applicability of this multiscale model has been demonstrated in epoxy-silica system. It is expected this model can be applied to other polymer-mineral systems in

which the simple grid system model can still describe the polymer network in the mesoscale. For a more robust modeling, the choice of force field and the calculation of partial charges should be studied carefully. Future studies could extend the theoretical framework reported here for capturing the effect of the surrounding (e.g. moisture) to the bonded system. The intrinsic strength presented here applies to the individual domains and can be linked up with the meso-, micro-, and macroscale levels with the capability to overcome the both the time scale and length scale limitation in which this theoretical prediction may have interesting implications for designing mechanically strong material consisting organic-inorganic interfaces, such as the application in medical field including artificial bone and tissue.

3.4 Summary Comments

The connection between atomistic and macroscale has been demonstrated using epoxy-silica interface as an example. This work outlines a possible approach using which the intrinsic strength of epoxy-silica interface derived from molecular dynamics simulation can be used to predict the macroscale structural behavior at the interface. It is found that the intrinsic strength at epoxy-silica interface is 134 pN at the single molecule level. This intrinsic strength was used to predict the global structural behavior of epoxy-silica interface by applying cohesive elements with an appropriate mesh in the finite element model and such an approach has been compared with the existing experimental data and a good agreement is obtained. The basic assumptions and the input parameters involved in the derivation are universal and may be used to explain the interfacial fracture phenomena in other organic-inorganic system through a proper characterization of fracture energy and traction-separation relationships at the interface. The use of metadynamics for reconstructing the FES of the system is an efficient method in finding the surface energy of an interfacial layer that can be broadly applied. This predictive model may have interesting implications for designing mechanically strong interface consisting organic and inorganic materials, such as the application in medical field including artificial bone and tissue.

Chapter 4

Experimental Verification: Nano-scale

4.1 Background on Nanoindentation

The term "nanoindentation" refers to depth-sensing indentation (DSI) techniques used to obtain mechanical properties from very small volumes of material and the observed deformation process is within the nanoscale range. Traditionally, an indenter is pressed into a sample with a known load and is then released during an indentation test. The hardness is defined as the load divided by the area of the residual indentation, which gives a measure of the resistance of the material to plastic deformation. In DSI, the applied load and the displacement of the indenter are continuously recorded as it is pressed into and removed from the tested sample. These data are subsequently analyzed to determine mechanical properties, such as Young's modulus and hardness. Furthermore, since there is no need to image the residual indentations, these properties can be easily obtained from indentations with depths as small as a few nanometers. Nanoindentation is commonly used to determine the mechanical properties of thin films and coatings, particles and fibers, embedded phases, patterned structures, and other small volumes. Nanoindentation is believed to be versatile and powerful means of measuring mechanical properties at the nanoscale, since the modern nanoindentation instruments are very precise.

A number of DSI instruments capable of making sub-micrometer indentations (nanoindenters) have been developed. An indenter tip is attached to a suspended shaft which can be either load-controlled or displacement-controlled. For practical reasons, the majority of these instruments are load-controlled. Typically, load is applied electromagnetically, electrostatically, or by deformation of a spring. In general, displacements are measured by a capacitance gauge. In some machines, linear variable differential transformers (LVDTs), and optical systems are also used. Contemporary instruments have load and displacement resolutions significantly better than 1 μN and 1 nm, respectively.
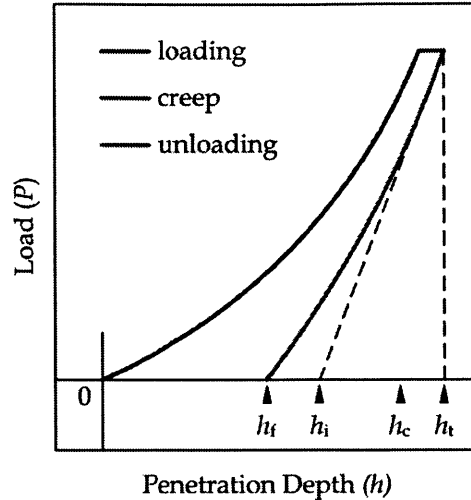
Fig 4.1 Typical *P-h* curve measured from the nanoindentation in fused silica

Fused silica is usually used as the reference material for the nanoindentation experiment. Typical nanoindentation data from fused silica, in the form of *P-h* curve, are shown in Fig. 4.1. After contact has been established at a low load intensity (typically 1 μN or less), the load is increased and the indenter penetrates the sample, owing to both elastic and plastic deformation of the tested sample. Typically, the load is then held constant for a certain period of time (usually around 1 min) to allow for indentation creep. As the load is subsequently reduced, the indenter moves back out of the sample, owing primarily to elastic recovery. After the complete unloading process, the indenter rests a certain distance below the original surface of the tested sample before nanoindentation because of the permanent plastic deformation in the vicinity of the indenter tip.

The indentation process can be visualized as shown in Fig. 4.2. At maximum load P_{max} as shown in Fig. 4.2(a), the indenter is pressed into the material by an amount h_t (the total depth) with respect to the original surface. The indenter is in contact with the material for a distance h_c (the contact depth) along the axis of the indenter. There is a region of plastic deformation near the tip (shaded), generally thought to be roughly hemispherical (Johnson 1970). When the indenter is unloaded, the indentation recovers elastically. At the final point of unloading as shown in Fig. 4.2(b), the indenter rests in the recovered indentation at a depth h_f (the final depth). If the unloading process were truly elastic, then upon reloading to P_{max}, the load and the penetration depth data would just retrace the unloading data.

46
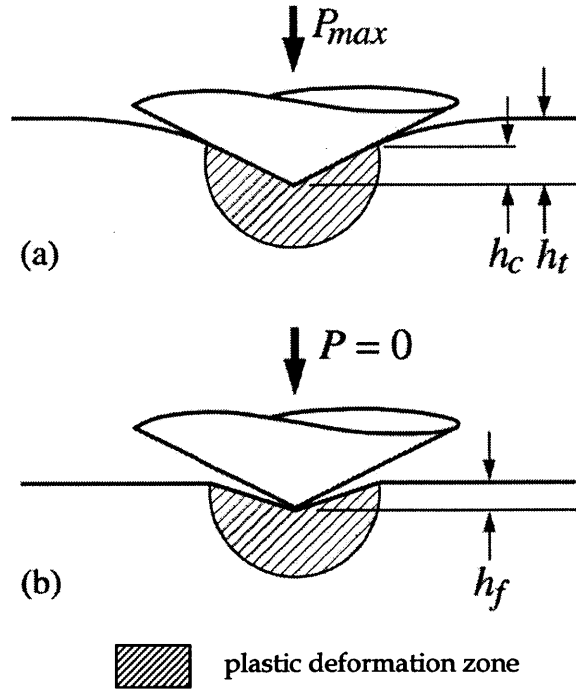
Fig 4.2 Schematic cross-section of indentation (a) at maximum load and (b) after complete unloading

Several mechanical properties including hardness, elastic modulus, and time-dependent deformation characteristics can be measured with a high degree of precision in volumes as small as a few hundred cubic nanometers during the process of nanoindentation. The simplest and most widespread analyses are those in which the deformation on unloading is assumed to be purely elastic. The form of this elastic contact approach most often used today is that presented by (Oliver and Pharr 1992) and the approach is usually referred as O&P analysis. In the O&P analysis, the unloading process is modeled as a contact between an isotropic elastic indenter and an isotropic elastic half space using expressions developed by (Sneddon 1965). For a variety of tip shapes, Sneddon's analytical solutions predict that the unloading data should follow a power law relationship as shown in Eq. (4.1).

$$P = \alpha(h - h_f)^m \tag{4.1}$$

where P and h are load and penetration depth, respectively, and m and α are constants depending on the tip shape. The contact depth, h_c, can be expressed as:

$$h_c = h_t - \kappa(h_t - h_i) \tag{4.2}$$

where hi is the intercept depth, which is defined as the intercept with the depth axis of the tangent to the unloading curve at P_{max}, and κ is a constant that depends on tip shape. For a range of tip shapes (conical, parabolic, pyramidal), m is close to 1.5 and κ is close to 0.75.

The O&P method is implemented to obtain hardness as follows: a power law fit

47

as shown in Eq. (4.1) is applied to the unloading data. The derivative of the fit at P_{max} is used to determine h_i and Eq. (4.2) is used to obtain h_c. An area function, expressed as $A_c = f(h_c)$, is used to determine the contact area, A_c. The hardness is then defined as $H_c = P_{max}/A_c$. It is important to note that this definition of hardness is different from the conventional one. The elastic contact solution returns the contact area at maximum load, not the residual plastic indentation area recorded in a traditional hardness measurement. Thus, this definition of hardness is a measure of the resistance of a body to any indentation deformation, elastic or plastic. In the extreme case of a perfectly elastic indentation (e.g., in rubber), the O&P method would return a finite hardness where the hardness determined by an imaging method would be infinite as there is no permanent deformation.

For measuring the elastic modulus of the tested sample, the total measured compliance, C_t, which refers to the machine-sample system, has to be quantified first. C_t can be written as:

$$C_t = \left.\frac{\partial h}{\partial P}\right|_{elastic} = C_m + C_c = C_m + \frac{\sqrt{\pi}}{2E_r}\frac{1}{\sqrt{A_c}} \tag{4.3}$$

where C_m is the machine compliance and C_c is the contact compliance. E_r is the reduced modulus of the contact, which can be expressed as shown in Eq. (4.4).

$$\frac{1}{E_r} = \left(\frac{1-\nu_i^2}{E_i}\right) + \left(\frac{1-\nu_m^2}{E_m}\right) \tag{4.4}$$

where E and ν are the isotropic Young's modulus and Poisson's ratio, and the subscripts i and m refer to the indenter and sample materials respectively. If the machine compliance and the elastic properties of the indenter are known, the indentation modulus, I, defined as $I = E_m/(1-\nu_m^2)$, can be determined from the contact area and the derivative of the unloading data (which is the contact stiffness, $S_c = 1/C_c$) at P_{max}.

4.2 Materials and Methods

In this experimental program of nanoindentation, fused silica and an epoxy based polymer are used. Fused Silica is a high purity synthetic amorphous silicon dioxide (SiO_2). This non-crystalline, colorless, silica glass combines a very low thermal expansion coefficient with excellent optical qualities. It is resistant to scratching and thermal shock. Fused silica is available in a number of grades for different applications. One of the important applications is High Energy Laser Optics. No other optical material matches the purity of fused silica and therefore its ability to withstand and transmit high energy laser pulses with limited absorption or damage to the material. Fused Silica is used for windows, lenses, and prisms in the transmission range 0.16 mm to 3 mm. Its refractive index varies from 1.55 to 1.40 through the transmission range. Traditionally, it is used as the reference material for nanoindentation experiment.

Figure 4.3 shows the fused silica samples that were used in this experimental program.
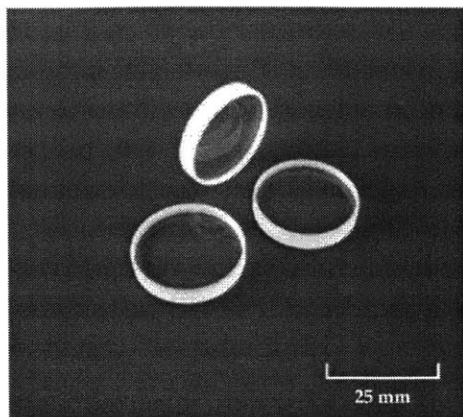
Fig 4.3 Sample of fused silica
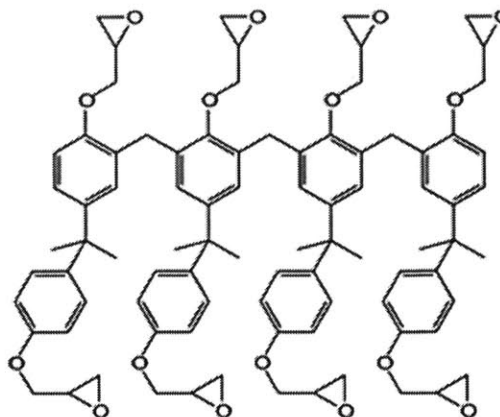
Fig 4.4 Chemical formula of SU-8

SU-8 2000 is chosen as the epoxy based polymer which is used in the nanoscale experiment. The chemical formula of SU-8 is shown in Fig. 4.3. This epoxy based polymer does not need another liquid curing agent for cross-link formation, instead the cross lining process can under ultraviolet (UV) radiation. It is a high contrast, epoxy based photoresist designed for micromachining and other microelectronic applications, where a thick, chemically and thermally stable image is desired. SU-8 2000 is an improved formulation of SU-8, which has been widely used by MEMS producers for many years. SU-8 2000 is available in twelve standard viscosities. Film thicknesses of 0.5 to >200 μm can be achieved with a single coat process. The exposed and subsequently thermally cross-linked portions of the film are rendered insoluble to liquid developers. SU-8 2000 has excellent imaging characteristics and is capable of producing very high aspect ratio structures. SU-8 2000 has very high optical transmission above 360 nm, which makes it ideally suited for imaging near vertical sidewalls in very thick films. SU-8 2000 is best suited for permanent applications where it is imaged, cured and left on the device.

The SU-8 is coated onto the fused silica surface through spin coat as shown in Fig. 4.5. In order to generate 20 μm thick film, the spin coater should rotate with a speed 2,500 rpm for 30 s after the uncured and unbaked SU-8 (liquid state) is placed onto the substrate. After spinning, the sample is placed in vacuum for 1 hr to get rid of the solvent in SU-8. Then, the sample should be treated under UV for 90 s so that the SU-8 can develop extensive cross-link in the following baking process. At the final step, the sample is placed in the 95 °C laboratory oven (see Fig. 4.6) for 20 hr to make sure that SU-8 is fully cured with an extensive cross-link network.

Fig 4.5 Spin coater
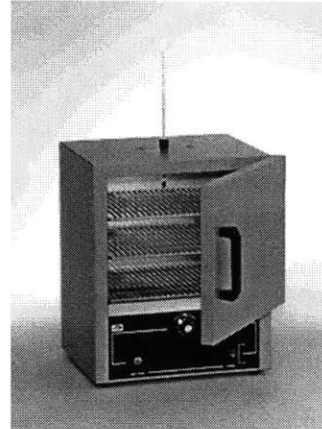
Fig 4.6 Laboratory oven

After fabricating the epoxy-silica bonded samples consisting of fused silica substrate with a SU-8 thin film attachment, they were conditioned in a water bath under different duration, ranging from 0 week (dry) to 8 weeks. These conditioned samples were used for characterizing the effect of moisture to various mechanical properties through nanoindentation. The Hysitron TriboIndenter, as shown in Fig 4.7, was used for conducting the nanoindentation. The load range for this machine is between 10 μN and 10 mN, and the depth range is between 20 nm and 5 μm.
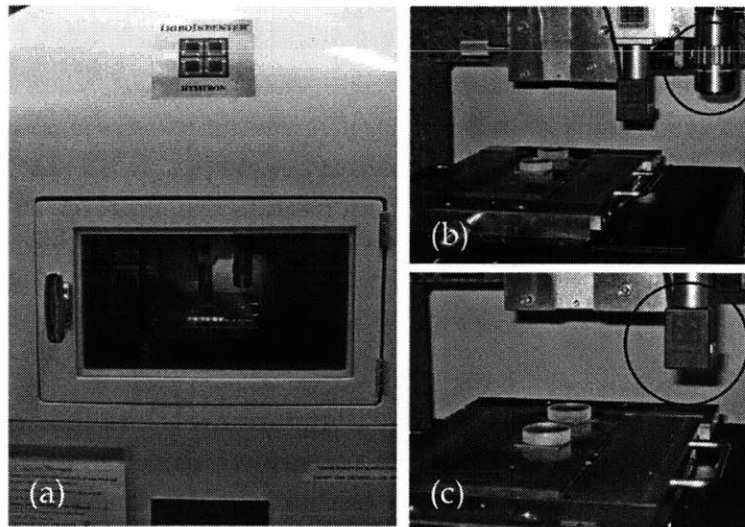
Fig 4.7 Hysitron TriboIndenter (a) machine outlook, (b) optics as circled in red, (c) nanoindenter as circled in red

4.3 Procedure of Nanoindentation Using Hysitron TriboIndenter

Before getting started, there are two things that should be borne in mind. (1) The maximum applied load is 10 mN for the one dimensional force transducer. The maximum measurable depth is 5 μm for the transducer. (2) Below the chamber, there are three control units, namely, the power for the piezo tube attached to the transducer,

the transducer to which the tip is attached, and the *xy* stage on which the samples sit. They should be always on.

When getting started, it is important to check for correct stand-by conditions. The blue light inside the chamber should be on. It should always be left on. There is a red button inside the chamber that turns it off and on. The chamber door is closed. It should never be left open. It should be kept closed at all times except when placing the samples on the stage and, if necessary, when manually moving the tip towards the sample during the H-calibration. For the middle transducer controller unit, it should be ensured that its knobs have the following settings: 1,000 for "low pass filter", 100 for "displacement gain", 1,000 for "microscope feedback gain", and 100 for "display gain". The "LOAD (mg)" LCD display should read within ±5.000. It is very important to confirm this before starting the software. If the force display is not within ±5.000 mg, the "AUTO ZERO" button should be pressed. Finally, the optical light and the software should both be off.

After the above checking, the software can be turned on. The optics light should be turned on at this stage. The logbook should be read carefully to see if there are any important messages. The TriboScan icon on the desktop should be double clicked to log into the computer system. When asked to zero the load, it means that the "LOAD (mg)" LCD display should read within ±0.030. The coarse and fine knobs can be used to achieve this.

After turning on the software, indentation axis calibration is required to be conducted. The key steps of this calibration are summarized as follows:

- ➢ Go to Calibration tab and then System Calibrations sub tab.
- ➢ Confirm that the correct transducer file is loaded.
- ➢ Unclick the "Auto detect front panel gains" box and make sure that the "System Setup" software settings match the hardware settings.
- ➢ Before doing the indentation axis calibration, both the hardware and software settings for the microscope feedback gain should be changed to 100.
- ➢ Perform the Indentation Axis calibration. The desired load function is triangular with 10 second time segments and a 700 µN peak load.
- ➢ Click "Cal Air Indent". Accept the calibration by clicking "Yes" if the red squiggly line overlaps the blue line in the Electrostatic force (ESF) vs. Displacement window. Record the results into the logbook.
- ➢ Return both the software and hardware settings for the "microscope feedback gain" to 1,000.

After the indentation axis calibration, H-calibration should be conducted if necessary. The H-calibration is necessary if the tip has been changed. It is a stage offset determination between the optics and the indenter probe. If the H-calibration is required, it will be the first time you need to load a sample and trace its boundary. Extra care should be paid when loading a sample and tracing its boundary. It should be mentioned that the transducer and tip are very vulnerable to being damaged. User

should be very careful not to let the tip ram into the stage. When making the calibration indents with blunt tips, use 10,000 µN for the one dimensional force transducer. When done with the H-calibration, the "H" should be turned into an "A" or "∀" so that it will not be confused with future H patterns. The Navigation window can be used to move the optics cursor to either the bottom middle or top middle of the "H" pattern in order to create the "A" or "∀" pattern.

After all these calibrations, the research samples can be set up for testing. The sample needs to be mounted on a magnetic substrate such as a one-inch square magnetic stainless steel piece as shown in Fig 4.8. The sample should be mounted at the locations in which there are three magnets under the stage marked by little dimples. The sample surfaces should be focused and their boundaries should be traced using the focused image. After all your research samples have been traced, user can go from one sample to another by right clicking the mouse within its traced boundary to activate the sample of interest. In order to make sure that there is a non-zero contact value between the indenter and the sample surface, a "Quick Approach" for each traced boundary should be conducted before actually indenting the sample.
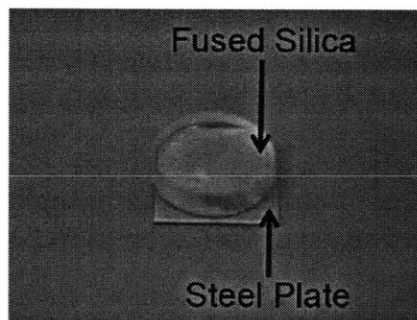
Fig 4.8 Fused silica sample mounted on a stainless steel plate

4.4 Results and Discussions

The fused silica sample was indented under a 7× 3 grid (i.e. 21 indents in total). It was noticed that there was no observable change in the measured mechanical properties for different moisture conditioned samples. Fig 4.9 shows the *P-h* curves from the 21 indents. The different colored lines refer to different loading rates ranging from 20 µN/s to 2,000 µN/s. Based on the nanoindentation result, the Young's modulus of silica is 69.58 ± 0.42 GPa and its hardness is 8.93 ± 0.05 GPa. These tested results are very close to the data from the existing literature. The small difference between the experimental measurements and the existing literature data, as well as the small standard deviation of the experimental measurement, implies that the experiment was correctly conducted.

Compared with fused silica, it was observed that the epoxy based polymer, SU-8, has an observable change in appearance under the effect of moisture. Fig. 4.10 shows

the material texture of SU-8 under optical microscope. The thickness of the SU-8 layer was 20 μm. It is noticed that SU-8 is highly transparent under dry condition. However, after 2 week moisture conditioning, the texture of SU-8 changes a lot as shown in Fig 4.10. There are lots of black dots as captured under optical microscope. It is expected that hydrolysis of epoxy occurs when sufficient water molecules diffuse into the bulk SU-8 thin film layer. The hydrolysis process may involve the release of oxygen which results in the formation of bubbles (black dots as shown in Fig 4.10). This observation under optical microscope further consolidate the importance of studying the effect of moisture towards the mechanical properties of epoxy based polymer, SU-8, as well as the interfacial properties between SU-8 and silica. In fact, after analyzing the *P-h* curves from SU-8, it is noticed that the moisture effect is most critical to the interface which affects the integrity of the epoxy-silica bonded system significantly.
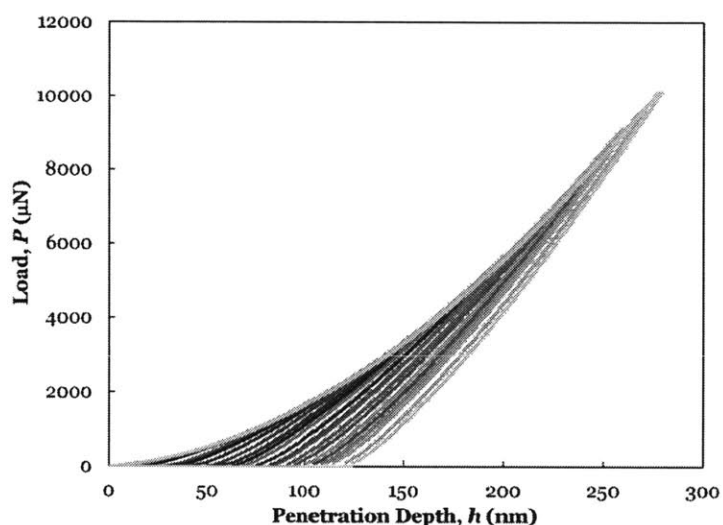
Fig 4.9 *P-h* curves for fused silica under different loading rate ranging from 20 μN/s to 2,000 μN/s

The 20 μm thick SU-8 thin film deposited on the fused silica substrate was indented under three 7× 7 grids (i.e. 147 indents in total). Each 7× 7 grid corresponded to a single load rate. In this experiment, three different loading rates were considered, namely 20 μN/s, 200 μN/s and 2,000 μN/s. The *P-h* curves of nanoindentation in SU-8 were analyzed based on the description in section 4.1. Fig 4.11 shows the *P-h* curves for the nanoindentation in SU-8 under both dry and wet conditions. Table 4.1 summarizes the measured Young's modulus and hardness for both dry and wet SU-8 samples. It is noticed that the mean value of the measured mechanical properties were very close between the dry and wet samples, while the measured Young's modulus from the wet samples had a larger standard deviation. The change of hardness and Young's modulus of SU-8 with respect to the duration of moisture conditioning is shown in Fig. 4.12. Surprisingly, both the hardness and Young's modulus of SU-8 does not change significantly under the effect of moisture. In fact, based on the nanoindentation result of both silica and SU-8, it can be concluded that moisture has minimal effect on the bulk material properties of the constituent materials in the epoxy-silica bonded system. This

motivates a more robust characterization of the interfacial properties between epoxy and silica because interfacial degradation is the key reason for the overall deterioration of the bonded system. In what follows, a new approach to quantify the interfacial fracture toughness will be described.

Dry condition (0 week)

2.5x   10x   20x   50x

Moisture conditioning for 2 weeks

2.5x   10x   20x   50x
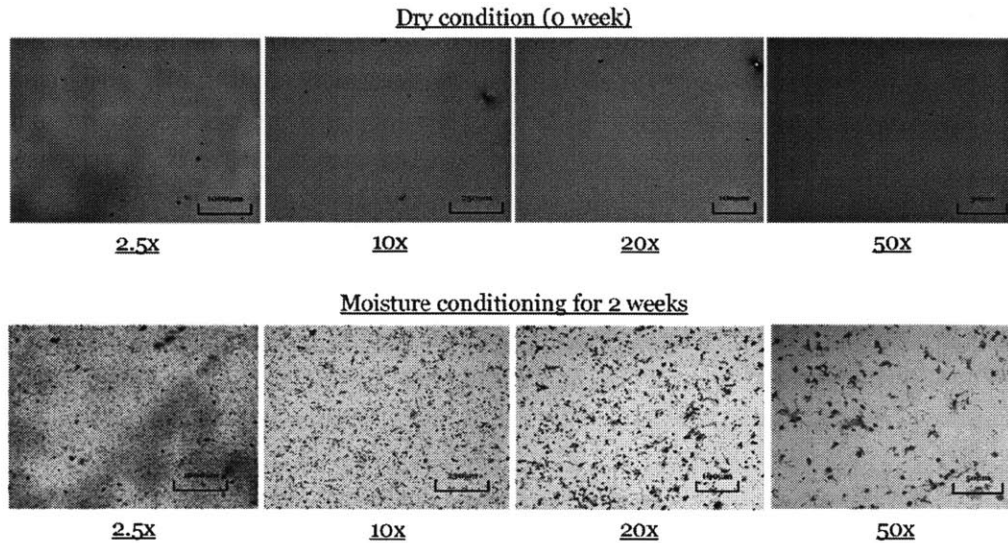
Fig 4.10 Epoxy based polymer, SU-8, under optical microscope
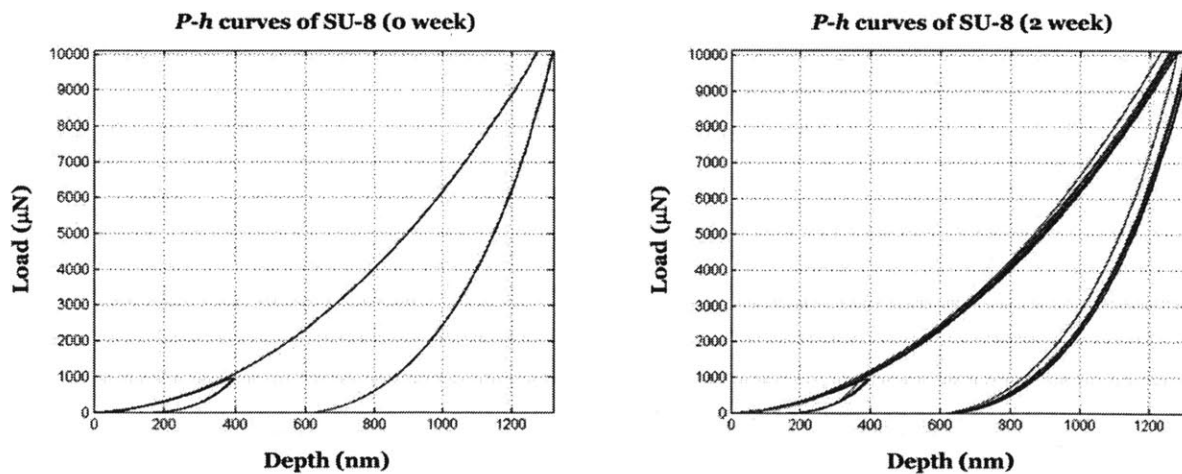
Fig 4.11 *P-h* curves for nanoindentation in SU-8:
(a) dry condition (b) wet condition (2 week moisture conditioning)

Table 4.1 Summary of the Young's Modulus and the Hardness for both dry (0 week) and wet (2 week) SU-8 samples

Moisture Duration (week)	Loading Rate (μN/s)	E (GPa)	H (GPa)
0	20	4.80 ± 0.15	0.35 ± 0.01
	200	4.77 ± 0.05	0.29 ± 0.002
	2000	5.00 ± 0.06	0.29 ± 0.002
2	20	5.20 ± 0.23	0.37 ± 0.02
	200	5.23 ± 0.42	0.32 ± 0.03
	2000	5.22 ± 0.12	0.29 ± 0.01
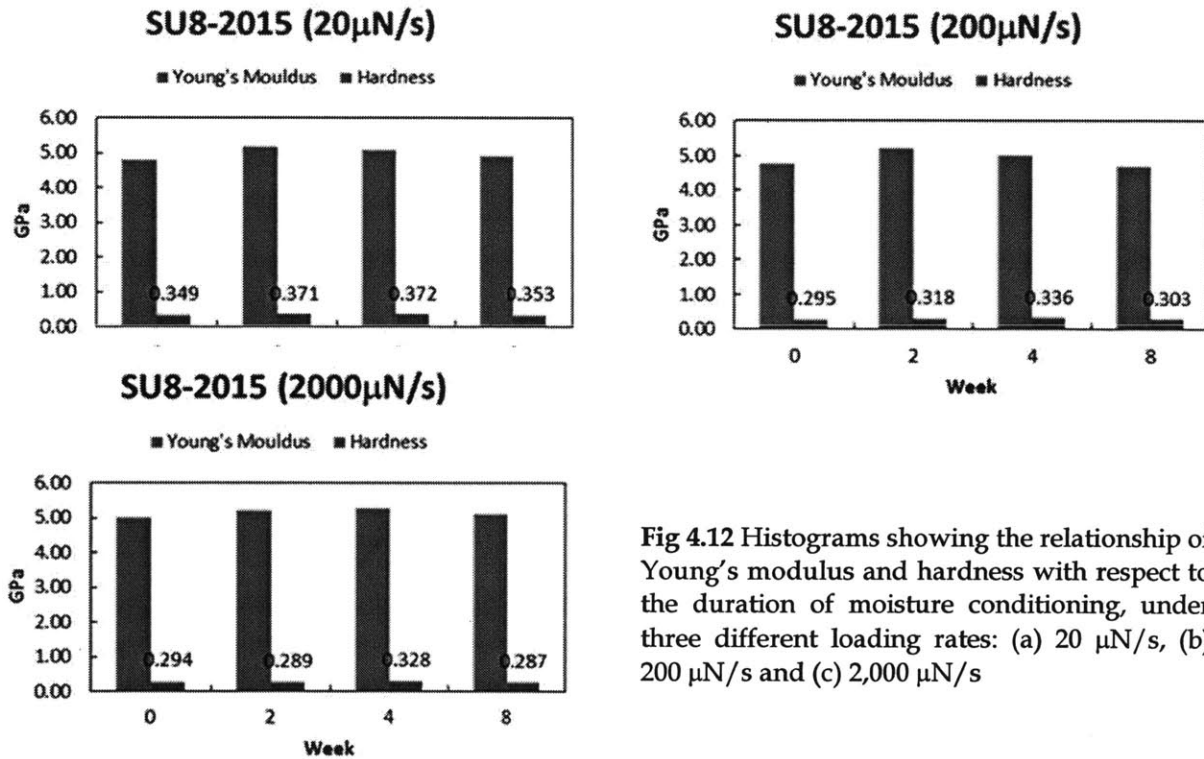
Fig 4.12 Histograms showing the relationship of Young's modulus and hardness with respect to the duration of moisture conditioning, under three different loading rates: (a) 20 μN/s, (b) 200 μN/s and (c) 2,000 μN/s

4.5 Characterizing Interface Fracture Toughness Using Nanoindentation Approach

In bi-layer systems such as film-substrate systems, as the indentation load increases, several kinds of damage can appear. These can be cracks (originating from the edges of the indenter), delamination (loss of contact between the thin film and substrate), or chipping (removal of coating segments) (Etienne-Calas et al. 2004). These damages can be seen from the load-displacement curves obtained from nanoindentation. These failures are represented by discontinuities in the graphs, as shown in Fig 4.13.
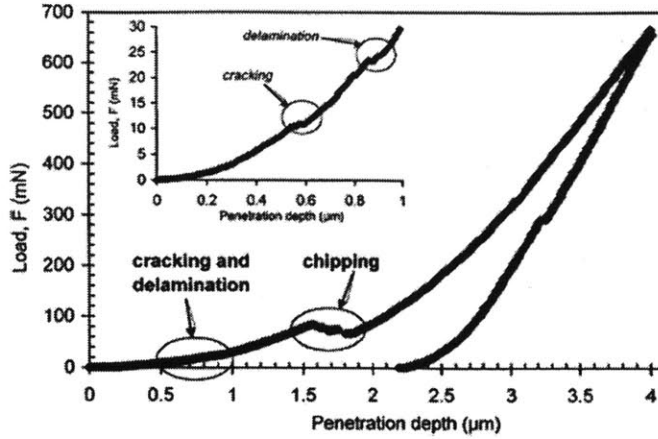
Fig 4.13 Typical *P-h* curve shows the details of the cracking and delamination area (Etienne-Calas et al. 2004).

(Marshall and Evans 1984) developed a method for analyzing conical-indentation induced thin film delamination, based on residual stresses and the mechanical properties (Young's modulus and Poisson ratio) of the film. The strain energy release rate, G, is given by the following equation:

$$G = \frac{1-v_f}{E_f}\left[\frac{h\sigma_I^2(1+v_f)}{2E_f} + (1-\alpha)h\sigma_r^2 - (1-\alpha)h(\sigma_I - \sigma_b)^2\right] \quad (4.5)$$

where E_f and v_f are the Young's modulus and the Poisson's ratio of the thin film, respectively, h is the film thickness, and σ_r is the residual stress in the film. The unit of G is J/m². The value σ_I, the indentation stress, is given by the following:

$$\sigma_I = \frac{E_f V_I}{2\pi a^2 h(1-v_f)} \quad (4.6)$$

where V_I is the indentation volume, which can be determined from the indenter geometry and a is the crack length, which can be obtained through microscopy. The value σ_b, the Euler buckling stress, is given by the following:

$$\sigma_b = \frac{\mu^2 h^2 E_f}{12a^2(1-v_f)} \quad (4.7)$$

where $\mu^2 = 14.68$ for single buckling and 42.67 for double buckling (Volinsky et al. 2002). Schematics for single and double buckled films are shown in Fig 4.14.

56
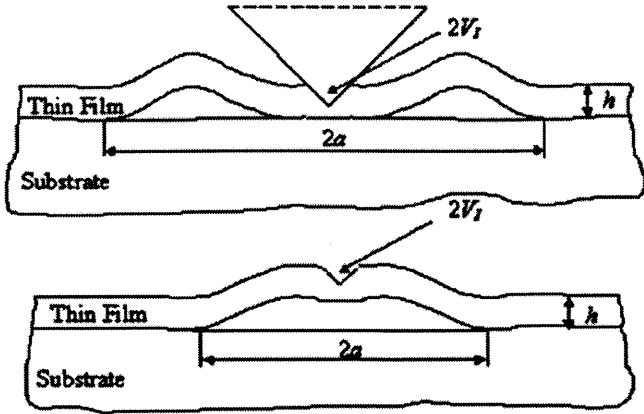
Fig 4.14 Schematic diagram showing the single buckling and double buckling during nanoindentation (Volinsky et al. 2002)

If the film is not buckled, $\alpha = 1$. Otherwise, α can be expressed as:

$$\alpha = 1 - \frac{1}{1 + 0.902(1 - v_f)} \tag{4.8}$$

If $\alpha = 1$, the delamination is only driven by the indentation stress and the residual stress does not come into play ($\sigma_r = 0$). However, the accuracy of experimental measurement using the above approach relies much on the proper quantification of the residual stress. It is known that the characterization of the residual stress in the thin film is very complicated since it is governed by various parameters, including the material texture, the condition during thin film deposition, the coating thickness, etc. Therefore, with the advancements in technology and refinements in methodology, characterization of interface fracture energy and toughness using an energy approach is recommended, which does not rely on residual stresses.

The energy approach requires the dissipated energy, U, to be separated into its different events, U_{crack}, U_c (chipping), and U_d (delamination). This can be achieved by plotting the dissipated energy as a function of maximum load F during indentation. Fig 4.15 depicts this and is taken from the same experiment as Fig 4.12 (Etienne-Calas et al. 2004).

After determination of U_d from the energy dissipation vs. load graph, the interface fracture energy, Γ_{int}, can be determined using the following equation:

$$\Gamma_{int} = \frac{U_d}{\pi \varphi_d^{\,2}} \tag{4.9}$$

where φ_d is the diameter of delamination area. Γ_{int} is analogous to G (strain energy release rate) described in Eq. (4.5). The interface fracture toughness (units of MPa m$^{1/2}$) can then be determined by the following:

$$K_{int} = \sqrt{\Gamma_{int} E_{int}} \tag{4.10}$$

where E_{int}, the interfacial modulus, is defined as:

$$\frac{1}{E_{int}} = \frac{1}{2}\left(\frac{1}{E_c} + \frac{1}{E_s}\right) \tag{4.11}$$

where E_c and E_s represent the elastic modulus of the film coating and the substrate, respectively (Hutchinson and Suo 1992).
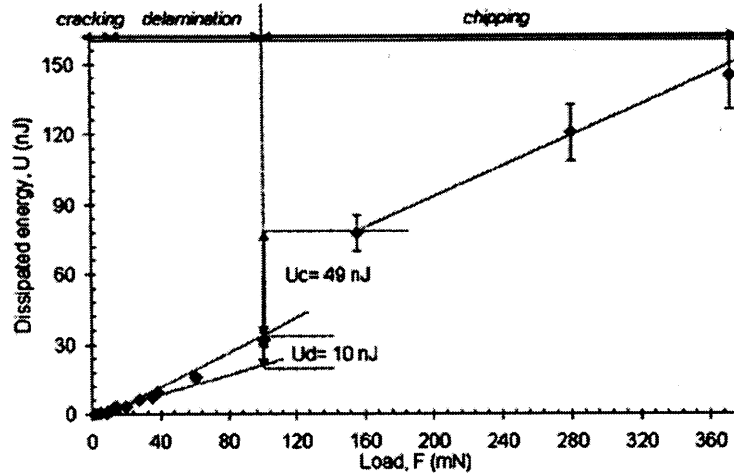
Fig 4.15 Relationship between dissipated energy and the maximum load recorded during nanoindentation (Etienne-Calas et al. 2004)

Equipped with the above knowledge, nanoindentation was conducted such that the indenter reached a depth of 20 μm such that the interface fracture toughness can be quantified accordingly. The dry epoxy-silica bonded system was tested and the corresponding P-h curves are shown in Fig 4.16. Three different loading rates, namely 50 μN/s, 500 μN/s and 5,000 μN/s, were adopted and again the results were not sensitive to the loading rate. Red circle region in the P-h curves refers to possible damage of the epoxy-silica bonded system. However, it is very difficult to ensure that the kink on the P-h curves is really related to the debonding mechanism. A meaningful cross section cut is extremely hard to be carried out because the indent region is so small that the cut cannot intersect the indent region. Meanwhile, it is still questionnable in the research field of solid mechanics that whether an indentation force can really initiate an interfacial debonding. It is believed that the applicability of such approach really depends on the chosen materials and hence the above presented approach is not robust enough for general interface fracture toughness characterization. In view of all these limitations, another new approach of quantifying the interface fracture toughness, which can avoid the much plasticity during the debonding process, will be presented in the next chapter.
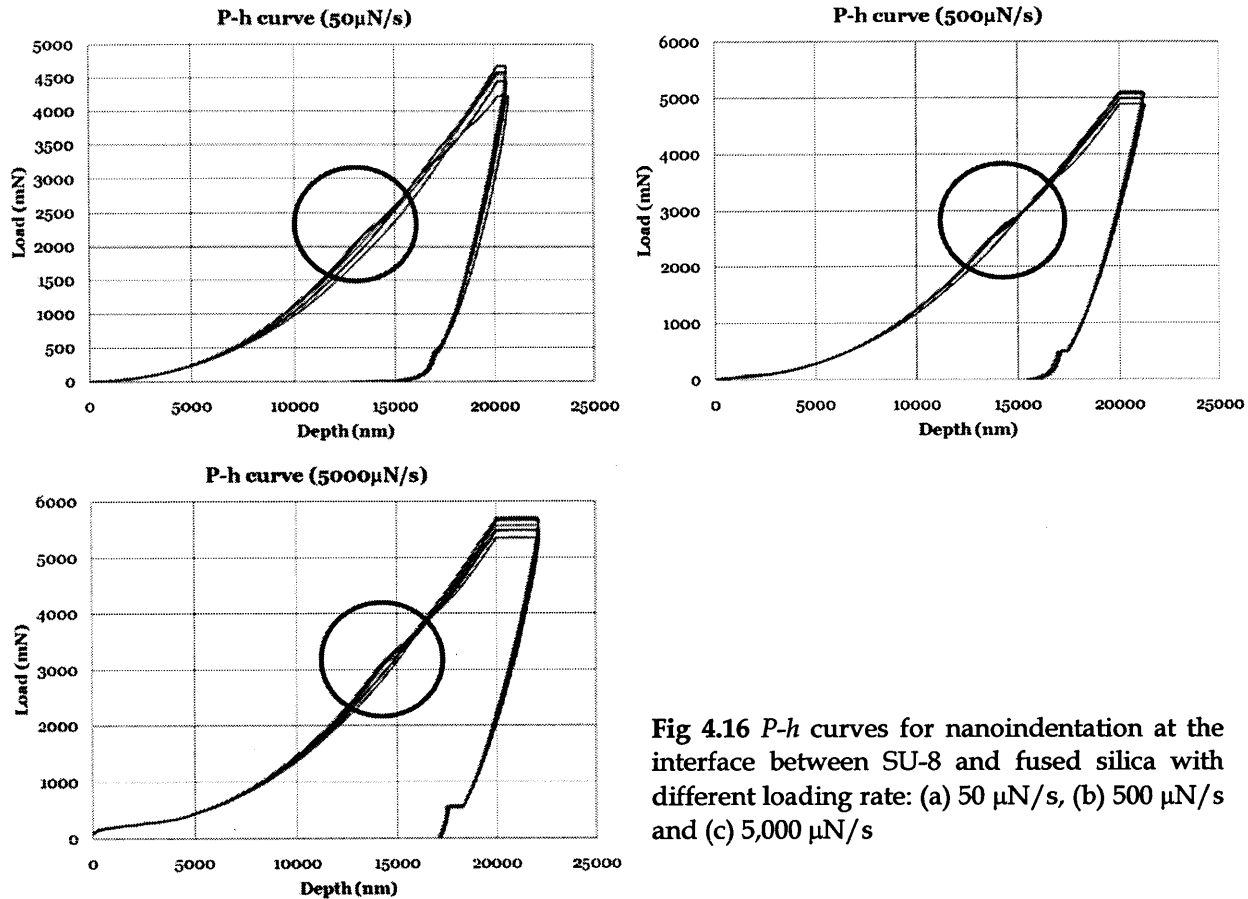
Fig 4.16 *P-h* curves for nanoindentation at the interface between SU-8 and fused silica with different loading rate: (a) 50 μN/s, (b) 500 μN/s and (c) 5,000 μN/s

4.6 Summary Comments

The nanoindentation in fused silica and SU-8 has been conducted successfully. In such a small scale characterization, it is noticed that moisture has little effect on the change of bulk material properties in terms of Young's modulus and hardness. With the observable change of SU-8 under the optical microscope, it is expected that the overall deterioration of the epoxy-silica bonded system is originated from the interface. Nanoindentation at the interface has been attempted. However, with the limitations of this approach as mentioned in section 4.5, a new approach called "superlayer approach", which involves another layer of material (e.g. chromium or nickel) that can create a large tensile residual stress as the driving force of the interface debonding, is used. Such new approach can avoid much plasticity such that the fracture energy can be more accurately measured. The details of superlayer approach will be given in Chapter 5.

Experimental Verification: Micro-scale

5.1 Background on the Characterization of Interfacial Fracture Energy

There are several straightforward measurement methods for quantifying the interface fracture energy on large specimens, such as Brazilian disk specimen (Hutchinson 1990) and sandwiched beam specimen (Büyüköztürk and Lee 1993; Lee and Büyüköztürk 1995). But it has been difficult to directly measure this parameter for micro-scale specimens, such as thin film systems. A list of four common approaches for measuring the interface fracture energy in thin film systems is presented in Table 5.1. More detail descriptions can be found in reviews by (Bagchi and Evans 1996) and others (Valli 1986; Steinmann and Hintermann 1989; Chalker et al. 1991). Unlike the nanoindentation approach, the following approaches involve direct debonding from the external load (in the form of peel force or residual tensile tensile) with high fidelity.

Table 5.1 Summary of adhesion tests

Test	Method	Remarks
Microscratch	A stylus load is drawn across the film with increasing load until spallation occurs.	Pros: It is simple and can be applied to thin, strongly adhering ceramic and metallic films. Cons: Critical load at failure is influenced by many extrinsic parameters which restricts quantification.
Peel	A strip of film is peeled at fixed angle to the substrate.	Pros: The steady-state peel force is a direct measurement of interface fracture energy if there is no plastic deformation. Cons: Plastic dissipation becomes predominant with decreasing film thickness.
Blister	A fluid is injected to the interface between the substrate and the thin film to create a blister.	Pros: It is a sensitive test that can yield high fidelity of the interface fracture energy data. Cons: Sample preparation is tedious and applications are limited to compliant films that do not yield.
Superlayer	A metal superlayer, usually chromium or nickel, is deposited onto the thin film/substrate system which induces debonding by residual strain.	Pros: Interface fracture energy can be measured with high fidelity over a range of phase angle. Cons: Sample preparation is tedious.

The microscratch test has been widely applied to metallic and ceramic films (Wu 1991). Its main advantage is the ease in implementation. However, the critical load is influenced by many factors. The models developed to predict interface fracture energy

are generally approximate in nature (Venkatraman et al. 1992; Venkatraman et al. 1993). They use a point contact to approximate film stresses around the indenter using the elastic field. The elastic strain energy contained in the film above the delamination is obtained from the stress. This energy is considered to be available for the interface decohesion, together with a contribution from the substrate which is assumed to be equal to that from the film. Using this approach, the residual stresses present in the film are difficult to take into the account because the sign of the stress relative to that from the point force varies spatially around the scratch. In order to evaluate the interface fracture energy, a measurement of the delamination geometry from scanning electron microscopy observations of the scratch track is required.

Peel tests have been applied primarily to flexible thick films (typical thicknesses ~10 μm to 1 mm). It was originally developed by the aerospace industry as a quality control measure for laminated structural components (Spies 1953). Recently, the test has been embraced by the electronics industry to assess the adhesion of metallic and polymeric thick films, deposited on various dielectric substrates (Chen and Flavin 1972; Kim 1991). More recently, this test setup has been adopted to quantify the interface fracture energy for the multilayer material system found in civil infrastructures, such as the FRP-epoxy-concrete system (Au and Büyüköztürk 2006b; Tuakta and Büyüköztürk 2011b). The characteristic of this test is that the peeling force is measured in steady state condition when the shape of the strip remains invariant. This force is in fact the direct measure of the interface fracture energy.

Blister tests are commonly used for thin polymeric films spun onto a substrate having a circular or square perforation (Allen and Senturia 1988; Allen and Senturia 1989). A blister is created by a hydrostatic loading through the perforation, leading to progressive interfacial debonding. The critical pressure needed to initiate the debonding process is related to the interface fracture energy. The effects of residual stress can be readily included using this test approach (Jensen and Thouless 1993). One basic approach of introducing the pressure is to use a constant volumetric flow rate which causes progressive debonding. The area under the pressure-time plots relates to the interface fracture energy (Jeong and White 1993).

Superlayer test involves the use of residual stress which can generate a steady-state loading on a thin film system at the mode mixities relevant to thin film and multilayer decohesion. For typical thin films (h < 1 μm), and representative residual stresses (σ_R ~ 100 MPa), the induced energy release rate is generally below the interface fracture energy of bonded system having practical interest. A procedure that substantially increases steady-state energy release rate, G_{ss}, is required. Such a procedure involves the deposition of a superlayer that increases the effective film thickness and also elevates the residual stress. The superlayer is selected in accordance with four characteristics, namely:

1. The deposition can be conducted at ambient temperature.
2. The layer should not react with the existing film.

3. It should have good adhesion.
4. The superlayer should be subjected to a large residual tension upon deposition.

Chromium (Cr) or nickel (Ni) films, deposited by electron beam evaporation, meet all four criteria (Evans and Hu 1989).

5.2 Materials

In this superlayer approach experiment, silicon wafer with an oxide layer and an epoxy based polymer (SU-8) as discussed in Chapter 4 were used. Silicon (Si) is a blue gray, brittle, chemical element in the same group as carbon (C). At 27.8%, it is second only to Oxygen (O), as the most common element on the surface of the earth. Silicon is the main ingredient of glasses, quartz, soil and sand. It contributes to hardness and structural strength to many metals such as aluminum-silicon alloy and bronze. The majority of semiconductors and microchips are built on silicon. Before a semiconductor can be built, silicon must be transformed into a wafer. This begins with the growth of a silicon ingot. A single silicon crystal is a solid composed of atoms arranged in a three dimensional periodic pattern that extends throughout the material. Because silica is the interest of this study, silicon wafers with a 0.9 nm thick thermal oxide were used. The thermal oxide layer is also crystalline in nature with [1 0 0] orientation. The diameter of the silicon wafer used here was 152.4 mm with a thickness 0.525 mm. Fig 5.1 shows the typical [1 0 0] silicon wafer used in this experimental work.
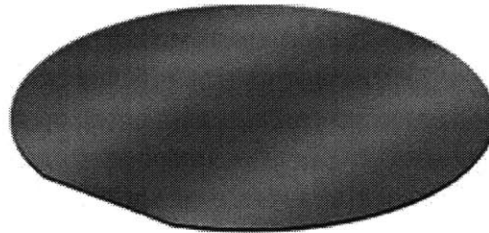
Fig 5.1 Typical silicon wafer with thermal oxide layer that crystalline orientation [1 0 0]

5.3 Procedure of Superlayer Test

This experiment relies mainly on measuring the curvature of the thin film system using profilometer. Based on the curvature measurement, the stress in the film can be calculation with the associated standard deviation. With the calculated stress, the interface fracture energy can be quantified accordingly. Deposition and photolithography were conducted. Residual stresses were measured from beam deflections using the mechanical surface profilometer (Dektak 150) at MIT Microsystem Technology Laboratories (MTL) as shown in Fig 5.2(a). Then, film severing above the pre-crack is conducted. The films were inspected to assess the critical thickness, h_c,

using the scanning electron microscopy (SEM) as shown in Fig 5.2(b). Finally, this critical thickness was used to determine the interface fracture energy.
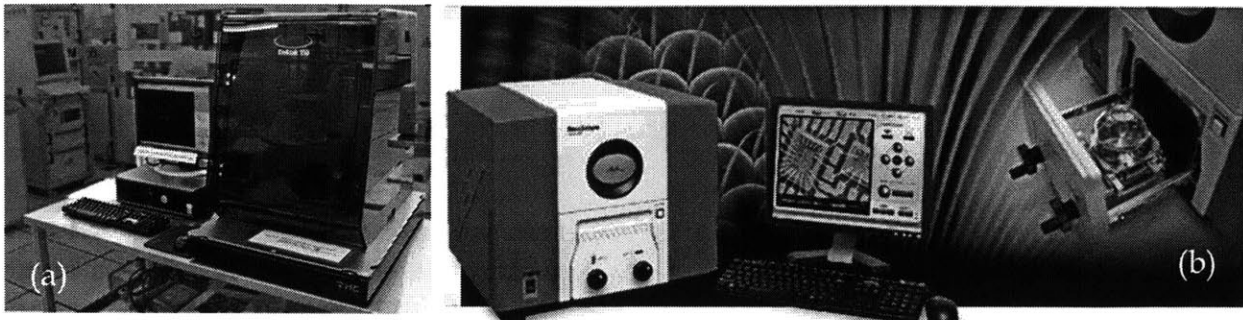
Fig 5.2 Equipment at MTL: (a) mechanical surface profilometer, Dektak 150, (b) SEM, a Joel/Nikon Neoscope JCM-5000

Fig 5.3 describes the fabrication of the tested specimen used for the superlayer test. Preliminary experiments have been carried out by using SU-8 films and silica substrates (silicon wafer with thermal oxide). The choice of SU-8 is particularly attractive due to its emerging importance as an adhesive that is usually used in various engineering fields including micro-electro-mechanical systems (MEMS), optics and bio-engineering. Careful substrate cleaning is essential. For this purpose, the silica substrate (silicon wafer with thermal oxide) was solvent cleaned in trichloroethylene, acetone, and isopropyl alcohol in order to remove organic contaminants. Then, the wafer was water cleaned, followed by etchcleaning in buffered hydrofluoric acid, in order to remove all inorganic contaminants. Finally, the wafer was rinsed in de-ionized water and dried by putting it on the 105°C hot plate for 10 min. In order to achieve the Au pattern, a negative photoresist (AZ5214) was first coated onto the silicon wafer with thermal oxide using a spin coater with a speed 3,000 rpm for 30 s. After that, the wafer was soft-baked with compression on a 105°C hot plate for 3 min. Then, the wafer was exposed under ultraviolet (UV) light for 20 s using hard contact approach with the transparency mask shown in Fig 5.4(a). It should be mentioned that the hard contact approach involves a clean glass plate and a transparency mask (ink is down) placed on top of the wafer. Post-exposure bake was conducted on a 105°C hot plate for another 3 min, followed by flood exposure under UV light for another 1 min without transparency mask, which is regarded as soft contact. Finally, the negative photoresist was developed in AZ422 for 1 min, followed by rinsing using deionized water. Gold (Au) layer (thickness ~30 Å) was then deposited onto the negative photoresist patterned wafer by electron beam evaporation. The Au pattern, as shown in Fig 5.3(a), was achieved by removing the AZ5214. The stripper for the AZ5214 used to "lift off" the Au, was an n-methyl-2-pyrrolidone (NMP) based solution called Microstrip 2001. The Au pattern acts as the pre-crack region for the epoxy-silica bonded system.
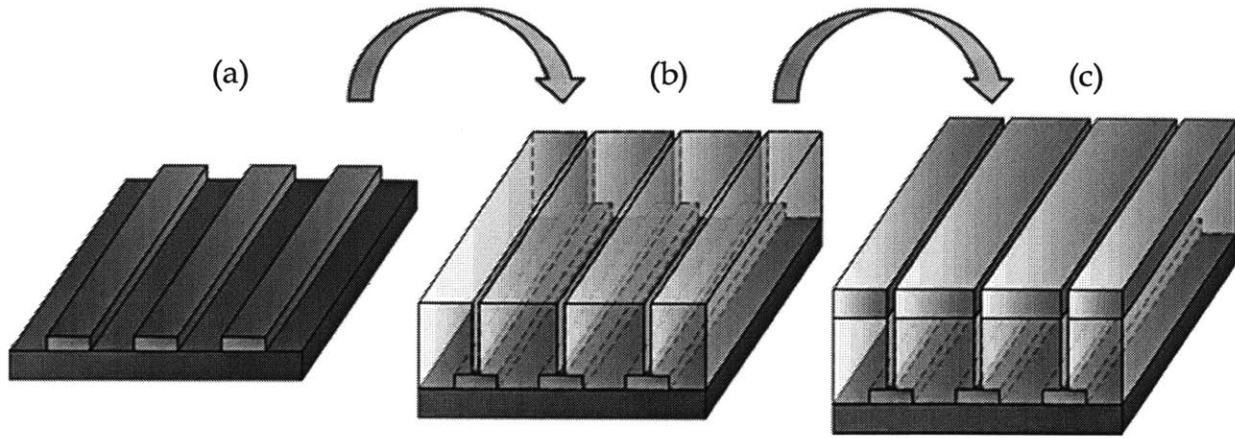
Fig 5.3 (a) Au pattern on Si wafer with a layer of thermal oxide (0.9nm), (b) SU-8 was spin-coated on the wafer with a thickness 20μm, (c) Cr was deposited onto the SU-8 surface by the sputterer. The residual tensile stress in Cr leads to the crack initiation at the SU8-SiO_2 interface when the critical Cr thickness is achieved.

After achieving the Au pattern, SU-8 was coated on Au strips using spin coater. SU-8 2015 was spin-coated onto the Au patterned wafer using a speed 3,000 rpm for 30 s. After that, the wafer was soft-baked on a 95°C hot plate for 5 min. Then, the wafer was exposed under ultraviolet (UV) light for 45 s using hard contact approach with the transparency mask shown in Fig 5.4(b). It should be mentioned that the solid and hollow square marks shown in Fig 5.4 are for the aligning purpose during the patterning process. Post-exposure bake was conducted on a 95°C hot plate for another 5 min. Finally, SU-8 was developed on the spin coater with PM Acetate, followed by rinsing in isopropyl alcohol (IPA) and the SU-8 pattern was achieved as shown in Fig 5.3(b).

After having the epoxy-silica bonded system as shown in Fig 5.3(b), the wafer was broken into smaller specimens for the chromium deposition afterwards. Each wafer could generate 21 specimens as shown in Fig 5.4(b) with the red dash boundary. 18 specimens were conditioned in a water bath for 4 weeks and they were regarded as wet, while another 18 specimens were placed in a 65°C oven for 2 weeks to minimize the water content in the specimen and those specimens were regarded as dry. Chromium (Cr) was then deposited by sputterer as shown in Fig 5.6. Two targets were used during the deposition and hence the Cr deposition rate of 3 Å/s could be achieved. Three different Cr thicknesses were achieved, namely, 1 μm, 2 μm and 3 μm. For the thickest superlayer (3 μm), the deposition took about 3 hr to complete. Once the critical Cr thickness was reached, the SU-8 debonded from the wafer. The interfacial crack was initiated at the tip of the pre-crack (Au) and propagated along the interface between SU-8 and the wafer. Fig 5.3(c) shows the schematic diagram of epoxy-silica bonded system with a Cr superlayer on top after deposition.
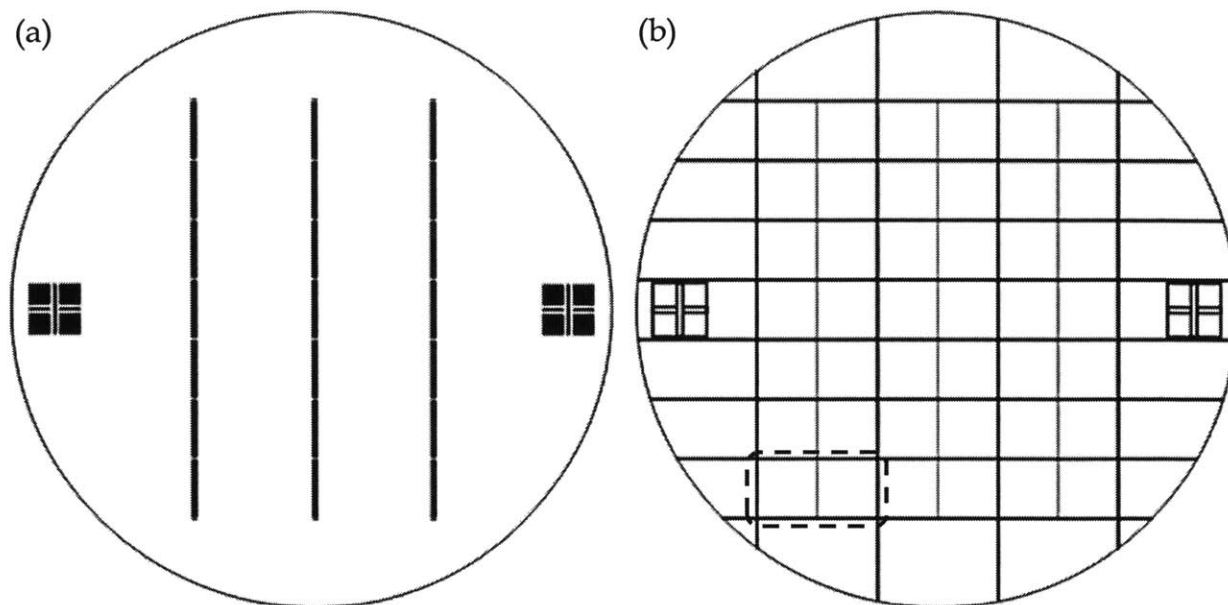
Fig 5.4 (a) Transparency mask for Au pattern with three 1 mm wide vertical black strips, (b) transparency mask for SU-8 pattern with 0.5 mm wide black darker lines and 0.2 mm wide black lighter lines. The diameter of both transparencies is 152.4 mm. The wafer was broken into 21 smaller pieces which were then coated by chromium. The rectangular box with red dash line indicates the size of the single specimen.
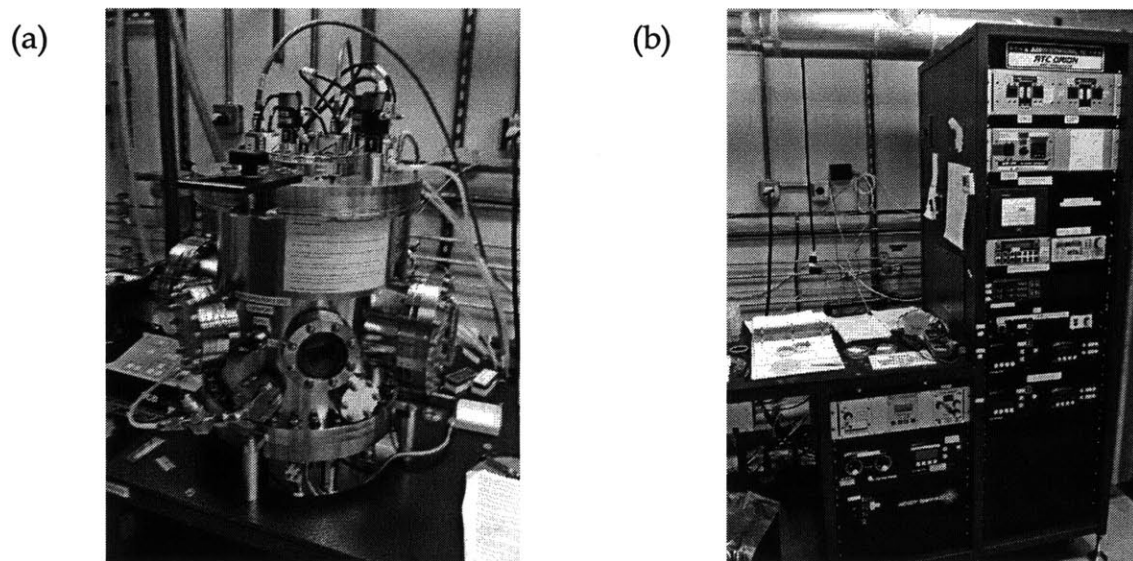
Fig 5.5 (a) Chamber of the sputter, (b) control panel of the sputter

5.4 Measurement of Residual Stress

The residual stress was measured by using a standard procedure that relies on determination of the film/substrate system (Stoney 1909). For this purpose, a profilometer is used to measure substrate curvature (Thomas et al. 1988). The profilometer uses a metallic stylus, which is horizontally scanned while its vertical movement is converted to an electrical signal. The substrate often has an initial curvature. Therefore, two scans are made in order to measure the radius of curvature of the substrate. These are made both with and without the film attached. The residual stress in the film is related to the measured radius of curvature by:

$$\sigma_R = \frac{E_s h_s^2 \kappa}{6 h_f (1 - v_s)} \tag{5.1}$$

where h_s is the substrate thickness, h_f is the film thickness, E_s, v_s are the substrate Young's modulus and Poisson's ratio respectively. This procedure is used to evaluate the residual stress in the SU-8 and then the residual stress in the Cr deposited onto the SU-8. The total stress, σ_{tot}, associated with both is

$$\sigma_{tot} = \sigma_{SU8} H_{SU8} + \sigma_{Cr} H_{Cr} = \sigma_{SU8} + (\sigma_{Cr} - \sigma_{SU8}) H_{Cr} \tag{5.2}$$

where H is the relative thickness, *i.e.* $H = h/(h_{SU8} + h_{Cr})$. Consequently, if the stresses are essentially independent of the film thicknesses, there would be a linear dependence of the total stress on the relative thickness, H. This approach was used to assess the experimental results.

Residual stress measurements have been performed on a batch of three samples with the same nominal SU-8 thickness (20 µm) and with three Cr thicknesses: 1 µm, 2 µm, and 3 µm. On each sample, five profilometer scans were made before and after depositing the film onto the substrate. A least square regression fitting to the data gave the measured radius of curvatures and their respective standard deviations. The film thickness was also obtained from the scans by making small scratches on the coated surface. The level difference measured by the profilometer indicated the film thickness accordingly. The stresses obtained in this manner are plotted in Fig 5.7. A linear fit appears to obtain, consistent with stresses in each separate layer being independent of thin film thickness as shown in Eq. (5.2). This fit indicates that the residual stresses in the SU-8 and Cr layers are 17 MPa and 1,248 MPa, respectively, with standard deviations ~5%. The former is consistent with the tensile strength of SU-8 films, and both values are within the range measured by others (Abermann 1992; Bagchi et al. 1994).
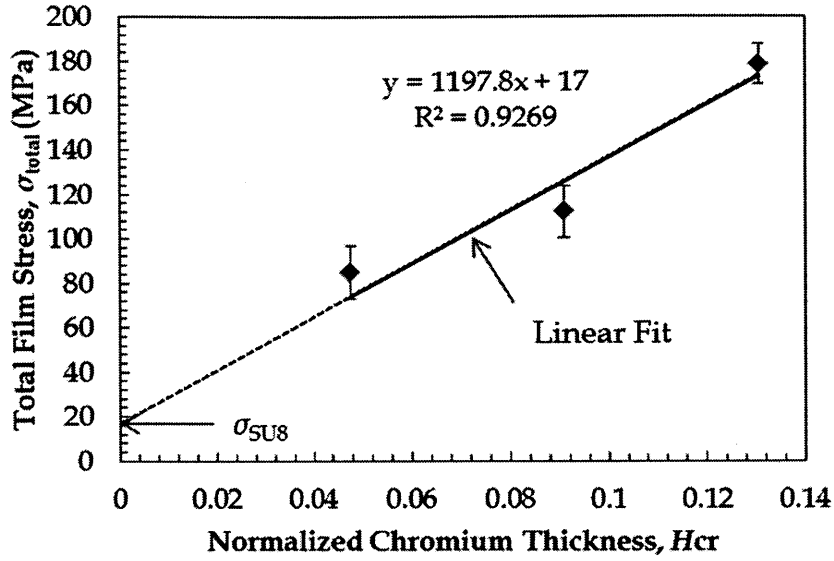
Fig 5.7 A plot of the total film stress with the normalized Cr layer thickness

5.5 Calculation of Interface Fracture Energy

The steady-state energy release rate, G_{ss}, control the interfacial debonding which motivated by residual stresses in deposited thin film layers when the interfacial flaw size, a_0, exceeds the film thickness (Hutchinson and Suo 1992). Moreover, since the film stress diminishes once the interfacial debonding occurs, this energy release behavior is entirely controlled by elasticity. For thin film system as shown in Fig 5.8, G_{ss} can be calculated by considering the strain energy far ahead and far behind the growing interfacial crack. It should be mentioned that the interfacial crack in the thin film/substrate system is propagating under the plain strain condition. If U_a and U_b denote the strain energies in the two volume elements having the width Δa as shown in Fig 5.8, then

$$G_{ss} = \frac{U_a - U_b}{\Delta a} \tag{5.3}$$

This result is valid provided that the substrate thickness is much larger than the film thickness. The element far ahead of the crack tip is in biaxial plane stress:

$$\sigma_x^i = \sigma_y^i = \sigma_i$$

$$\sigma_i = \frac{E_i}{1 - v_i} \varepsilon_i = E_i' \varepsilon_i$$

$$\sigma_z^i = \tau_{xy}^i = \tau_{yz}^i = \tau_{zx}^i = 0 \tag{5.4}$$

67

where σ_1, σ_2 are the residual stresses in the two layers, ε_1, ε_2 are the corresponding residual strains and E_i' is the biaxial modulus of the film layers. The elastic strain energy density associated with each layer (*i.e.* $i = 1,2$), per unit width, can be written as:

$$\frac{U_a^i}{h_i \Delta a} = \frac{\sigma_i^2}{E_i'}$$ (5.5)

Consequently, for a bilayer, the strain energy far ahead of the crack tip can be written as:

$$U_a = \sum_i U_a^i = \left(\frac{\sigma_1^2 h_1}{E_1'} + \frac{\sigma_2^2 h_2}{E_2'} \right) \Delta a$$ (5.6)
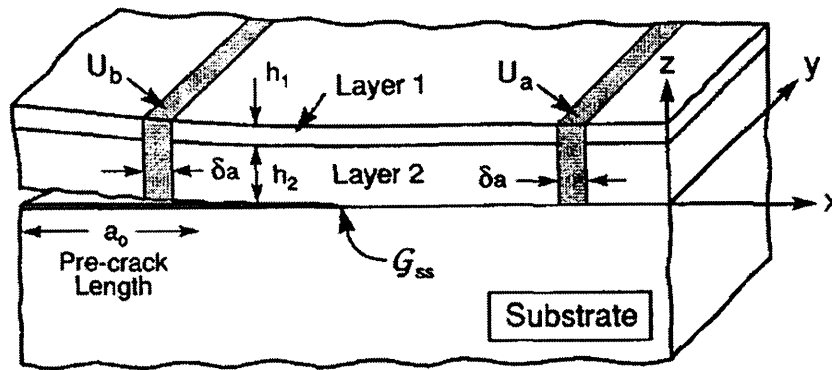
Fig 5.8 A schematic diagram showing the energy balance approach to find the strain energy release rate for a bi-layer thin film system (Bagchi et al. 1994)

Fig 5.9 shows the free body diagram of the bi-layer thin film system corresponding to the situation when both layers are under residual tensile stresses and $\varepsilon_1 > \varepsilon_2$. The film bends upward after decohesion in order to release the strain energy. The resultant stresses in each layer can be related to the forces, P_i, moments M_i, and curvature, κ, defined in Fig 5.11(b) as shown below (Timoshenko 1925):

$$\sigma_i(z) = \frac{P_i}{h_i} + \frac{zM_i}{I_i}$$

$$\frac{M_i}{I_i} = E_i' \kappa$$

$$I_i = \frac{h_i^3}{12}$$ (5.7)

where z denotes the vertical distance from the neutral axis in each layer, and I_i is the sectional modulus.

Based on the set of equations shown in Eq. (5.7), the strain energy far behind the crack tip can be written as:

$$U_b = \sum_i \frac{1}{E_i'} \left(\frac{P_i^2}{h_i} + \frac{M_i^2}{I_i} \right) \Delta a \tag{5.8}$$

(a)   (b)
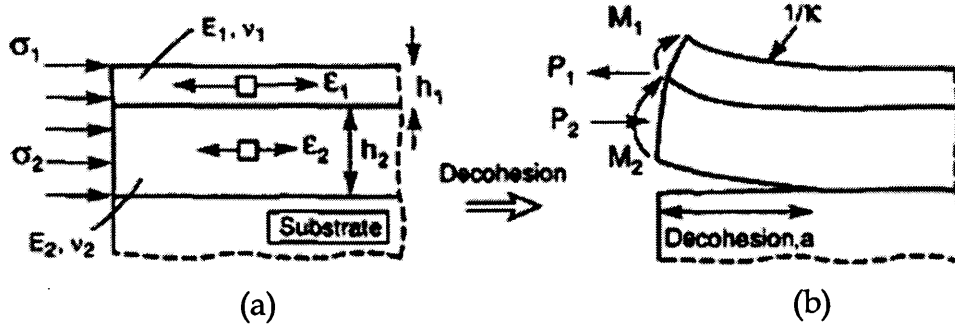
Fig 5.9 A schematic diagram showing the deformation of a bi-layer thin film system when subjected to residual tensile stresses, resulting in interfacial debonding. The stresses σ1 and σ2 (a) are the misfit stresses in the Cr (subscript i=1) and SU-8 (subscript i=2), which provide the forces, P_i, and the moments, M_i, in the bi-layer thin film system above the decohesion. The curvature of the debonded bi-layer thin film is κ (Bagchi et al. 1994).

At this stage, it is required to link up P_1, P_2, M_1, M_2 and κ to the residual tensile stresses (σ1 and σ2) and the film thickness (h_1 and h_2) which are the known parameters. This procedure involves five linear equations with five unknowns (*i.e.* P_1, P_2, M_1, M_2 and κ). Two equations are obtained from the consideration of equilibrium:

$$\sum_i P_i = 0 \rightarrow P_1 + P_2 = P$$

$$\sum_i M_i = 0 \rightarrow M_1 + M_2 = P\left(\frac{h_1 + h_2}{2}\right) \tag{5.9}$$

Another two equations are obtained from the consideration of geometry between the moments and the curvature:

$$M_1 = E_1' I_1 \kappa \text{ and } M_2 = E_2' I_2 \kappa \tag{5.10}$$

Finally, by considering the strain compatibility at the interface between Cr (subscript i=1) and SU-8 (subscript i=2), one more equation can be obtained:

$$-\varepsilon_1 + \frac{P_1}{E_1' h_1} + \frac{h_1 \kappa}{2} = -\varepsilon_2 - \frac{P_2}{E_2' h_2} - \frac{h_2 \kappa}{2} \tag{5.11}$$

Hence, an analytical solution for P ($P = P_1 = P_2$), M_1, M_2 and κ can be obtained:

$$M_i = E_i' I_i \kappa$$

$$P = \left[\frac{E_1' h_1^3 + E_2' h_2^3}{6(h_1 + h_2)} \right] \kappa$$

69

$$\kappa = \frac{6(h_1 + h_2)(\varepsilon_1 - \varepsilon_2)}{\left[h_1^2 + \dfrac{E_2' h_2^3}{E_1' h_1} + \dfrac{E_1' h_1^3}{E_2' h_2} + h_2^2 + 3(h_1 + h_2)^2 \right]} \qquad (5.12)$$

Substituting Eq. (5.6) and Eq. (5.8) into Eq. (5.3), together with the solved P, M_1, M_2, κ and the measured residual stress $\sigma 1$ and $\sigma 2$, the steady-state energy release rate is:

$$G_{ss} = \sum_i \frac{\sigma_i^2 h_i}{E_i'} - \sum_i \frac{1}{E_i'}\left(\frac{P^2}{h_i} + \frac{12 M_i^2}{h_i^3} \right) \qquad (5.13)$$

For a silicon wafer with thermal oxide layer coated by a 20 μm thick SU-8 film, the results are summarized in Fig. 5.10 and Fig 5.11. For the dry specimens, the bilayer remained attached to the substrate when the Cr superlayer was 1 μm thick. Conversely, when the Cr layer was either 2 μm or 3 μm thick, debonding occurred, followed by curling of the film as shown in Fig 5.12. Consequently, h_c was between 2 μm and 3 μm for the dry specimens. For the wet specimens, debonding occurred, followed by curling of the film, for all three tested Cr thickness (1 μm, 2 μm and 3 μm) and hence h_c is less than 1 μm for the wet specimens. After getting these values, together with the measured residual stresses as described in section 5.4, bounds for the interface fracture energy can be calculated using Eq. (5.13).

By introducing these values into the energy release rate formula for the bilayer as shown in Eq. (5.13), bounds are placed on the interface fracture energy. For this purpose, the elastic modulus of the film is needed. Generally, polycrystalline thin films can have a lower modulus than the bulk material, because of porosity at the boundaries of the columnar grains. Consequently, for completeness, independent measurement of E_f would be needed. Such measurements have not been performed completely in this study. The Young's modulus of SU-8 (E_2) was measured using the nanoindentation approach as mentioned in Chapter 4; while literature values of polycrystalline Cr thin films ($E_1 = 93$ GPa) is used instead (Janda 1986). With the chosen E_1 and E_2, the bounds on the interface fracture energy are 12.0 J/m² $\leq \Gamma_i \leq$ 24.5 J/m² for the dry specimens as shown in Fig 5.10. For the wet specimens, only the upper bound can be found based on the chosen Cr thicknesses (1 μm, 2 μm and 3 μm) and the results show that $\Gamma_i \leq$ 12.7 J/m² as shown in Fig 5.11. It is noticed that the interfacial crack does not separate SU-8 and silica in a clean manner; instead the interfacial crack propagates in a random zigzag path inside the SU-layer and remains closely to the interface. Such phenomenon is observed for both dry and wet specimens. Earlier study of concrete/epoxy interfaces indicated that Γ_i usually ranged between 10 and 20 J/m² for the dry case and between 5 and 10 J/m² for the wet case (Lau and Büyüköztürk 2010). Such consistency implies that using silica to substitute concrete in our molecular dynamics simulation and the corresponding multi-scale model is a reasonable approach. The measured interface fracture energy between the epoxy-silica system and the epoxy-concrete system are close to each other, probably because the nature of the interfacial bonding of these two

system is similar, which is dominated by the non-bonded and non-directional van der Waals forces and Coulombic interaction.

Dry Samples
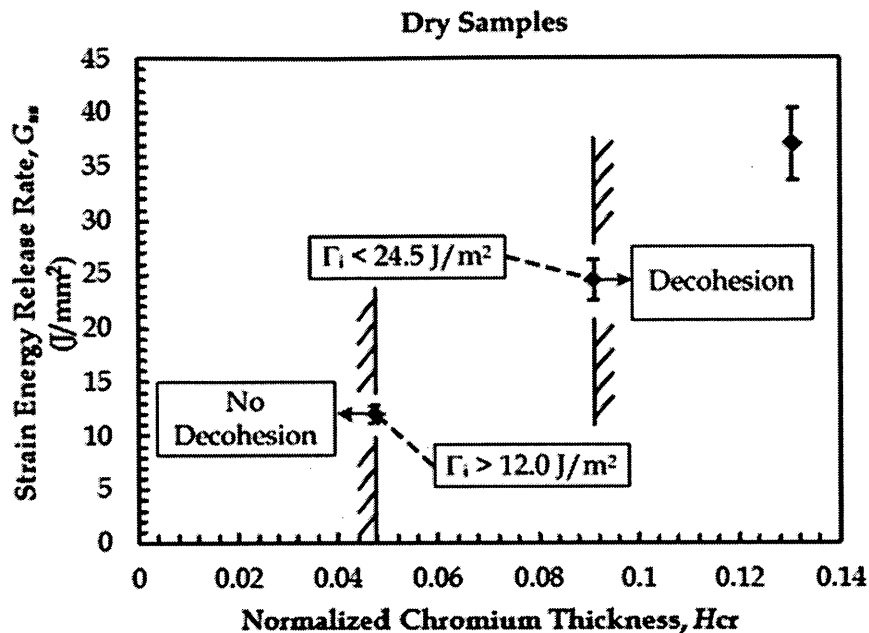
Fig 5.10 A plot of the calculated energy release rates with the normalized Cr layer thickness. The red lines show the lower and upper bounds that the critical energy release rate of epoxy-silica bonded system in dry condition.

Wet Samples (4 weeks)
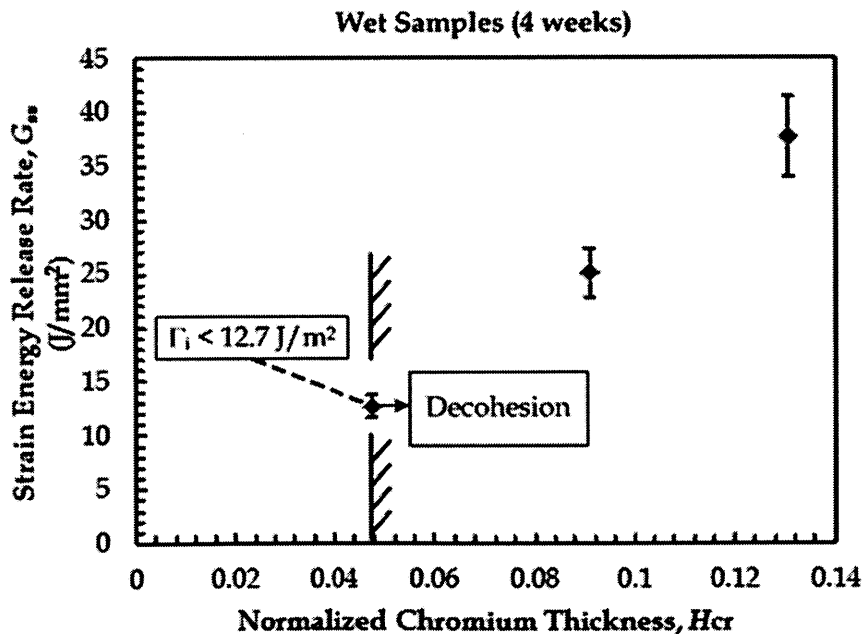
Fig 5.11 A plot of the calculated energy release rates with the normalized Cr layer thickness. The blue lines show the upper bound that the critical energy release rate of epoxy-silica bonded system after 4 week moisture conditioning.

71
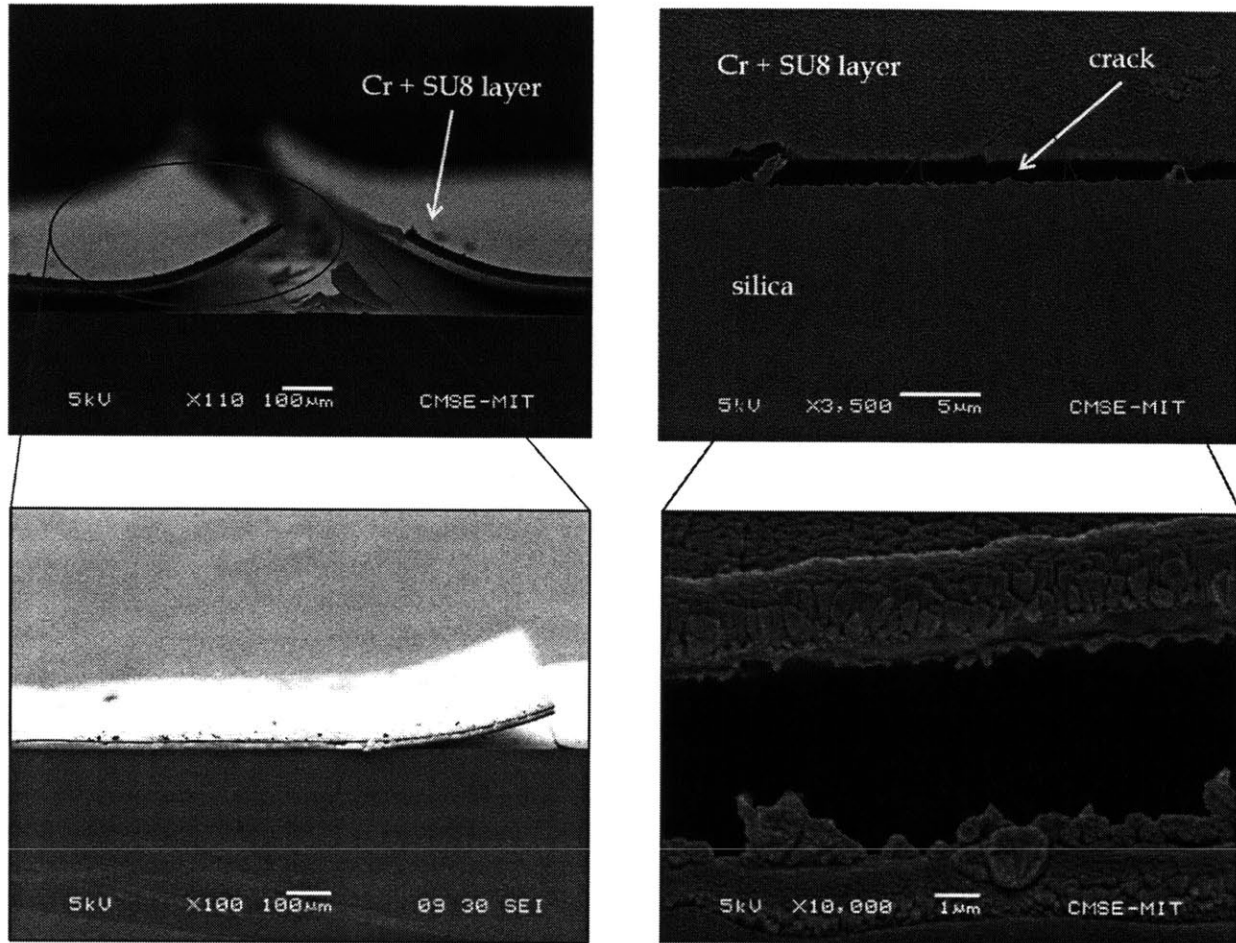
Fig 5.12 Scanning electron microscopy (SEM) of the epoxy-silica bonded system with Cr superlayer. (a) interfacial debonding was observed when the Cr thickness is 3 μm, (b) a cross section of the specimen with 3 μm thick Cr superlayer, (c) a SEM was taken with a magnification ×3,500 at the vicinity of the interfacial crack tip was taken, (d) a more detailed SEM with magnification ×10,000 was taken at the debonding surfaces. It is noticed that the interfacial crack does not separate SU-8 and silica in a clean manner; instead the interfacial crack propagates in a random zigzag path inside the SU-8 layer and remains closely to the interface. Such phenomenon is observed for both dry and wet specimens.

5.6 Summary Comments

The superlayer test for quantifying the interface fracture energy between epoxy (SU-8) and silica has been conducted successfully. In this micro-scale characterization, it is noticed that moisture has significant effect on the interface fracture energy of the epoxy-silica bonded system. Instead of finding an exact value of the interface fracture energy, the experiments using the Cr superlayer enable us to confine the range of the actual interface fracture energy with high fidelity. By considering the upper and lower

bounds of the interface fracture energy for both the dry and wet specimens, it is suspected that the interface fracture energy of epoxy-silica bonded system can decrease down to 50% of its original value in the presence of water. Our measured interface fracture energy of the epoxy-silica bonded system is in line with the literature values of the epoxy-concrete bonded system. Such consistency implies that using silica to substitute concrete in our molecular dynamics simulation and the corresponding multi-scale model is a reasonable approach. The measured interface fracture energy between the epoxy-silica system and the epoxy-concrete system are close to each other, probably because the nature of the interfacial bonding of these two system is similar, which is dominated by the non-bonded and non-directional van der Waals forces and Coulombic interaction. In the next chapter, the interface fracture energy of the epoxy-silica bonded system will be quantified using the molecular dynamics simulation approach such that the free energy profiles describing the debonding process under both dry and wet conditions can be reconstructed through the metadynamics approach as mentioned in Chapter 3.

6.1 Background on the Multiscale Modeling Approach

When studying the deformation behavior of materials, multiscale analysis is in general necessary because there are many factors causing the difference in mechanical properties measured at various length scales. For example, the change of deformation mechanisms across different length scales leads to the change of mechanical properties accordingly. Also, the disparity in time- and length-scales inherited in the molecular dynamics simulation leads to the discrepancies between nano-scale predicted mechanical properties and the experimental measurement conducted at longer time- and length-scales. Although there are several examples where mechanical properties from molecular simulations match reasonably well with those measured experimentally at larger scales, such as the properties in ideal gases, defect-free crystalline structure, it is definitely necessary to connect the atomistic level to macroscale such that a prediction on mechanical properties using a bottom-up approach becomes feasible for a majority of materials.

6.2 Cohesive Zone Model

Bi-layer material systems are found in various engineering applications ranging from nano-scale components, such as thin films in circuit boards (Nied 2003), to macroscale structures, such as adhesive bonding in aerospace and civil infrastructures (Higgins 2000; Teng et al. 2001). They are also found in many natural and biological materials. The structural integrity of a bi-layer system depends on properties of both the interface and the constitutive materials. In particular, interfacial delamination has been observed as a major integrity issue. Standard implementations of cohesive zone model (CZM) are available in several commercial finite element analysis packages and CZM has been used to successfully study fracture process in polymers, metals, bi-material systems, and fiber reinforced polymer composites (Espinosa et al. 2000; Rahulkumar et al. 2000; Siegmund and Brocks 2000; Jin and Sun 2005; Chen and Mai 2010).

As discussed in Chapter 3, CZM was first introduced as a technique to study fracture or void nucleation in quasi-brittle materials such as ceramic and concrete. It was developed upon the concept of cohesive zones proposed by (Dugdale 1960) and (Barenblatt 1962). CZM collectively describes all the mechanisms related to fracture, such as plastic deformation, void growth, and crack coalescence, in the process zone ahead of the crack tip as shown in Fig 6.1. With the advancement of finite element method, CZM has become a popular tool for studying fracture process because of its easy implementation in a finite element code. During modeling, a layer of cohesive elements is located along a potential crack path, usually as an extension from an

existing crack tip. When normal or shear stress (or crack opening displacements) reaches the critical values (t_n^0 for maximum normal stress or t_s^0 for maximum shear stress), damage is initiated in the material modeled with cohesive elements. Damage causes the material to lose its load-bearing capacity, which results in decreasing stress or softening behavior. The manner in which stress decreases during this stage is governed by a given traction-separation relation as shown in Fig 6.2. Widely used softening behaviors are a simple linear curve and an exponential curve, while more complex softening curve may be required for certain types of problem (Needleman 1987; Rice and Wang 1989; Needleman 1990a; Needleman 1990b; Tvergaard 1990; Tvergaard and Hutchinson 1992; Xu and Needleman 1993; Camacho and Ortiz 1996; Geubelle and Baylor 1998). The linear curve of the traction-separation relation was assumed to describe the behavior of epoxy-silica interface in Chapter 3 for the concern of simplicity. In fact, an accurate characterization of specific material interfaces with detailed traction-separation relations has only been accomplished on a limited scale and generally calibrated with results from micromechanical modeling or experimental result from fracture specimens of various configurations, which may be found in (Karbhari and Engineer 1996; Elices et al. 2002; Qiao and Xu 2004; Au and Büyüköztürk 2006a; Frigione et al. 2006; Ouyang and Guoqiang 2009). Recently, there are various empirical approaches in quantifying the traction-separation relation for bi-layer material systems have been proposed when experimental data is not available (Ferracuti et al. 2007; Wang 2007; Subramaniam et al. 2008). However, the limitation of these empirical approaches is the lack of scientific support in explaining the interaction between two materials at the interfacial region from the physics and chemistry point of view.
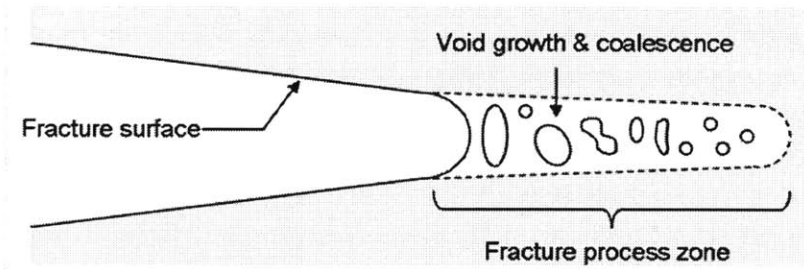
Fig 6.1 Fracture process zone ahead of a crack tip

The derivation of the traction-separation relation using either experimental or empirical approaches is generally confined in a large length scale. The values of strength and toughness that are input to the CZM represent the responses of millions of atoms in the constitutive materials, and the defects within the specimens from which they are obtained. Hence, these macro-scale values do not represent the unique response of a particular interface at which a local fracture event might occur. If the small length scale predictions are to become quantitative, consideration of the local nano-scale properties is required. One possible means of making this connection is to use atomistic approach to quantify the traction-separation relation at the interface as input to the CZM (Yamakov et al. 2006; Zhou et al. 2009; Krull and Yuan 2011). This

connection allows more realistic simulations leading to accurate predictions of the failure properties of a large class of materials and microstructures. Meanwhile, this approach is able to describe the interactions among various atoms at the interfacial region and does not require any experimental data in the derivation process.
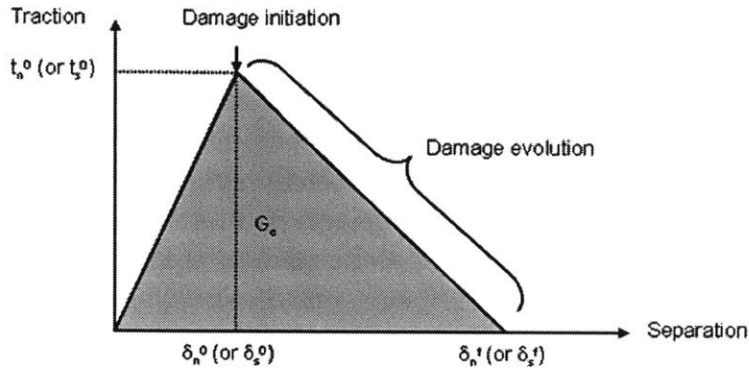
Fig 6.2 Elastic Traction-Separation Law with Linear Damage Evolution

The objective of this chapter is to provide an atomistic approach to quantify the traction-separation relation of the epoxy-silica system through the understanding of the change of the free energy during the interfacial debonding process with the consideration of moisture effect. The traction-separation relation derived by this method is no longer empirical, but based on the actual free energy change during the interfacial debonding process. Eventually, a multiscale model is proposed which can link the result from the molecular dynamics simulation to the finite element modeling through the CZM, which is similar to that described in Chapter 3. The method used here also provides a better understanding on how the nano-mechanical properties are deliverable to material properties in macro-scales.

6.3 Derivation of Traction-Separation Relation

In the nano-scale study, an atomistic model is constructed for quantifying the nano-mechanical properties of the bonded system using a free energy approach. The construction of a reliable free energy surface has always been a challenging task until recently, there is a method using metadynamics which is capable in reconstructing the entire free energy profile and is compatible with many existing molecular dynamics codes. The details of metadynamics have been described in Chapter 3. Here, the application of the reconstructed free energy profile is further extended to characterize the free energy surface with the consideration of the moisture effect. The success in reconstructing the free energy profile enables us to track the energy change of the system along the reaction coordinates, and leads to the accurate prediction of various mechanical properties from the energy point of view, including the debonding stress and the interface fracture energy as mentioned in Chapter 3. The approach described in

this chapter enable us to conduct a direct derivation of the traction-separation relation of the bonded system based on the reconstructed free energy surface, such that the entire shape and the critical values of the traction-separation relation can all be obtained. In what follows, the steps in deriving the traction-separation relation, starting from the atomistic model, will be described using epoxy-silica system as an example.

The atomistic model consists of a slab of crystalline silica (SiO_2) and a single chain of epoxy which is similar to that in Chapters 2 and 3. The atomistic model used in this chapter is based on the one developed in Chapter 3. The size of SiO_2 substrate is the same as that described in Chapter 3 and consists of 4,749 atoms. The epoxy employed in this study is still the diglycidyl ether of bisphenol A (DGEBA) with only one repeating unit and consists of 49 atoms. In order to study the moisture effect on the epoxy-silica bonded system, a water box consisting of 45843 atoms is used to surround the epoxy-silica bonded system. Three-site water models are commonly adopted in molecular dynamics simulation because of their simplicity, computational efficiency, and yet a fairly accurate prediction can be made. They have three interaction sites, corresponding to the three atoms of the water molecule. Each atom gets assigned a point charge, and the oxygen atom also gets the Lennard-Jones (LJ) parameters. Commonly used three-site water models are TIP3P (transferable intermolecular potential 3P) (Jorgensen et al. 1983; Neria et al. 1996), SPC (simple point charge) (Berendsen et al. 1981; Berweger et al. 1995) or SPC/E (extended simple point charge) (Berendsen et al. 1987). These three water models are similar in nature, but the LJ and Coulombic terms differ and give significant differences in calculated bulk properties for liquid water. The water model used here is TIP3P. The 104° H-O-H angle in TIP3P has slightly better structural and thermodynamic properties when compared with SPC or SPC/E models. Based on the prior work on epoxy-silica system shown in Chapters 2 and 3 in which CVFF was used to govern the interaction between epoxy and silica, the non-reactive forcefield CVFF is used to govern the interactions between epoxy and silica in the presence of water. It should be emphasized that the breaking of bonds of interest here are weak bonds, not covalent, which can be described with CVFF. Also, by using the non-reactive forcefield CVFF, it is understood that the partial charges in the system do not change in the entire molecular dynamics simulation process. Although the partial charges along the interface may not be accurately described in the entire debonding process by using CVFF, the case demonstrated in this chapter is based on the prior work (Büyüköztürk et al. 2011; Lau et al. 2012a). The partial charge calculation, the energy minimization and the equilibration of the system were conducted as those described in Chapters 2 and 3.

After setting up the atomistic model, the free energy surface (FES) of the epoxy-silica system from an attached stage to a detached stage is then reconstructed by the metadynamics approach as described in Chapter 3 (Laio and Parrinello 2002; Laio and Gervasio 2008). FES for both dry case (without waterbox) and wet case (with waterbox) are reconstructed. Similar to what have been described in Chapter 3, the distance between the center of mass (CM) of the epoxy chain and the silica surface is chosen to

be the independent variable for monitoring the free energy of the system in this study for both dry and wet cases. It should be mentioned that the simulation time for the wet case can take up to couples of week because of the enormous amount of water molecules. In fact, in most of the simulations conducted in bio-engineering field, they are required to be done in a water surrounded environment because most of the bio-molecules are unstable in vacuum condition. In these simulations, most of the computational power is used for simulating the movement of water molecules and hence parallel computing is usually preferable in order to shorten the actual time required in the simulation.

Fig 6.3 shows the reconstructed FES of the epoxy-silica bonded system under both dry and wet cases. The result from molecular dynamics simulation shows that there is a severe reduction of the adhesion energy. It should be mentioned that the energy barrier measured during the entire simulation process (*i.e.* the free energy difference between the attached and detached states) is equal to the adhesion energy. This reduction trend is in line with the observation from the peel and shear fracture tests (Au and Büyüköztürk 2006b; Tuakta and Büyüköztürk 2011b), and the sandwiched beam fracture tests (Lau and Büyüköztürk 2010), which were conducted using concrete as a substrate at the meso-scale level. In order to make sure that silica can be used as a representative of concrete in the molecular dynamics simulation, peel tests on FRP-epoxy-silica bonded system have also been conducted. The configuration of this peel specimen was the same as the FRP-epoxy-concrete bonded system as shown in Fig 3.7. There were two groups of specimens in this peel test. One group was regarded as "dry" in which they were conditioned in standard laboratory condition (without water bath) for 4 weeks; while the other group was regarded as "wet" as the specimens were moisture-conditioned in a water bath for 4 weeks. Fig 6.5 shows the measured load-displacement curves for both dry and wet cases and a severe deterioration due to the effect of moisture can be clearly observed, which is very similar to the observation from the epoxy-concrete system. Such agreement indicates that the moisture effect is down to the nano-scale level and the adhesion governed van der Waals forces and Coulombic interactions is serious weakened in the presence of water as demonstrated in the molecular dynamics simulation. Also, the assumptions of no covalent bond breaking and the unchanged partial charges during the debonding process are good engineering approaches to tackle this complex debonding problem. After having obtained the FES of the epoxy-silica interface under both dry and wet cases, the traction-separation relation can be evaluated by considering the first derivative of the FES, which is then used as a direct input for the CZM in the finite element modeling (Lau et al. 2012b). The entire derivation process is schematically shown in Fig. 6.4. The structural behavior of larger-scale structures can then be predicted at the continuum level via finite element simulation using the same approach as described in Chapter 3.
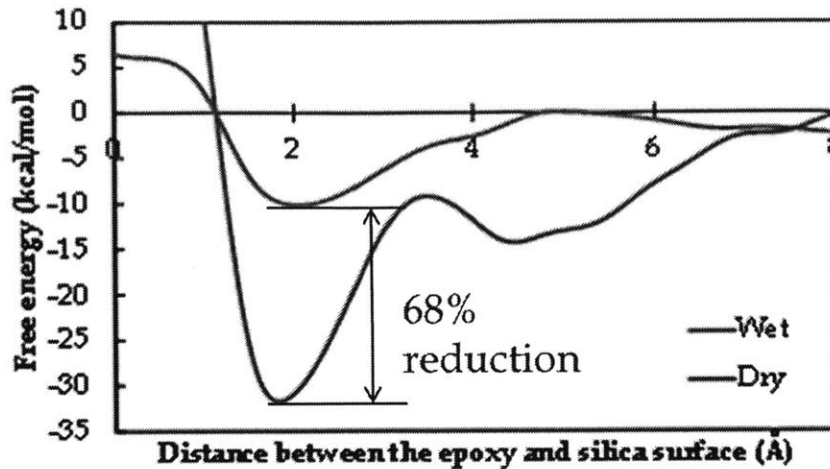
Fig 6.3 The reconstructed FES for both dry and wet cases using metadynamics approach (Laio and Parrinello 2002; Laio and Gervasio 2008). The minimum point in the FES is the equilibrium state of the epoxy-silica bonded system referring to the attached stage. A 68% reduction in term of the free energy is recorded. This free energy difference indicates that the epoxy-silica bonded system is much more vulnerable against the debonding process because the energy barrier between the attached and the detached states reduces significantly as shown in the reconstructed FES.
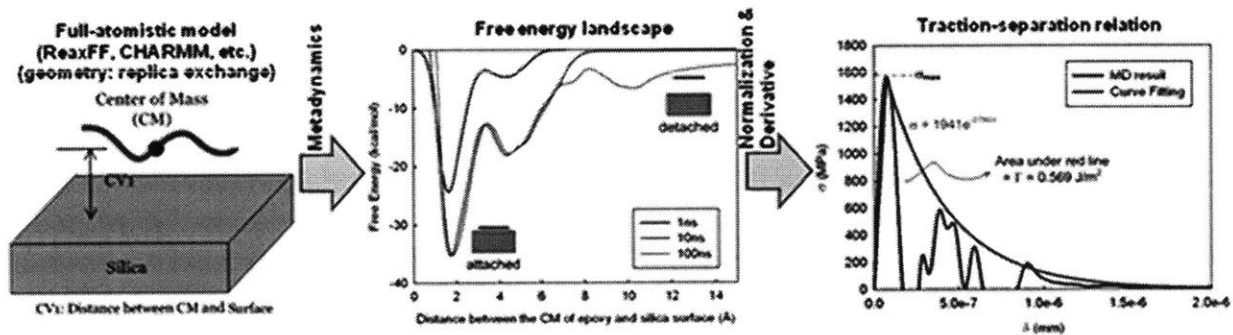
Fig 6.4 Illustration of the process of using MD simulation (left) to determine the free energy landscape (center) using advanced MD methods such as Parrinello's metadynamics (to sample for rare events while reconstructing the FES), to identify the traction-separation relation that can be directly fit to continuum CZM models.
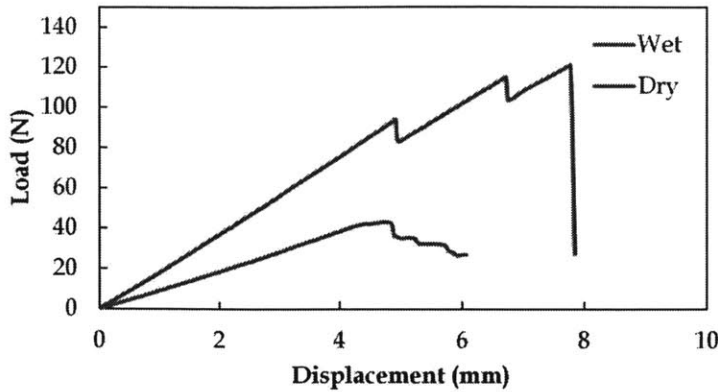
Fig 6.5 The load-displacement curves of FRP-epoxy-silica system for both dry and wet cases. There is severe deterioration due to the presence of water. Both the stiffness and the maximum load capacity in such bonded system reduce significantly under the effect of moisture.

Based on the reconstructed FES as shown in Fig 6.3, the traction-separation relation for both dry and wet cases are evaluated as shown in Fig 6.6. Curve fitting are also conducted for the ease of implementation in the finite element modeling. For the dry case, the curve fitting is done in a way such that the pre-peak region is linear, while the post-peak region is described by the exponential fit. For the wet case, a bi-linear curve fitting is conducted accordingly. It should be mentioned that the area under the traction-separation relation refers to the interface fracture energy and hence the area under the blue dotted curve is about one third of the area under the red dotted curve as shown in Fig 6.6.
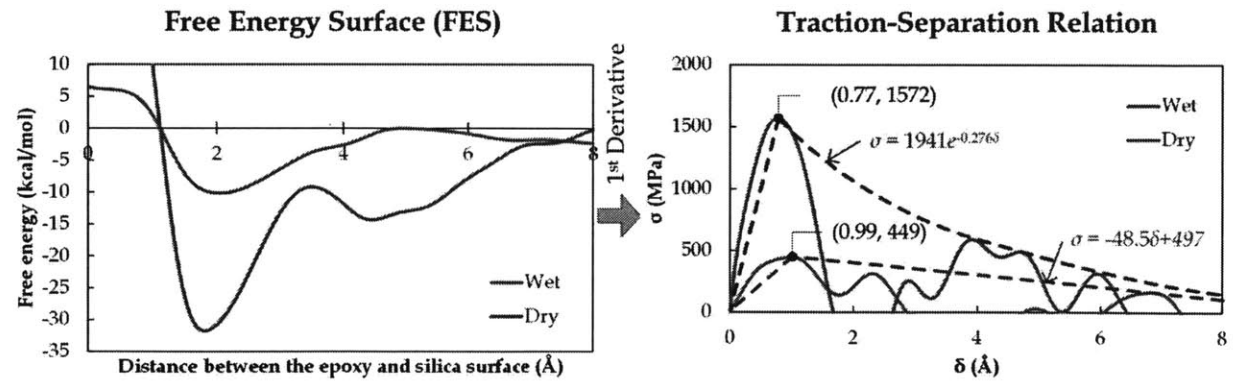
Fig 6.6 The traction-separation relation can be obtained by considering the 1st derivative of the FES with respect to the interface separation (δ).

6.4 Summary Comments

The free energy surfaces of the epoxy-silica bonded system under both dry and wet case have been reconstructed using the metadynamics approach. A 68% reduction

in the adhesion energy is measured in the molecular dynamics simulation which is in line with the meso-scale tests conducted using FRP-epoxy-concrete specimens, as well as the FRP-epoxy-silica specimens. It should be mentioned that such reduction reported in this chapter is more than the value reported in Chapter 2 and is more reliable because the maximum force used in the Bell model is subjected to a high fluctuation in general. The results from the molecular dynamics simulation imply that silica is a good representative of concrete at the nano-scale for studying the structural behavior of the interface mainly governed by van der Waals forces and Coulombic interactions. On one hand, the reconstructed free energy surface can be used to quantify various mechanical properties (*e.g.* interface fracture energy). On the other hand, it can be converted to traction-separation relation by considering the 1st derivation of the free energy surface with respect to the interface separation, which is particularly useful for the multiscale modeling of interface because the evaluated traction-separation relation can act as a bridge between the atomistic level and the continuum regime. The multiscale approach involves the implementation of finite element modeling using the traction-separation relation derived from the atomistic perspective, such that the information from the nano-scale can be passed to the macro-scale. With this multiscale approach, the global structural behavior of epoxy-silica interface can be predicted by applying cohesive elements with an appropriate mesh in the finite element model as demonstrated in Chapter 3. The use of metadynamics for reconstructing the free energy surface of a bonded system is an efficient method in finding the interface fracture energy and it has a great potential to be broadly applied in many other engineering application involving interface, in particular, the cell adhesion on inorganic substrate.

Chapter 7
Summary, Conclusions and Future Work

The objective of this research is to develop a methodology to apply molecular dynamics simulation to the study of interface fracture in bi-layer material systems with and without moisture effect. This research consists of a number of experimentations and computational simulations. An experimental program for characterization of nano-scale bulk material properties and the interface fracture energy of epoxy-silica bonded system was conducted with the consideration of moisture effect. Molecular dynamics simulation was performed to study how water molecules affect the adhesion between epoxy and silica at a nano-scale. In addition, to extend the applicability of molecular dynamics simulation to meso-scale structure, a multiscale analysis technique, which is capable to link the molecular dynamics simulation and the finite element modeling, was proposed.

7.1 Summary

The structural integrity of bi-layer material systems has been investigated comprehensively through both experimental and computational approaches, using an epoxy-silica bonded system as an example. The moisture effect on various mechanical properties of the epoxy-silica system including the bulk material properties and the interface fracture energy has been studied using nanoindentation and superlayer approaches. Even though moisture has little effect on the bulk material properties, it results in a detrimental effect on the interface fracture energy eventually leading to premature failure of the bonded system, causing a durability problem. Superlayer approach is known to be able to quantify the interface fracture energy with high fidelity over a range of phase angle. Using this approach, the upper and lower bounds of the interface fracture energy in the epoxy-silica system can be measured accurately. It is observed that the interface fracture energy decreases significantly after 4 week moisture conditioning with approximately 50% reduction of the measured upper bound. The morphology of material in the vicinity of the interface has also been captured using the scanning electronic microscope (SEM). It is noticed that the interfacial crack does not separate SU-8 and silica in a clean manner; instead the interfacial crack propagates in a random zigzag path inside the SU-8 layer and remains closely to the interface. Such phenomenon is observed for both dry and wet specimens. In order to understand the moisture effect in a more comprehensive way, the free energy profile of the epoxy-silica bonded system describing the debonding process has been reconstructed for both dry and wet conditions and it is noticed that the adhesion between epoxy and silica, which is dominated by the van der Waals force and Coulombic interaction, can be weakened significantly (more than 68% reduction) in the presence of water. Both the

experimental and computational results show that water plays the main role in the interfacial deterioration. The interfacial deterioration can be explained using molecular dynamics simulation and a multiscale model of the epoxy-silica bonded system is presented which is capable in predicting the macro-scale structural behavior based on the reconstructed free energy profile of the bonded system at the nano-scale. The reconstructed free energy profile of the epoxy-silica system derived from the molecular level is used to quantify the traction-separation relation at epoxy-silica interface, which is a necessary property for defining the cohesive zone model used in the finite element modeling. This technique can be applied to model a general organic-inorganic system that primarily features non-bonded and non-directional van der Waals and Coulombic interactions. The prediction from our multiscale model shows a good agreement with experimental data of the interfacial fracture toughness. The multiscale modeling used in this research provides a powerful new approach to link nano to macro for complex material systems.

7.2 Conclusions

This thesis research has shown that water molecules can have detrimental effects on epoxy-silica bonded systems. Although the bulk material properties of the constituent materials are not affected much by the presence of water at the nano-scale perspective, the interface fracture energy can reduce by 68% under the effect of moisture based on the simulation result, leading to the premature failure observed at the macro-scale.

Fracture mechanics approach implemented in finite element analysis using the cohesive zone model (CZM) has proven to be a useful tool to link the molecular dynamics simulation and the finite element modeling together for investigating the debonding behavior of epoxy-silica bonded system. Such multiscale approach is capable of predicting the global structural behavior of the epoxy-silica interface based on the traction-separation relation derived from the molecular dynamics simulation.

As FRP-retrofitted concrete structure is one of the major examples in civil infrastructure that involves epoxy-silica interface, where silica is a good representative of concrete at nano-scale as demonstrated in various simulations in this thesis, it is recommended that special attention should be paid when strengthening or retrofitting existing concrete structures using FRP. Protection of the epoxy-concrete interface against moisture should be provided while the strengthened/retrofitted structures can be designed according to the design guideline which is based on the short-term experimental results.

The studies in this thesis contribute towards the understanding of debonding mechanisms in epoxy-silica bonded system with the consideration of moisture effect. In particular, the intellectual contributions of this thesis are stated as follows:

83

➢ Advance multi-disciplinary areas of fracture mechanics experimentation, molecular dynamics simulation, durability mechanics, and multiscale modeling of material and structure.

➢ Provide scientific knowledge, as well as expanded quantitative and qualitative information on moisture-affected deterioration at organic-inorganic interface, using epoxy-silica bonded system as an example.

➢ Provide a multiscale model for analyzing macro-scale structural behavior of epoxy-silica interface based on the measured nano-scale mechanical properties from molecular dynamics simulation, which can be integrated into the design guideline as a preliminary safety check of the civil infrastructures involving epoxy-concrete interfaces.

➢ Enhance our understanding of interface in bi-layer material systems and how interfacial properties play an important role in the debonding problems by observing the physical movement of the atoms and their interactions in molecular dynamics simulation.

It is believed that this thesis research will have a direct impact on professional practices because organic-inorganic interfaces exist in many natural and synthetic material systems and it is always the common goal in various engineering fields to improve the structural integrity of such interface. From the civil engineering perspective, the findings and methodology developed in this thesis research will form the basis for future qualitative and quantitative assessment of the behavior of epoxy-concrete system, and for the development of design guideline involving strengthening and retrofitting of existing concrete structures using advanced composite materials.

7.3 Future Work

7.3.1 Meso-scale coupled stress-diffusion

In a service condition, strengthened concrete structures are subjected to mechanical and environmental stresses simultaneously. The studies on the durability of FRP-bonded concrete system reported in this thesis have not addressed the problem of stress-coupled deterioration. However, a preliminary work reported in (Tuakta and Büyüköztürk 2011a) was conducted. In this preliminary investigation, fracture tests on peel specimens under coupled moisture diffusion and stress were conducted. In all concerned levels of sustained load, there was a brief jump in deflection during the first few hours, which could be attributed to instantaneous microcracking in the epoxy. The deflection then increased in small magnitudes owing to the creep effect in the bond line. This effect is significantly pronounced in specimen under high intensity of sustained load at high temperature. On the other hand, the effect of coupled stress-diffusion on bond strength was not obvious under low stress intensity. Such effect of sustained stress coupled with moisture diffusion can further degrade the strength of FRP-concrete interface leading to premature failure at load levels much lower than prediction. The

84

effect of sustained load on interface fracture toughness in a specimen under moisture effects needs to be further studied for the implementation in long term performance model to take into account the effect of stress-diffusion coupling.

7.3.2 Atomistic model describing concrete

The development of the reactive force field (ReaxFF) core model of concrete, which is capable in describing the possible reaction inside concrete, is essential for a more accurate atomic model. The development process will require the knowledge in quantum mechanics (QM). Observables to be included in the force field training set are bond order, valence angle, torsion angle, heat of formation, and Mulliken charge distribution. Successive optimization should be conducted in order to find optimal ReaxFF parameters that fit the training set. Fig 7.1 is a schematic diagram showing all these simulation approaches against different length scales.
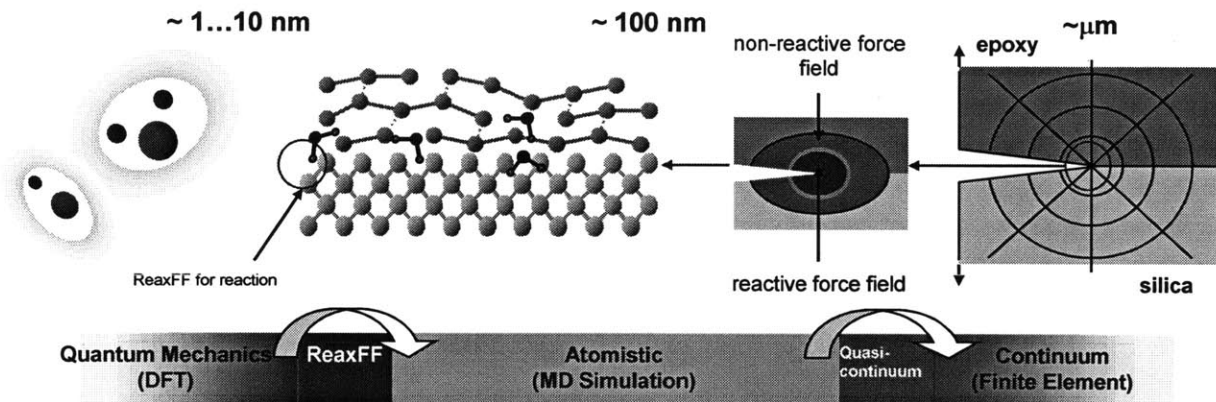
Fig 7.1 Multiscale simulation involving QM, ReaxFF, MD simulation and finite element modeling

7.3.3 Finite element modeling coupled with molecular dynamics

In practice, the length scale of structural models is much larger than that of the atomistic models. In order to implement the fundamental knowledge of local interface behavior in the entire model of the structural system, molecular dynamics (MD) modeling should be coupled with the conventional finite element modeling (FEM). Due to the limitation of MD modeling on both length and time scales, bridging between MD and FEM needs to be established. In a multi-scale simulation framework, this would allow the exchange of information between atomistic and continuum regions. This process, in most cases, takes place in a region called hand-shaking region, which interconnects the two descriptions of materials. The location of atoms in this specialized region usually coincides with the nodes of finite elements adjacent to the atomistic region. The size of the interface region must ensure that information can be transferred seamlessly between the two regions. A conceptual description of various length scales and relationship of atomistic to continuum approaches is given in Fig 7.2.

~ 0.1 nm

~ 1000 m

Hand-shaking region
~ 1 - 100 μm

~ 1 m

~ 10 nm

~ 1 mm

~ 100 nm

☐ Finite Element
○ Atom
– Bond

Atomistic Approach

Continuum Approach

Hybrid Atomistic/
Continuum Approach
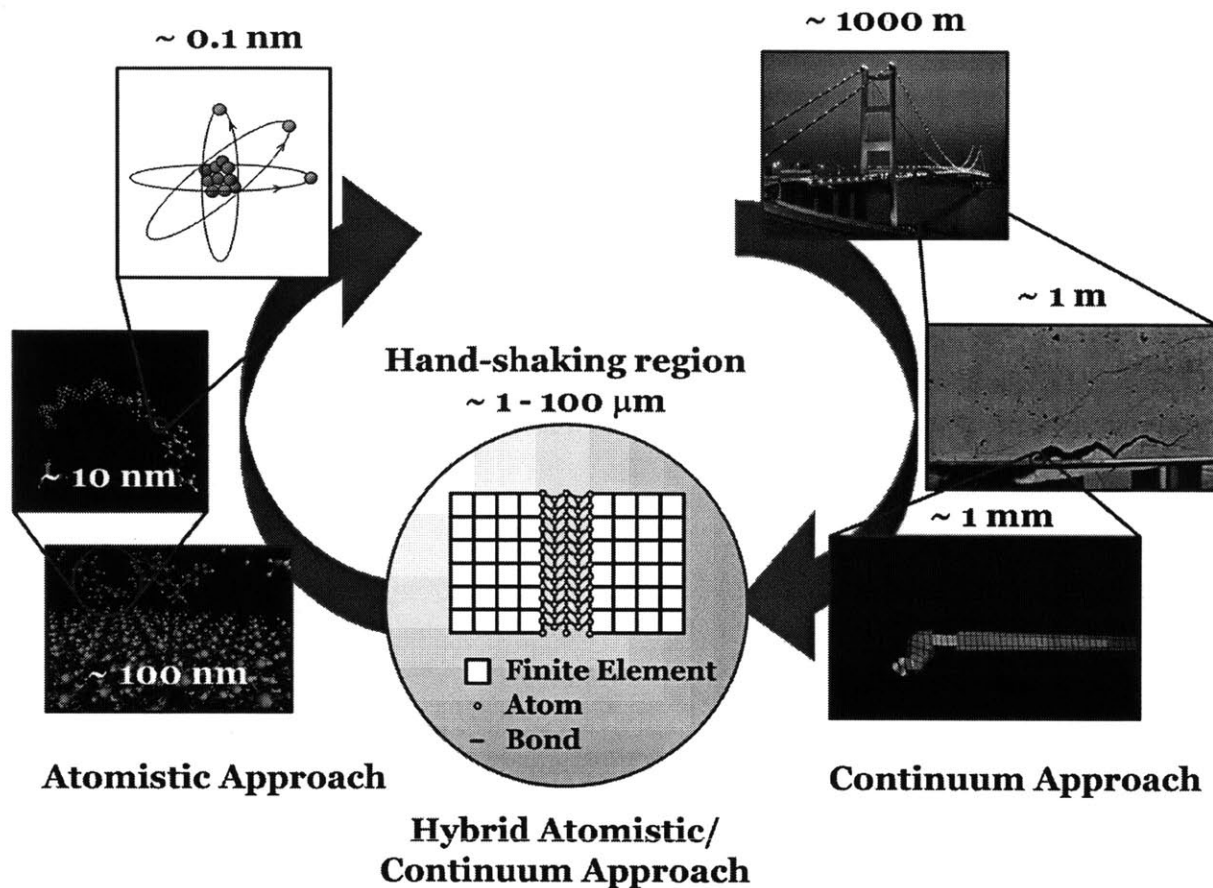
Fig 7.2 Atomistic and continuum approaches connected in the hand-shaking region (Büyüköztürk et al. 2011)

Several techniques have become available to bridge FEM and MD (Nakano et al. 2001; Fish 2006; Liu et al. 2006). The main objective of these techniques is to avoid wave reflection at MD and FE interface. A concurrent coupling technique based on the idea of quasicontinuum method is found to be suitable in bridging the atomistic and continuum paradigms. This technique reduces the degree of freedoms in the atomistic region by employing the Cauchy-Born (CB) rule, which postulates that a uniform deformation gradient at the macro-scale can be mapped to the same uniform deformation at atomistic scale (Klein and Gao 1998; Miller and Tadmor 2002). It is noted that the FEM internal force can be obtained using the CB hypothesis in conjunction with the atomistic forces utilizing the same interatomic potential. The connection between the FEM equations of motion can be achieved if a CB continuum model is used and the FEM mesh is meshed down to the atomic spacing. A correction can be made to the CB rule to account for non-uniform deformation in some materials (Tadmor et al. 1999; Zhang et al. 2002) and free surfaces when extracting information at continuum scale (i.e. force and energy) from representative atoms in the atomistic region and subsequently performing energy minimization (Park et al. 2006; Park and

Klein 2008). This will allow seamless information transfer between FEM and MD regions because, unlike other techniques, no boundary will be present between them.

Abermann, R. (1992). Thin films: stresses and mechanical properties III. Materials Research Society Symposium Proceeding, Pittsburgh, PA.

ACI440.2R-08 (2008). Guide for the design and construction of externally bonded FRP systems for strengthening concrete structures. Michigan (U.S.A.), American Concrete Institute (ACI), Committee 440.

Ackbarow, T., Chen, X., Keten, S. and Buehler, M. J. (2007). "Hierarchies, multiple energy barriers, and robustness govern the fracture mechanics of α-helical and β-sheet protein domains." Progress of National Academy of Sciences of the United States of America 104(42): 16410-16415.

Akisanya, A. R. and Fleck, N. A. (1992). "Brittle fracture of adhesive joints." International Journal of Fracture 58: 93-114.

Alder, B. J. and Wainwright, T. E. (1957). "Phase transition for a hard sphere system." Journal of Chemical Physics 27: 1208-1209.

Allen, M. G. and Senturia, S. D. (1988). "Analysis of critical debonding pressures of stressed thin fihns in the blister test." Journal of Adhesion 25: 303-315.

Allen, M. G. and Senturia, S. D. (1989). "Application of the island blister test for thin film adhesion measurement." Journal of Adhesion 29: 219-231.

Allen, M. P. and Tildesley, D. J. (1989). Computer Simulation of Liquids, Oxford University Press.

Au, C. and Büyüköztürk, O. (2006a). "Debonding of FRP plated concrete: a tri-layer fracture treatment." Engineering Fracture Mechanics 73(3): 348-365.

Au, C. and Büyüköztürk, O. (2006b). "Peel and shear fracture characterization of debonding in FRP plated concrete affected by moisture." Journal of Composites for Construction, ASCE 10(1): 35-47.

Bagchi, A. and Evans, A. G. (1996). "The mechanics and physics of thin film decohesion and its measurement." Interface Science 3: 169-193.

Bagchi, A., Lucas, G. E., Suo, Z. and Evans, A. G. (1994). "A new procedure for measuring the decohesion energy for thin ductile films on substrates." Journal of Materials Research 9(7): 1734-1741.

Barenblatt, G. I. (1962). The mathematical theory of equilibrium cracks in brittle fracture. Advances in Applied Mechanics. H. L. Dryden and T. Von Karman, Academic Press: 55-129.

Bell, G. I. (1978). "Models for the specific adhesion of cells to cells." Science 200: 618-627.

Berendsen, H. J. C., Grigera, J. R. and Straatsma, T. P. (1987). "The missing term in effective pair potentials." Journal of Physical Chemistry 91(24): 6269–6271.

Berendsen, H. J. C., Postma, J. P. M., van Gunsteren, W. F. and Hermans, J. (1981). Intermolecular Forces. The Fourteenth Jerusalem Symposium on Quantum Chemistry and Biochemistry, Jerusalem, Israel, Dordrecht Reidel.

Berweger, C. D., van Gunsteren, W. F. and Muller-Plathe, F. (1995). "Force field parametrization by weak coupling. Re-engineering SPC water." Chemical Physics Letters 232(5-6): 429-436.

Bonomi, M., Branduardi, D., Bussi, G., Camilloni, C., Provasi, D., Raiteri, P., Donadio, D., Marinelli, F., Pietrucci, F., Broglia, R. A. and Parrinello, M. (2009). "PLUMED: a portable plugin for free-energy calculations with molecular dynamics." Computer Physics Communications 180(10): 1961-1972.

Brooks, B. R., Bruccoleri, R. E., Olafson, B. D., States, D. J., Swaminathan, S. and Karplus, M. (1983). "CHARMM: a program for macromolecular energy, minimization, and dynamics calculations." Journal of Computational Chemistry 4(2): 187-217.

Buehler, M. J. (2008). Atomistic Modeling of Materials Failure. New York, Springer.

Buehler, M. J. and Ackbarow, T. (2007). "Fracture mechanics of protein materials." Materials Today 10(9): 46-58.

Bustamante, C., Smith, S. B., Liphardt, J. and Smith, D. (2000). "Single-molecule studies of DNA mechanics." Current Opinion in Structural Biology 10: 279.

Büyüköztürk, O., Buehler, M. J., Lau, D. and Tuakta, C. (2011). "Structural solution using molecular dynamics: Fundamentals and a case study of epoxy-silica interface." International Journal of Solids and Structures 48(14-15): 2131.

Büyüköztürk, O., Gunes, O. and Karaca, E. (2004). "Progress on understanding debonding problems in reinforced concrete and steel members strengthened using FRP composites." Construction and Building Materials 18: 9-19.

Büyüköztürk, O. and Lee, K.-M. (1993). "Assessment of interfacial fracture toughness in concrete composites." Cement and Concrete Composites 15(3): 143-151.

Camacho, G. T. and Ortiz, M. (1996). "Computational modeling of impact damage in brittle materials." International Journal of Solids and Structures 33: 2899-2938.

Chalker, P. R., Bull, S. J. and Rickerby, D. S. (1991). "A review of the methods for the evaluation of cating-substrate adhesion." Materials Science and Engineering: A 140: 385-392.

Chen, C. R. and Mai, Y. W. (2010). "Comparison of cohesive zone model and linear elastic fracture mechanics for a mode I crack near a compliant/stiff interface." Engineering Fracture Mechanics 77: 3408-3417.

Chen, W. T. and Flavin, T. F. (1972). "Mechanics of film adhesion: Elastic and elastic-plastic behavior." IBM Journal of Research and Development 116: 203-213.

Dauber-Osguthorpe, P., Roberts, V. A., Osguthorpe, D. J., Wolff, J., Genest, M. and Hagler, A. T. (1988). "Structure and energetics of ligand binding to proteins: E. coli dihydrofolate reductase-trimethoprim, a drug-receptor system." Proteins: Structure, Function and Genetics 4: 31-47.

Diehl, T. (2008). "On using a penalty-based cohesive-zone finite element approach: Part II – Inelastic peeling of an epoxy-bonded aluminum strip." International Journal of Adhesion and Adhesives 28(4-5): 256.

Dugdale, D. S. (1960). "Yielding in steel sheets containing slits." Journal of the Mechanics and Physics of Solids 8: 100-104.

Elices, M., Guinea, G. V., Gomez, J. and Planas, J. (2002). "The cohesive zone model:

advantages, limitations and challenges." <u>Engineering Fracture Mechanics</u> **69**(2): 137-163.

Espinosa, H. D., Dwivedi, S. and Lu, H. C. (2000). "Modeling impact induced delamination of woven fiber reinforced composites with contact/cohesive laws." <u>Computer Methods in Applied Mechanics and Engineering</u> **183**(3-4): 259-290.

Etienne-Calas, S., A., D. and Etienne, P. (2004). "Fracture study of organic-inorganic coatings using nanoindentation technique." <u>Journal of Non-Crystalline Solids</u> **344**: 60-65.

Evans, A. G. and Hu, M. S. (1989). "The cracking and decohesion of thin films on ductile substrates." <u>Acta Metallurgica et Materialia</u> **37**: 917-925.

Fermeglia, M., Ferrone, M. and Pricl, S. (2003). "Computer simulation of nylon-6/organoclay nanocomposites: prediction of the binding energy." <u>Fluid Phase Equilibria</u> **212**(1-2): 315-329.

Fermeglia, M., Ferrone, M. and Pricl, S. (2004). "Estimation of the binding energy in random poly(butylene terephtalate-co-thiodiethylene terephtalate) copolyesters/clay nanocomposites via molecular simulation." <u>Molecular Simulation</u> **30**(5): 289-300.

Ferracuti, B., Savoia, M. and Mazzotti, C. (2007). "Interface law for FRP–concrete delamination." <u>Composite Structures</u> **80**: 523–531.

Fish, J. J. (2006). "Bridging the scales in nano engineering and science." <u>Journal of Nanoparticle Research</u> **8**: 577-584.

Fisher, T. E., Oberhauser, A. F., Carrion-Vazquez, M., Marszalek, P. E. and Fernandez, J. M. (1999). "The study of protein mechanics with the atomic force microscope." <u>Trends in Biochemical Sciences</u> **24**: 379.

Frigione, M., Aiello, M. A. and Naddeo, C. (2006). "Water Effect on the Bond Strength of Concrete/Concrete Adhesive Joints." <u>Construction and Building Materials</u> **20**: 957-970.

Galema, S. A., Howardb, E., Engberts, J. B. F. N. and Grigera, J. R. (1994). "The effect of stereochemistry upon carbohydrate hydration. A molecular dynamicsnext term simulation of β-d-galactopyranose and (α,β)-d-talopyranose " <u>Carbohydrate Research</u> **265**(2): 215-225

Gardebien, F., Gaudel-Siri, A., Jean-Luc Brédas and Lazzaroni, R. (2004). "Molecular dynamics simulations of intercalated poly(ε-caprolactone)-montmorillonite clay nanocomposites." <u>Jounral of Physical Chemistry B</u> **108**(30): 10678-10686.

Geubelle, P. H. and Baylor, J. (1998). "The impact-induced delamination of laminated composites: A 2D simulation." <u>Composites Part B: Engineering</u> **29**: 589-602.

Gunsteren, W. F. V., Luque, F. J., Timms, D. and Torda, A. E. (1994). "Molecular Mechanics in Biology: From Structure to Function, Taking Account of Solvation." <u>Annual Review of Biophysics and Biomolecular Structure</u> **23**: 847-863.

Hagler, A. T. and Ewig, C. S. (1994). "On the use of quantum energy surfaces in the derivation of molecular force fields." <u>Computer Physics Communication</u> **84**(1-3): 131-155.

Higgins, A. (2000). "Adhesive bonding of aircraft structures." <u>International Journal of</u>

Adhesion and Adhesives 20: 367-376.

Hutchinson, J. W. (1990). Mixed mode fracture mechanics of interfaces. Metal-Ceramic Interfaces, Acta-Scripta Metallurgica, Proceedings Series 4. A. G. E. M. Ruhle, M. F. Ashby and J. P. Hirth, Pergamon Press: 295-306.

Hutchinson, J. W. and Suo, Z. (1992). "Mixed mode cracking in layered materials." Advances in Applied Mechanics 29: 63-191.

Hwang, M., Stockfisch, T. P. and Hagler, A. T. (1994). "Derivation of class II force fields. 2. Derivation and characterization of a class II force field, CFF93, for the alkyl functional group and alkane molecules." Journal of the American Chemical Society 116(6): 2515-2525.

Janda, M. (1986). "On the intrinsic stress in thin chromium films." Thin Solid Films 142(1): 37-45.

Jensen, H. M. and Thouless, M. D. (1993). "Effect of residual stresses in the blister test." International Journal of Solids and Structures 30: 779-795.

Jeong, H.-S. and White, R. C. (1993). "Variational principle of thin film adhesion." Journal of Vacuum Science and Technology A 11: 1373-1376.

Jin, Z.-H. and Sun, C. T. (2005). "Cohesive zone modeling of interface fracture in elastic bi-materials." Engineering Fracture Mechanics 72: 1805-1817.

Johnson, K. L. (1970). "The correlation of indentation experiments." Journal of the Mechanics and Physics of Solids 18: 115-126.

Jorgensen, W. L., Chandrasekhar, J., Madura, J. D., Impey, R. W. and Klein, M. L. (1983). "Comparison of simple potential functions for simulating liquid water." Journal of Chemical Physics 79(2): 926-935.

Karbhari, V. M. and Engineer, M. (1996). "Effects of Environmental Exposure on the External Strengthening of Concrete with Composites - Short Term Bond Durability." Journal of Reinforced Plastics and Composites 15(1194-1216).

Keten, S. and Buehler, M. J. (2008). "Asymptotic strength limit of hydrogen-bond assemblies in protein at vanishing pulling rates." Physical Review Letters 100(19): 198301.

Kim, S. (1991). The role of plastic package adhesion in IC performance. Proceedings: 41 st Electronic Components and Technology Conference, IEEE, New York.

Klein, P. and Gao, H. (1998). "Crack nucleation and growth as strain localization in a virtual-bond continuum." Engineering Fracture Mechanics 61: 21-48.

Korzhinsky, M. A., Tkachenko, S. I., Shmulovich, K. I. and Steinberg, G. S. (1995). "Native Al and Si formation " Nature 375: 544.

Krull, H. and Yuan, H. (2011). "Suggestions to the cohesive traction–separation law from atomistic simulations." Engineering Fracture Mechanics 78: 525–533.

Laio, A. and Gervasio, F. L. (2008). "Metadynamics: a method to simulate rare events and reconstruct the free energy in biophysics, chemistry and material science." Reports on Progress in Physics 71(12): 126601.

Laio, A. and Parrinello, M. (2002). "Escaping free-energy minima." Progress of National Academy of Sciences of the United States of America 99(20): 12562-12566.

Lau, D. and Büyüköztürk, O. (2010). "Fracture characterization of concrete/epoxy

interface affected by moisture." Mechanics of Materials 42(12): 1031-1042.

Lau, D., Büyüköztürk, O. and Buehler, M. J. (2012a). "Characterization of the adhesive strength between epoxy and silica using a multiscale approach." Journal of Materials Research in press.

Lau, D., Büyüköztürk, O. and Buehler, M. J. (2012b). Multiscale modeling of organic-inorganic interface: From molecular dynamics simulation to finite element modeling. 2012 Materials Research Society Spring Meeting. San Francisco, CA.

Lau, K. F., Alper, H. E., Thacher, T. S. and Stouch, T. R. (1994). "Effects of Switching Functions on the Behavior of Liquid Water in Molecular Dynamics Simulations." Journal of Physical Chemistry 98: 8785.

Lee, K.-M. and Büyüköztürk, O. (1995). "Fracture toughness of mortar-aggregate interface in high-strength concrete." ACI Materials Journal 92(6): 634-642.

Lewis, G. V. and Catlow, C. R. A. (1985). "Potential models for ionic oxides " Journal of Physics C: Solid State Physics 18(6): 1149-1161.

Liu, W. K., Park, H. S., Qian, D., Karpov, E. G., Kadowaki, H. and Wagner, G. J. (2006). "Bridging scale methods for nanomechanics and materials." Computer Methods in Applied Mechanics and Engineering 195: 1407-1421.

Maple, J. R., Dinur, U. and Hagler, A. T. (1988). "Derivation of force fields for molecular mechanics and dynamics from ab initio energy surfaces." Progress of National Academy of Sciences of the United States of America 85: 5350-5354.

Maple, J. R., Hwang, M. J., Stockfisch, T. P., Dinur, U., Waldman, M., Ewig, C. S. and Hagler, A. (1994). "Derivation of class II force fields. 1. Methodology and quantum force field for the alkyl functional group and alkane molecules." Journal of Computational Chemistry 15(2): 162-182.

Marko, J. F. and Siggia, E. D. (1995). "Stretching DNA." Macromolecules 28(26): 8759.

Marshall, D. B. and Evans, A. G. (1984). "Measurement of adherence of residually stressed thin films by indentation. I. Mechanics of interface delamination." Journal of Applied Physics 56(10): 2632-2638.

May, C. A. (1987). Epoxy Resins: Chemistry and Technology. New York, Marcel Dekker Inc.

Miller, R. E. and Tadmor, E. B. (2002). "The quasicontinuum method: overview, application, and concurrent directions." Journal of Computer-Aided Materials Design 9: 203-239.

Minisini, B. and Tsobnang, F. (2005). "Molecular mechanics studies of specific interactions in organomodified clay nanocomposite." Composites Part A: Applied Science and Manufacturing 36(4): 531-537.

Momany, F. A. and Rone, R. (1992). "Validation of the general purpose QUANTA ®3.2/CHARMm® force field." Journal of Computational Chemistry 13(7): 888-900.

Nakano, A., Bachlechner, M. E., Kalia, R. K., Lidorikis, E., Vashishta, P., Voyiadjis, G. Z., Campbell, T. J., Ogata, S. and Shimojo, F. (2001). "Multiscale simulation of nanosystems." Computing in Science & Engineering 3: 56-66.

Needleman, A. (1987). "A continuum model for void nucleation by inclusion

debonding." Journal of Applied Mechanics, Transactions of the ASME 54: 525-531.

Needleman, A. (1990a). "An analysis of decohesion along and imperfect interface." International Journal of Fracture 42: 21-40.

Needleman, A. (1990b). "An analysis of tensile decohesion along an interface." Journal of the Mechanics and Physics of Solids 38: 289-324.

Neria, E., Fischer, S. and Karplus, M. (1996). "Simulation of activation free energies in molecular systems " Journal of Chemical Physics 105(5): 1902-1921.

Nied, H. F. (2003). "Mechanics of interface fracture with applications in electronic packaging." IEEE Transactions on Device and Materials Reliability 3: 129-143.

Nishioka, T., Syano, S. and Fujimoto, T. (2003). "Concepts of separated J-integrals, separated energy release rates, and the component separation method of the J-integral for interfacial fracture mechanics." Journal of Applied Mechanics-Transactions of the ASME 70(4): 505-516.

Oberhauser, A. F., Marszalek, P. E., Erickson, H. P. and Fernandez, J. M. (1998). "The molecular elasticity of the extracellular matrix protein tenascin." Nature 393(181): 181.

Oliver, W. C. and Pharr, G. M. (1992). "An improved technique for determining hardness and elastic modulus using load and displacement sensing indentation experiments." Journal of Materials Research 7: 1564-1583.

Ouyang, Z. and Guoqiang, L. (2009). "Nonlinear interface shear fracture of end notched flexure specimens." International Journal of Solids and Structures 46: 2659-2668.

Park, H. S. and Klein, P. A. (2008). "Surface stress effects on the resonant properties of metal nanowires: The importance of finite deformation kinematics and the impact of the residual surface stress." Journal of the Mechanics and Physics of Solids 56: 3144-3166.

Park, H. S., Klein, P. A. and Wagner, G. J. (2006). "A surface Cauchy–Born model for nanoscale materials." International Journal for Numerical Methods in Engineering 68: 1072-1095.

Pellenq, R. J.-M., Kushima, A., Shahsavari, R., Van Vliet, K. J., Buehler, M. J., Yip, S. and Ulm, F.-J. (2009). "A realistic molecular model of cement hydrates." Progress of National Academy of Sciences of the United States of America 106(38): 16102-16107.

Plimpton, S. (1995). "Fast Parallel Algorithms for Short-Range Molecular Dynamics." Journal of Computational Physics 117: 1-19.

Qiao, P. and Xu, Y. (2004). "Effects of Freeze-thaw and Dry-wet Conditionings on the Mode-I Fracture of FRP-concrete Interface Bonds." Engineering, Construction and Operations in Challenging Environments: Earth and Space, ASCE: 601-608.

Rahulkumar, P., Jagota, A., Bennison, S. J. and Saigal, S. (2000). "Cohesive element modeling of viscoelastic fracture: Application to peel testing of polymers." International Journal of Solids and Structures 37: 1873-1897.

Rapaport, D. C. (1997). The Art of Molecular Dynamics Simulation. Cambridge, Cambridge University Press.

Rappe, A. K. and Goddard, W. A. I. (1991). "Charge equilibration for molecular

dynamics simulations." <u>Journal of Physical Chemistry</u> **95**(8): 3358-3363.

Rice, J. R. and Wang, J. (1989). "Embrittlement of interfaces by solute segregation." <u>Materials Science and Engineering: A</u> **107**: 23-40.

Rief, M., Fernandez, J. M. and Gaub, H. E. (1998). "Elastically coupled two-level systems as a model for biopolymer extensibility." <u>Physical Review Letters</u> **84**(21): 4764.

Rief, M., Gautel, M., Oesterhelt, F., Fernandez, J. M. and Gaub, H. E. (1997). "Reversible unfolding of individual titin immunoglobulin domains by AFM." <u>Science</u> **276**(5315): 1109.

Ritschla, F., Faitb, M., Fiedlera, K., JKohlerc, J. E. H., Kubiasb, B. and Meisela, M. (2002). "An Extension of the Consistent Valence Force Field (CVFF) with the Aim to Simulate the Structures of Vanadium Phosphorus Oxides and the Adsorption of n-Butane and of 1-Butene on their Crystal Planes." <u>ZAAC Zeitschrift für anorganische und allgemeine Chemie</u> **628**: 1385-1396.

Sharratt, B. M., Wang, L. C. and Dauskardt, R. H. (2007). "Anomalous debonding behavior of a polymer/inorganic interface." <u>Acta Materialia</u> **55**: 3601.

Shevade, A. V., Ryan, M. A., Homer, M. L., Manfreda, A. M., Zhou, H. and Manatt, K. S. (2003). "Molecular modeling of polymer composite - analyte interactions in electronic nose sensor." <u>Sensor and Actuators B</u> **93**(1-3): 84-91.

Siegmund, T. and Brocks, W. (2000). "A numerical study on the correlation between the work of separation and the dissipation rate in ductile fracture." <u>Engineering Fracture Mechanics</u> **67**: 139-154.

Sneddon, I. N. (1965). "The relation between load and penetration in the axisymmetric boussinesq problem for a punch of arbitrary profile." <u>International Journal of Engineering Science</u> **3**: 47-57.

Sotomayor, M. and Schulten, K. (2007). "Single-Molecule Experiments in Vitro and in Silico." <u>Science</u> **316**(1144-1148).

Spies, G. J. (1953). "The peeling test on redux-bonded joints." <u>Journal of Aircraft Engineering</u> **25**: 64-70.

Sprous, D., Young, M. A. and Beveridge, D. L. (1999). "Molecular dynamics studies of axis bending in d(G5-(GA4T4C)2-C5) and d(G5-(GT4A4C)2-C5): effects of sequence polarity on DNA curvature." <u>Journal of Molecular Biology</u> **285**(4): 1623-1632

Steinmann, P. A. and Hintermann, H. I. (1989). "A review of the mechanical tests for assessment of thin-film adhesion." <u>Journal of Vacuum Science and Technology A</u> **7**: 2267-2272.

Stoney, G. G. (1909). "The tension of metallic films deposited by electrolysis." <u>Proceedings of the Royal Society London Series A</u> **82**: 172-175.

Subramaniam, K. V., Ali-Ahmad, M. and Ghosn, M. (2008). "Freeze–thaw degradation of FRP–concrete interface: Impact on cohesive fracture response." <u>Engineering Fracture Mechanics</u> **75**: 3924–3940.

Tadmor, E. B., Smith, G. S., Bernstein, N. and Kaxiras, E. (1999). "Mixed finite element and atomistic formulation for complex crystals." <u>Physical Review B</u> **59**: 235-245.

Teng, J. G., Chen, J. F., Smith, S. T. and Lam, L. (2001). <u>FRP-strengthened RC Structures</u>.

West Sussex, England, Wiley & Sons, Ltd.

Thomas, M. E., Hartnett, M. P. and Mckay, J. E. (1988). "The use of surface profilometers for the measurement of wafer curvature." Journal of Vacuum Science and Technology A 6(4): 2570-2571.

Timoshenko, S. (1925). "Analysis of bi-metal thermostats." Journal of the Optical Society of America 11: 233-256.

Tuakta, C. and Büyüköztürk, O. (2011a). "Conceptual model for prediction of FRP-concrete bond strength under moisture cycles." Journal of Composites for Construction, ASCE 15(5): 743-756.

Tuakta, C. and Büyüköztürk, O. (2011b). "Deterioration of FRP/concrete bond system under variable moisture conditions quantified by fracture mechanics." Composites Part B: Engineering 42: 145-154.

Tvergaard, V. (1990). "Effect of fiber debonding in a whisker-reinforced metal." Materials Science and Engineering: A 125: 203-213.

Tvergaard, V. and Hutchinson, J. W. (1992). "The relation between crack growth resistance and fracture process parameters in elastic-plastic solids." Journal of the Mechanics and Physics of Solids 40: 1377-1397.

Valli, J. (1986). "A review of adhesion test methods for thin hard coatings." Journal of Vacuum Science and Technology A 4: 3007-3014.

Venkatraman, S. K., Kohlstedt, D. L. and Gerberich, W. W. (1992). "Microscratch analysis of the work of adhesion for Pt thin films on NiO." Journal of Materials Research 7(1126-1132).

Venkatraman, S. K., Kohlstedt, D. L. and Gerberich, W. W. (1993). "Metal-ceramic interfacial fracture resistance using the continuous microscratch technique." Thin Solid Films 223: 269-275.

Volinsky, A. A., Moody, N. R. and Gerberich, W. W. (2002). "Interfacial toughness measurements for thin films on substrates." Acta Materialia 50: 441-466.

Wang, J. (2007). "Cohesive-bridging zone model of FRP–concrete interface debonding." Engineering Fracture Mechanics 74: 2643–2658.

Weiner, S. J., Kollman, P. A., Case, D. A., Singh, U. C., Ghio, C., Alagona, G., Profeta, S. and Weiner, P. (1984). "A new force field for molecular mechanical simulation of nucleic acids and proteins." Journal of the American Chemical Society 106(3): 765-784.

Weiner, S. J., Kollman, P. A., Nguyen, D. T. and Case, D. A. (1986). "An all atom force field for simulations of proteins and nucleic acids." Journal of Computational Chemistry 7(2): 230-252.

Wu, T. W. (1991). "Microscratch and load relaxation tests for ultrathin films." Journal of Materials Research 6: 407-426.

Xu, X. P. and Needleman, A. (1993). "Void nucleation by inclusion debonding in a crystal matrix." Modelling and Simulation in Materials Science and Engineering 1: 111-132.

Yamakov, V., Saether, E., Phillips, D. R. and Glaessgen, E. H. (2006). "Molecular-dynamics simulation-based cohesive zone representation of intergranular

fracture processes in aluminum." Journal of the Mechanics and Physics of Solids **54**: 1899–1928.

Yarovsky, I. and Evans, E. (2002). "Computer simulation of structure and properties of crosslinked polymers application to epoxy resins." Polymer **43**: 963.

Yuuki, R. and Xu, J. Q. (1992). "Stress based criterion for an interface crack kinking out of the interface in dissimilar materials." Engineering Fracture Mechanics **41**(5): 635-644.

Zhang, P., Huang, Y., Geubelle, P. H., Klein, P. A. and Hwang, K. C. (2002). "The elastic modulus of single-wall carbon nanotubes: a continuum analysis incorporating interatomic potentials." International Journal of Solids and Structures **39**: 3893-3906.

Zhou, X. W., Moody, N. R., Jones, R. E., Zimmerman, J. A. and Reedy, E. D. (2009). "Molecular-dynamics-based cohesive zone law for brittle interfacial fracture under mixed loading conditions: Effects of elastic constant mismatch." Acta Materialia **57**: 4671–4686.

CVFF Parameters

```
#atom_types      cvff

!Ver  Ref  Type  Mass        Element  Connections  Comment
!---- ---  ----  ----------  -------  -----------  ------------------------------------------
 1.0   1    h    1.007970    H            1        Hydrogen bonded to C. Masses from CRC 1973/74
pages B-250.
 1.0   1    ho   1.007970    H            1        Hydrogen bonded to O
 1.0   1    c    12.011150   C            4        Sp3 aliphatic carbon
 1.0   1    cp   12.011150   C            3        Sp2 aromatic carbon (partial double bonds)
 1.0   1    c2   12.011150   C            4        Sp3 carbon bonded to 2 H's, 2 heavy atoms
 1.0   1    c1   12.011150   C            4        Sp3 carbon bonded to 1 H, 3 Heavy atoms
 1.0   1    o    15.999400   O            2        Sp3 oxygen in ether or ester groups
 1.8  14    oz   15.999400   O            1        Oxygen in Zeolite
 1.0   1    oh   15.999400   O            2        Oxygen in hydroxyl (OH) group
 1.8  14    sz   28.086000   Si           1        Silicon atom in a Zeolite or Silicate


#quadratic_bond        cvff

> E = K2 * (R - R0)^2

!Ver  Ref   I     J         R0        K2
!---- ---   ----  ----      -------   --------
 1.0   1    c     o         1.4250    273.2000
 1.0   1    c     h         1.1050    340.6175
 1.0   1    c     c         1.5260    322.7158
 1.0   1    oh    ho        0.9600    540.6336
 1.0   1    oh    c         1.4200    384.0000
 1.0   1    cp    h         1.0800    363.4164
 1.0   1    cp    cp        1.3400    480.0000
 1.0   1    cp    c         1.5100    283.0924
 1.0   1    cp    o         1.3700    400.0000
 1.8  14    sz    oz        1.6150    392.8000
 1.8  14    sz    oh        1.6350    392.8000
 2.1  28    sz    sz        3.0900    392.8000


#quadratic_angle        cvff

> E = K2 * (Theta - Theta0)^2

!Ver  Ref   I     J     K     Theta0     K2
!---- ---   ----  ----  ----  --------   -------
 1.0   1    c     o     ho    106.0000    58.5000
 1.0   1    o     c     h     109.5000    57.0000
 1.0   1    c     c     o     109.5000    70.0000
 1.0   1    cp    cp    h     120.0000    37.0000
 1.0   1    cp    cp    cp    120.0000    90.0000
 1.0   1    h     c     cp    110.0000    44.4000
 1.0   1    c     cp    cp    120.0000    44.2000
 1.0   1    c     c     cp    110.5000    46.6000
 1.0   1    o     cp    cp    120.0000    60.0000
 1.0   1    cp    o     c     109.5000    50.0000
 1.0   1    cp    o     cp    109.5000    50.0000
 1.0   1    cp    c     cp    110.5000    46.6000
 1.0   1    c     o     c     109.5000    60.0000
 1.8  14    sz    oz    sz    149.8000    31.1000
 1.8  14    oz    sz    oz    109.4700   100.3000
 3.0  14    oh    sz    oz    109.4700   100.3000
 3.0  14    sz    oh    ho    113.4000    33.3000


#torsion_1      cvff

> E = Kphi * [ 1 + cos(n*Phi - Phi0) ]

!Ver  Ref   I     J     K     L       Kphi        n         Phi0
!---- ---   ----  ----  ----  ----    -------     ------    -------
 1.0   1    *     c     c     *       1.4225      3         0.0000
 1.0   1    *     c     o     *       0.3900      3         0.0000
 1.0   1    *     cp    cp    *      12.0000      2       180.0000
 1.0   1    *     cp    c     *       0.0000      2         0.0000
```

98

```
1.9  17   cp    cp    c    cp           0.6750    4        0.0000
1.0   1    *    cp    o     *           1.5000    2      180.0000
1.9  16   cp    cp    o     c           1.8000    2      180.0000
1.8  14   sz    oz   sz    oz           0.3000    3        0.0000
3.0  14   ho    oh   sz    oz           0.3000    3        0.0000
2.1  28    *    sz   oz     *           1.0000    3        0.0000
```

#nonbond(12-6) cvff

@type A-B
@combination geometric

> E = Aij/r^12 - Bij/r^6
> where Aij = sqrt(Ai * Aj)
>   Bij = sqrt(Bi * Bj)

```
!Ver  Ref   I          A              B
!----  ---  ----   -----------    -----------
 1.0   1    h        7108.4660       32.87076
 1.8  14    oz     272894.7846      498.87880
 1.0   1    c     1981049.2250     1125.99800
 1.8  14    sz    3149175.0000      710.00000
```

Sample Script of Atom Definition in LAMMPS

```
LAMMPS 2005 data file for quartz_alpha_1_0_0_SU8

    4798 atoms
    5726 bonds
   10455 angles
   15184 dihedrals
      12 impropers

   11 atom types
   14 bond types
   24 angle types
   28 dihedral types
    3 improper types

      9.968999863      77.805999756 xlo xhi
     10.333000183      73.518001556 ylo yhi
     12.860000610     103.845001221 zlo zhi

Masses

    1   15.999400
    2   15.999400
    3   28.086000
    4    1.007970
    5   12.011150
    6   12.011150
    7   12.011150
    8   15.999400
    9   12.011150
   10   12.011150
   11    1.007970

Pair Coeffs

    1    0.2280000124    2.8597848722
    2    0.2280000124    2.8597848722
    3    0.0400184175    4.0534337049
    4    0.0000000000    0.0000000000
    5    0.1479999981    3.6170487995
    6    0.1599999990    3.4745050026
    7    0.0389999952    3.8754094636
    8    0.2280000124    2.8597848722
    9    0.0389999952    3.8754094636
   10    0.0389999952    3.8754094636
   11    0.0380000011    2.4499714540

Bond Coeffs

    1    392.8000    1.6350
    2    540.6336    0.9600
    3    392.8000    1.6150
    4    480.0000    1.3400
    5    400.0000    1.3700
    6    363.4164    1.0800
    7    283.0924    1.5100
    8    322.7158    1.5260
    9    340.6175    1.1050
   10    273.2000    1.4250
   11    322.7158    1.5260
   12    340.6175    1.1050
   13    273.2000    1.4250
   14    340.6175    1.1050

Angle Coeffs

    1     33.3000    113.4000
    2     31.1000    149.8000
    3    100.3000    109.4700
    4    100.3000    109.4700
    5    100.3000    109.4700
```

```
  6      60.0000     120.0000
  7      90.0000     120.0000
  8      37.0000     120.0000
  9      44.2000     120.0000
 10      46.6000     110.5000
 11      46.6000     110.5000
 12      46.6000     110.5000
 13      44.4000     110.0000
 14      39.5000     106.4000
 15      50.0000     109.5000
 16      70.0000     109.5000
 17      57.0000     109.5000
 18      44.4000     110.0000
 19      39.5000     106.4000
 20      46.6000     110.5000
 21      70.0000     109.5000
 22      44.4000     110.0000
 23      57.0000     109.5000
 24      60.0000     109.5000
```

Dihedral Coeffs

```
  1      0.3000      1      3
  2      0.3000      1      3
  3      0.3333      1      3
  4      0.3000      1      3
  5      3.0000     -1      2
  6      3.0000     -1      2
  7      3.0000     -1      2
  8      3.0000     -1      2
  9      0.7500     -1      2
 10      3.0000     -1      2
 11      3.0000     -1      2
 12      3.0000     -1      2
 13      0.0000      1      2
 14      0.6750      1      4
 15      0.1581      1      3
 16      0.1581      1      3
 17      0.1300      1      3
 18      0.1300      1      3
 19      0.1581      1      3
 20      0.1581      1      3
 21      0.1581      1      3
 22      0.1581      1      3
 23      0.1581      1      3
 24      0.1581      1      3
 25      0.1300      1      3
 26      0.1300      1      3
 27      0.1300      1      3
 28      0.1300      1      3
```

Improper Coeffs

```
  1      0.0000     -1      2
  2      0.3700     -1      2
  3      0.3700     -1      2
```

Atoms

```
      1      0   1 -0.593300     19.968999863    20.333000183    43.241001129
      2      0   1 -0.619700     19.968999863    22.788000107    38.988998413
      3      0   1 -0.587600     19.968999863    20.333000183    34.736000061
...
   4798      0  11  0.100000     36.679000854    40.473999023    50.286998749
```

Bonds

```
      1   1      1     33
      2   2      1   4565
      3   1      2     77
...
   5726  12   4773   4798
```

Angles

```
      1   1     33      1   4565
      2   1     77      2   4566
      3   1     34      3   4567
...
  10455  24   4773   4774   4772
```

Dihedrals

```
    1    1    4565       1      33      12
    2    2    4565       1      33      21
    3    2    4565       1      33      24
...
15184   28    4772    4774    4773    4798
```

Impropers

```
    1    1    4751    4750    4755    4766
    2    2    4750    4751    4752    4775
    3    2    4751    4752    4753    4776
    4    3    4752    4753    4754    4756
    5    2    4753    4754    4755    4777
    6    2    4750    4755    4754    4778
    7    3    4758    4757    4762    4756
    8    2    4757    4758    4759    4779
    9    2    4758    4759    4760    4780
   10    1    4759    4760    4761    4765
   11    2    4760    4761    4762    4781
   12    2    4757    4762    4761    4782
```

```
# -----------------------------------------------------------
#
#        silica/epoxy atomistic model
#
#        Prepared by:   D. Lau
#
#        Revised:       September 29th, 2011
#
#        Current Model: silica  (4749 atoms)
#                       SU8      (49 atoms)
#                       TIP3P   (45843 atoms)
#
# -----------------------------------------------------------
# Initialization
processors              1 1 1
units                   real
atom_style              full
boundary                p p p
# Force Fields and Interactions
bond_style              harmonic
angle_style             harmonic
dihedral_style          harmonic
improper_style          cvff
pair_style              lj/cut/coul/cut 10.0 8.0
# Atom Definition - Indicate input geometry file
read_data               quartz_alpha_1_0_0_SU8_1_chain_wb_d_20.data
pair_modify             mix geometric
# Neighbor Setting
neighbor                2.0 bin
neigh_modify            delay 5
timestep                1.0
fix                     en0 all nve/limit 0.0005
# -----------------------------------------------------------
# Silica and Epoxy Group/Boundary Conditions
region                  1 block 18.0 68.0 18.0 68.0 22.5 26.0 units box
group                   hold_substrate region 1
group                   SU8 id <> 4750 4798
group                   water id > 4798
group                   substrate subtract all hold_substrate SU8 water
dump                    1 all xtc 10000 all_10ns.xtc
# -----------------------------------------------------------
# Step 1: Optimization
thermo_style            custom step temp etotal epair press vol
thermo                  500
min_style               cg
minimize                0.0 1.0e-8 10000 20000
min_modify              dmax 0.2
velocity                all create 300.00 376847
velocity                hold_substrate set 0.0 0.0 0.0 units box
fix                     bc1 hold_substrate setforce 0.0 0.0 0.0
run                     50000
unfix                   en0
fix                     en1 all nve
fix                     tempcontrol all temp/berendsen 300.0 300.0 100.0
run                     50000
minimize                0.0 1.0e-8 10000 20000
run                     50000
minimize                0.0 1.0e-8 10000 20000
run                     50000
minimize                0.0 1.0e-8 10000 20000
run                     50000

# -----------------------------------------------------------
#        END OF BASIC SET-UP
# -----------------------------------------------------------

fix                     cv1 all plumed plumedfile myfile.cfg outfile metaout.dat
run                     10000000
write_restart           all_10ns.*
```

Sample Input Script for PLUMED

```
# switching on metadynamics and Gaussian parameters
HILLS HEIGHT 0.005 W_STRIDE 100

# instruction for CVs printout
PRINT W_STRIDE 1000

# 1 CVs: distance
POSITION LIST <SU8> SIGMA 0.35 DIR Z
SU8->
LOOP 4750 4798 1
SU8<-

# wall potential
UWALL CV 1 LIMIT 103.0 KAPPA 100.0 EXP 4.0 EPS 1.0 OFF 0.0
LWALL CV 1 LIMIT 45.0 KAPPA 100.0 EXP 4.0 EPS 1.0 OFF 0.0

# end of the input
ENDMETA
```